

INVESTIGATION OF THE EFFECT OF ENERGY SHAPING VIA INTERCONNECTION AND DAMPING ASSIGNMENT PASSIVITY BASED CONTROL ON THE PERFORMANCE OF ACTIVE SUSPENSION SYSTEMS

Thesis

Submitted in partial fulfillment of the requirements for the degree of

DOCTOR OF PHILOSOPHY

by

S V PRAMOD



DEPARTMENT OF ELECTRICAL AND ELECTRONICS ENGINEERING

NATIONAL INSTITUTE OF TECHNOLOGY KARNATAKA

SURATHKAL, MANGALORE -575025

MARCH, 2023

DECLARATION

by the Ph.D. Research Scholar

I hereby *declare* that the Research Thesis entitled **Investigation Of The Effect Of Energy Shaping Via Interconnection And Damping Assignment Passivity Based Control On The Performance Of Active Suspension Systems** which is being submitted to the National Institute of Technology Karnataka, Surathkal in partial fulfilment of the requirement for the award of the Degree of Doctor of Philosophy in Electrical and Electronics Engineering is a *bonafide report of the research work carried out by me*. The material contained in this Research Thesis has not been submitted to any University or Institution for the award of any degree.

S. V. Pramod

.....
S V Pramod, 165058EE16F06

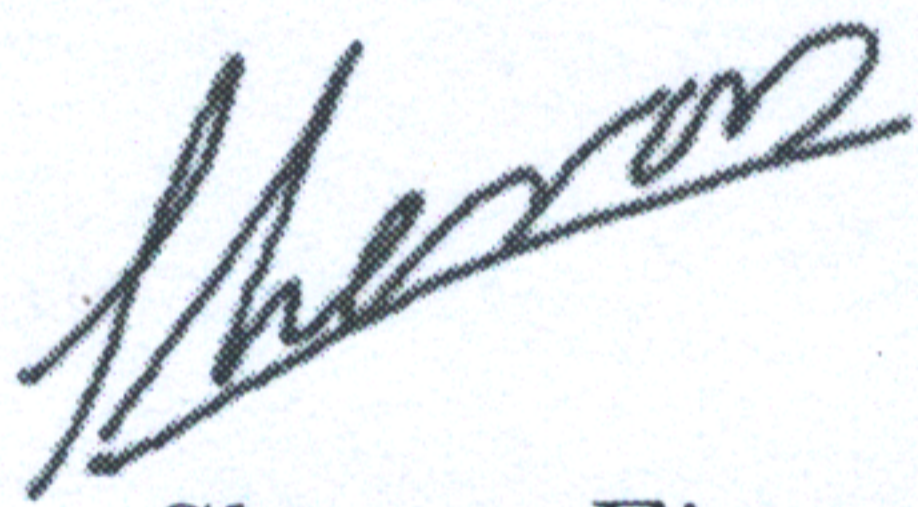
Department of Electrical and Electronics Engineering

Place: NITK-Surathkal

Date: *06-03-2023*

CERTIFICATE

This is to *certify* that the Research Thesis entitled **Investigation Of The Effect Of Energy Shaping Via Interconnection And Damping Assignment Passivity Based Control On The Performance Of Active Suspension Systems** submitted by S V Pramod (Register Number: 165058EE16F06) as the record of the research work carried out by him, is *accepted as the Research Thesis submission* in partial fulfilment of the requirements for the award of degree of Doctor of Philosophy.



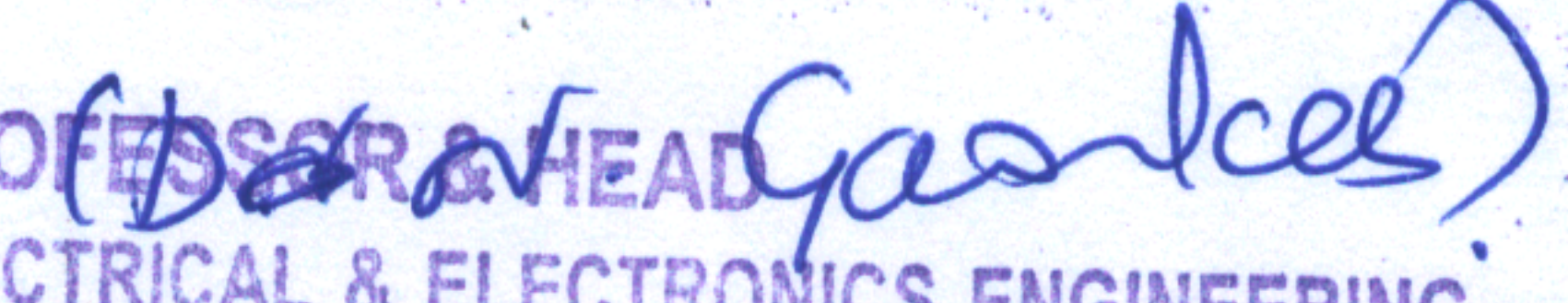
Dr. Sheron Figarado
(Research Guide)



Dr. Krishnan CMC
(Research Guide)



(Chairman-DRPC, EEE Dept.)


ASSOC. PROFESSOR & HEAD
DEPT. OF ELECTRICAL & ELECTRONICS ENGINEERING
NATIONAL INSTITUTE OF TECHNOLOGY KARNATAKA
SURATHKAL SRINIVASNAGAR P.O., MANGALORE-575025

Acknowledgements

I would like to thank a number of people who contributed to this dissertation in many different ways:

Firstly, I would like to express my deepest gratitude to my supervisors, Dr. Krishnan CMC, Assistant Professor, Department of Electrical and Electronics Engineering, and Dr. Sheron Figarado, Assistant Professor, School of Electrical Sciences (IIT Goa) for their guidance, encouragement and showing trust in me all the time.

I would like to thank my research progress assessment committee (RPAC) members Dr. Nagendrappa H and Dr. Sharnappa J, for their constructive feedback and guidance. Also, I would like to thank Dr. Dattatraya N. Gaonkar, Head of the Department of Electrical and Electronics Engineering, NITK, Surathkal. Thanks also go to Dr. Gururaj S Punekar, Dr. Shubhanga K N, Dr. Venkatesa Perumal and Dr. Vinatha U, former HODs for providing the necessary resources in the department to carry out my research. I also wish to thank the non-teaching staff of the EEE department for providing necessary support in day to day activities in the department.

I would like to thank Center for System Design (CSD) for their experimental facility and support. In particular, I am very grateful to Dr. K.V. Gangadharan, Professor, Department of Mechanical Engineering, for his technical and moral support.

I would like to thank Dr. Narayan Suresh Manjarekar, Faculty Member in Department of Electrical and Electronics Engineering, BITS Pilani KK Birla Goa Campus, for his valuable inputs to my research work.

I am truly grateful to Kiran Katari and Akshay for their support in carrying out my research work. I would like to express my heartfelt thanks

to all my colleagues, I have gained a lot from them through scholarly interactions.

I would like to express my deepest gratitude towards my parents, my wife and my sister for their love and patience which kept me going on this journey. Their faith and unconditional love towards me are the reason for whatever I have achieved in my life. I would like to dedicate this dissertation to my Late grandfather for his love, affection and inspiration.

S V PRAMOD

Abstract

Active suspension systems play a significant part in increasing the passenger ride comfort and vehicle ride stability. In addition to the spring and damping elements, active suspension systems have actuator that can inject additional force into the system to improve the performance characteristics. The performance of an active suspension system is determined by a feedback control law that governs the output of the actuator as well as the entire system. Design of a control law for active suspension system is a challenging control problem. This is owing to the fact that the performance objectives of increased ride comfort and stability while preserving suspension deflection limitations are incompatible. To address this issue, numerous control approaches have been developed and investigated in the literature.

Interconnection and Damping Assignment Passivity Based Control (IDA-PBC) is a popular passivity based control technique. The control law is designed by shaping the closed-loop energy function of the system and modifying the damping characteristics to a desired level required to improve the performance of the system. Modelling of the system in Port-Hamiltonian framework has an advantage when designing a control law using IDA-PBC. This is because the system is represented by its physical attributes in the port-Hamiltonian framework. The system can be represented by its inertia, stiffness, damping coefficients, and energy function, especially in mechanical systems. Therefore, while designing the control law using IDA-PBC, a Port Controlled Hamiltonian (PCH) model is typically used, particularly in mechanical systems where intrinsic physical features can be employed in control design and performance analysis.

Quarter-car active suspension system is a Two-Degree-Of-Freedom (2DOF) system representing a corner of a car. Although its capabilities are limited to solely vertical dynamics analysis and control, it can be utilised as a basis for the design and analysis of active suspension system controllers. IDA-PBC control law is designed for a quarter-car model of active suspension system. Different cases of the controller emerge after designing a general control law based on the structure of the desired inertia matrix. The choice of desired inertia matrix has a big impact on the dynamics

of the closed-loop system. As a result, a detailed analysis is carried out by examining the control structure with various inertia matrix scenarios. The results reveal that the design of the control law can be done using a choice of inertia matrices depending on the priority of the performance indices. The performance of a closed-loop system with various control law instances is analysed and compared using simulations and experiments on a bench scale prototype of an active suspension system.

On the quarter-car active suspension system, an observer design is developed and implemented. In general, a full-state feedback control law must be implemented to achieve better results in terms of various objectives. However, determining the unsprung mass states in the suspension system necessitates the deployment of many sensors. Furthermore, measuring velocities has been a long-standing issue in mechanical systems. A full-state observer is intended for quarter-car active suspension system to overcome these issues. The observer design is done to estimate the states of the PCH system for ease of implementation of IDA-PBC in PCH framework. On the experimental prototype, the performance of observer is evaluated. Furthermore, utilising the state estimates derived from the observer design, full-state IDA-PBC is realised on the experimental configuration. When state estimates are employed to execute the control law, the results reveal that the performance of closed-loop system is comparable to the case with full-state feedback.

Half-car active suspension is a Four-Degree-Of-Freedom (4DOF) system that represents one half of a four-wheeler system. It captures the vertical and pitch dynamics of the system. Complex analysis and the solution of several equations are required when designing a control law for a half-car active suspension system. The solution of partial differential equations is difficult to acquire, especially when designing an IDA-PBC control law. The IDA-PBC control law is designed using an algebraic method to overcome this complexity. Two controller scenarios are constructed based on the structure of the inertia matrix, and the performance of system is evaluated using performance indices in simulation in terms of their peak and RMS values, which show good improvement when compared to the uncontrolled system.

Contents

Acknowledgements	i
Abstract	iv
List of figures	ix
List of tables	xi
Acronyms and Abbreviations	xii
List of Symbols	xii
1 INTRODUCTION	1
1.1 Vehicle Suspension System	3
1.2 Modelling Of Active Suspension System	4
1.2.1 Full-Car Suspension Model	5
1.2.2 Half-Car Active Suspension Model	5
1.2.3 Quarter-Car Active Suspension Model	7
1.3 Performance Requirements And Constraints Of Suspension System	8
1.4 Port-Controlled Hamiltonian Systems	9
1.4.1 Example: 1DOF Mass Spring Damper System With Base Excitation	10
1.4.1.1 Case (i): Conservative System	13
1.4.1.2 Case (ii): System With Damping	13
1.4.1.3 Case (ii): System With External Inputs	14
1.5 Interconnection And Damping Assignment Passivity Based Control	14
1.5.1 Example: Control Of 1DOF Mass Spring Damper System With Base Excitation Using IDA-PBC	15
1.5.2 Effect Of Control Parameters On The Performance Indices And Constraints	16
1.6 Research Motivation	17

1.7	Thesis Organization	18
1.8	Summary	19
2	LITERATURE	20
2.1	Control Of Active Suspension Systems	21
2.1.1	Sliding Mode Control	21
2.1.2	H_∞ Control	23
2.1.3	Backstepping Control	24
2.1.4	Linear Quadratic Regulator	25
2.2	Port-Hamiltonian Systems And Passivity Based Control Methods	26
2.2.1	Interconnection And Damping Assignment Passivity Based Control	27
2.2.2	Recent Trends In IDA-PBC	28
2.2.3	On The Obstacle Of Solving Matching Equation	29
2.3	Observer Methods For PCH Systems	30
2.4	Summary Of Literature Survey	31
2.5	Identified Research Areas	32
2.6	Research Objectives	32
2.7	Summary	33
3	Design and performance comparison of IDA-PBC for vibration suppression in Active suspension systems	34
3.1	System Description	35
3.1.1	Port-Hamiltonian Model Of Active Suspension System	36
3.1.2	Control Objectives	37
3.2	Controller Design	37
3.3	Simulation And Discussion	41
3.3.1	Controller 1: Active Damping Injection (ADI)	42
3.3.2	Controller 2: Potential Energy Shaping And Damping Injection (PESADI)	44
3.3.3	Controller 3: Energy shaping and damping injection with coupled stiffness (ESDICS)	45
3.3.4	Controller 4: Energy shaping and damping injection with inertial decoupling (ESDIID)	47
3.3.5	Linear Quadratic Regulator (LQR)	51

3.4	Experimental Validation	53
3.4.1	Hardware Description	53
3.4.2	Experimental Results	54
3.4.2.1	Case 1: Square Wave Input	54
3.4.2.2	Case 2: Bump Input	56
3.4.2.3	Case 3: Continuously Varying Input	64
3.5	Summary	65
4	Design and Implementation of Port-Hamiltonian Observer for Active Suspension System	67
4.1	Observer Design	68
4.1.1	Choice Of Observer Parameters For Active Suspension Observer Design	70
4.2	Results and Discussion	71
4.3	Summary	74
5	Control Of Half-Car Active Suspension System Using Algebraic Interconnection And Damping Assignment Passivity Based Control	76
5.1	System Description: Half Car Active Suspension System	77
5.1.1	Port-Hamiltonian Model Of Half Car Active Suspension System	78
5.1.2	Control Objectives In Terms Of PCH Variables	81
5.2	Interconnection And Damping Assignment Passivity Based Control .	81
5.2.1	Algebraic Solution Of Matching Equation	82
5.2.2	Controller Design For Half-Car Active Suspension System . .	83
5.3	Case Studies	88
5.3.1	Controller-I: Potential Energy Shaping and Damping Injection (PESADI)	88
5.3.2	Controller-II: Inertial Decoupling	89
5.3.3	Quarter-Car IDA-PBC Method (QCAR IDA-PBC)	91
5.4	Simulation and Discussion	94
5.5	Summary	101
6	Conclusions and Future scope	102
6.1	Contributions	102
6.2	Conclusions and Remarks	103

6.2.1	Control Of Quarter-Car Active Suspension System	103
6.2.2	Control Of Half-Car Active Suspension System	104
6.3	Future Scope	104
A	Port-Hamiltonian Model Of Quarter-Car Active Suspension System	106
B	Port-Hamiltonian Model Of Half-Car Active Suspension System	109
	Bibliography	117
	PUBLICATIONS BASED ON THE THESIS	126

List of Figures

1.1	Pitch oriented Model of half-car active suspension system	6
1.2	Quarter car model of active suspension system	7
1.3	1DOF Mass Spring Damper System	11
1.4	Frequency response of Sprung mass acceleration to road displacement	17
3.1	Double mass-spring damper used to model active suspension experiment	35
3.2	Road profile for simulation analysis	42
3.3	Frequency response of $\ddot{x}_b(s)/x_r(s)$ with varying b_2	42
3.4	Time responses of ADI Controller design: (a) Sprung mass force,(b) Suspension deflection, (c) RDTL	43
3.5	Frequency response of $\ddot{x}_b(s)/x_r(s)$ for PESADI	44
3.6	Time responses of PESADI Controller design: (a) Sprung mass force,(b) Suspension deflection, (c) RDTL	46
3.7	Frequency response of $\ddot{x}_b(s)/x_r(s)$ for ESDICS	47
3.8	Time responses of ESDICS Controller design: (a) Sprung mass force,(b) Suspension deflection, (c) RDTL	48
3.9	Frequency response of $\ddot{x}_b(s)/x_r(s)$ for ESDIID	49
3.10	Time responses of ESDIID Controller design: (a) Sprung mass force,(b) Suspension deflection, (c) RDTL	50
3.11	Experimental setup	54
3.12	Implementation scheme of hardware setup.	55
3.13	Road profiles: (a) Square wave ,(b) Bump and (c) Random disturbance	56
3.14	Experimental results for square wave input: (a, b) Body acceleration ,(c, d) Suspension deflection, (e, f) Relative Dynamic Tire Load . . .	58
3.15	Experimental results for square wave input: (a, b) body displacement and (c, d) actuator force	59

3.16	Experimental results for bump input: (a, b) Body acceleration ,(c, d) Suspension deflection, (e, f) Relative Dynamic Tire Load	60
3.17	Experimental results for bump input: (a, b) body displacement and (c, d) actuator force	61
3.18	Experimental results for Continuously varying input: (a, b) Body acceleration ,(c, d) Suspension deflection, (e, f) Relative Dynamic Tire Load	62
3.19	Experimental results for Continuously varying input: (a, b) body displacement and (c, d) actuator force	63
4.1	Experimental results of observer in open-loop	72
4.2	Configuration of proposed controller with observer	72
4.3	Experimental results of observer in closed-loop	73
4.4	Experimental results of sprung mass acceleration	74
4.5	Experimental results of actuator force	74
5.1	Model of half car active suspension system	78
5.2	Control configurations (a) for PESADI, Inertial decoupling (b) QCAR IDA-PBC	93
5.3	Time responses of PESADI Controller design: (a) \dot{p}_1 ,(b) \dot{p}_2	95
5.4	Sequence of Inertial decoupling controller tuning	96
5.5	Time responses of Inertial decoupling Controller design: (a) $RDTL_f$, (b) $RDTL_r$, (c) \dot{p}_1 ,(d) \dot{p}_2 , (e) q_1 and (f) q_2	97
5.6	Simulation results for Acceleration: (a) Heave acceleration and (b) Pitch acceleration	98
5.7	Simulation results for Suspension deflection: (a) front and (b) rear	98
5.8	Simulation results for Relative dynamic tire load: (a) front and (b) rear	99
5.9	Simulation results for Actuator forces: (a) front and (b) rear	99

List of Tables

3.1	Quarter-Car Active Suspension System System Parameters	41
3.2	Values of control variables for different cases of IDA-PBC	49
3.3	Controller gains	52
3.4	Performance comparison of simulation results	52
3.5	Performance comparison of experimental results for square wave input	57
3.6	Performance comparison of experimental results for bump input . . .	57
3.7	Performance comparison of experimental results for continuously vary- ing input	64
4.1	Performance Indices of observer (Experimental Values)	75
4.2	RMS values of Acceleration (Experimental Values) \ddot{x}_b	75
5.1	RMS values of performance indices	99
5.2	RMS values of performance indices	100

Acronyms and Abbreviations

ADI	Active Damping Injection
DOF	Degree Of Freedom
ESDICS	Energy Shaping and Damping Injection with Coupled Stiffness
ESDIID	Energy Shaping and Damping Injection with Inertial Decoupling
IDA	Interconnection and Damping Assignment
IDA-PBC	Interconnection and Damping Assignment Passivity Based Control
LMI	Linear Matrix Inequality
LQR	Linear Quadratic Regulator
LTI	Linear Time Invariant
PBC	Passivity Based Control
PCH	Port Controlled Hamiltonian
PDE	Partial Differential Equation
PESADI	Potential Energy Shaping And Damping Injection
RDTL	Relative Dynamic Tire Load
RMS	Root Mean Square
SMC	Sliding Mode Control

List of Symbols

D	Damping Matrix
f	Disturbance Input
<i>g</i>	Acceleration due to Gravity
$H(\mathbf{x})$	Energy Function
J	Interconnection Matrix
K	Stiffness Matrix
<i>L</i>	Lagrangian
M	Inertia Matrix
p	Momenta Vector
q	Displacement Vector
R	Resistive/Dissipative Matrix
u	Actuator Input
x	State Vector
$\hat{\mathbf{x}}$	Estimate of State Vector x
y	Measurable Output Vector
$\tau(\mathbf{p})$	Kinetic Energy Function
$\nu(\mathbf{q})$	Potential Energy Function
\mathbb{R}^n	n-dimensional Vector of Real Numbers

Chapter 1

INTRODUCTION

Contents

1.1	Vehicle Suspension System	3
1.2	Modelling Of Active Suspension System	4
1.2.1	Full-Car Suspension Model	5
1.2.2	Half-Car Active Suspension Model	5
1.2.3	Quarter-Car Active Suspension Model	7
1.3	Performance Requirements And Constraints Of Suspension System	8
1.4	Port-Controlled Hamiltonian Systems	9
1.4.1	Example: 1DOF Mass Spring Damper System With Base Excitation	10
1.5	Interconnection And Damping Assignment Passivity Based Control	14
1.5.1	Example: Control Of 1DOF Mass Spring Damper System With Base Excitation Using IDA-PBC	15
1.5.2	Effect Of Control Parameters On The Performance Indices And Constraints	16
1.6	Research Motivation	17
1.7	Thesis Organization	18
1.8	Summary	19

Since the development of engineering and technology in the automotive industry to manufacture vehicles at a faster rate in the early 1900s, the use of commercial vehicles has increased, with an estimated global use of 1.4 billion vehicles. The increase in the commercial use of vehicles motivated the need to develop safe and comfortable transportation systems, optimise the use of road and fuel resources, and create minimal impact on the environment (Rajamani, 2011). These requirements are diverse and often difficult for manufacturers to meet. To achieve these conflicting requirements, automobiles are employed with electromechanical systems built with electronics, sensors and actuators.

An automobile is a dynamic system whose performance is effected by several forces acting on it when moving on road. It is a combination of large number of subsystems interacting with each other to perform and control multiple tasks. These subsystems can be broadly categorised as (a) driver assistance systems, (b) stability control systems, (c) ride quality improvement, (d) traffic congestion solutions, and (e) fuel economy and vehicle emissions (Rajamani, 2011).

In a broad sense, ride quality refers to the *level of comfort* experienced by the passengers onboard (Gillespie, 1992). Although it is difficult to distinguish the effects of individual components of disturbances, forces resulting from vehicle acceleration, braking, and cornering, internal vibrations from vehicle parts, and road unevenness all contribute to the discomfort felt by passengers in a vehicle. While the majority of the causes are attributable to driving circumstances and mechanical system design, road unevenness is a significant external element that contributes to vehicle vibration. Excitations to vibrations are caused by forces exerted on a vehicle's tires as it travels over a bumpy road. Road roughness is the difference in elevation of the road caused by a variety of factors ranging from potholes to localised pavement failures. This roughness causes ride vibrations by acting as a vertical input to the wheels. Through the tire/wheel assembly and suspension, these ride vibrations are communicated to the passengers (axle), producing discomfort. Vertical (heave) and horizontal (pitch, roll, and yaw) movements are caused by these vibrations (Liu et al., 2013). While the tire/wheel combination absorbs and attenuates some vibrations, the suspension system is responsible for the majority of vibration isolation.

1.1 Vehicle Suspension System

Suspension system connects the vehicle to the tires, and is responsible for isolating the passengers from vibrations caused due to road disturbances. In addition to provide vibration isolation, it is also responsible for keeping the tires in contact with the road while maintaining the rattle space requirements. Generally, suspensions can be broadly classified into two categories: Solid axle and independent suspension systems. Solid axle suspension systems are simple and inexpensive systems where the vertical motions of wheels connected to the axle are dependent on each other. Apart from being simple and inexpensive, they are strong and durable, due to which they are used in trucks and rear portion of some cars. These suspensions work well for applications where the ride comfort can be compromised, and are not suited well for improving ride comfort as the effect of disturbance experienced on one tire is transferred to another tire and their vertical movements cannot be controlled independently. These disadvantages are overcome by independent suspension systems where the vertical movement of tires is independent of each other. The vertical displacement at each wheel can be controlled independently in case of independent suspensions and the forces felt by one tire do not effect the movement of other tire. Other advantages of independent suspensions are increased suspension deflection limit, reduced weight of the vehicle due to relatively lighter suspension components. MacPherson strut and SLA suspension are two examples of widely used independent suspensions in cars (Gillespie, 1992).

Conventional suspension systems consist of a fixed spring (typically a coil, leaf or an air spring) and a damping element (typically a hydraulic shock absorber) along with other auxiliary components. The spring and damper are designed to achieve trade-off between multiple factors like static weight bearing capability, road holding and handling specifications. Due to the fixed nature of spring and damping properties of these components, the performance range of passive suspension is limited. To improve the performance of suspension system, several methods have been investigated and developed in literature. The developments in sensors and actuators led to the introduction of controllable elements into the automobiles. This led to the development of what are called as controllable suspension systems (Liu et al., 2013). Depending on the method of power induced/ dissipated from the suspension system, controllable suspension systems may be broadly classified into two categories:

Semi-active and active suspension systems. Semi-active suspension systems consist of controllable elements whose properties can be modified by using external control, and there is no external mechanical energy injected into the system. Few examples of such devices are dampers with magnetorheological (MR) fluids, electrorheological (ER) fluids, switchable shock absorbers, controllable springs etc. Active suspension systems consist of an additional element in parallel along with the spring and damper which is capable of injecting external mechanical energy into the system. This active element is mostly a hydraulic/pneumatic cylinder whose response can be controlled using electronic signal according to the desired ride behaviour. Active suspension using linear motor is also developed by Bose corporation. An active suspension system offers better performance characteristics compared to passive and semi-active counterparts due to its force injection capability.

1.2 Modelling Of Active Suspension System

The actuator (force generating element) in the active suspension system is controlled by processing signals from the sensors and generating a control signal and feeding it to the actuator input. Therefore, it is a control engineering problem which requires analysing the system dynamics and designing a control law to meet the performance requirements. Existence of large number of complex subsystems which are nonlinear makes the derivation of model of an exact system an impossible task. With mathematical and simulation tools in hand, an analytical model of the system based on the mechanics of interest can be used to understand the system properties and design a control law. A control engineer requires a model which captures the required dynamics and, at the same time simple enough to use it to design a controller (Rajamani, 2011).

When vehicle is moving on a road, all the components of the vehicle move together. Therefore, it can be considered as a point object with its mass located at the center of gravity. However, when analysing the vertical dynamics of a vehicle due to road disturbances, it is necessary to consider the components influenced by the vertical motion and components to be controlled to improve the performance. Some of the major assumptions in modelling and control for suspension system are:

- To analyse the effect of dynamics experienced by the passengers, the chassis is considered a separate lumped mass known as *sprung mass*.

- The tire/wheel assembly and its auxiliary components together are considered as a separate lumped mass termed as *unsprung mass*
- The mass of spring and damper are ignored while modelling the system.
- Tire is considered as a parallel combination of spring and damping elements.
- The wheel is always in contact with the road.

The suspension system consists of a spring, damper and a controllable force generator. Based on the dynamics of interest, three models of suspension system are mainly used for control design.

1.2.1 Full-Car Suspension Model

A full-car model consists of a sprung mass (vehicle body) supported by four unsprung masses at each corner of the vehicle. The suspension system consisting of spring, damper and an actuator connects the sprung mass to the unsprung masses. Full-car model is a complex model with Seven-Degrees-Of-Freedom (7DOF), namely vertical motions of four unsprung masses, heave (vertical motion), pitch and roll motions of sprung mass.

1.2.2 Half-Car Active Suspension Model

Based on the symmetry and design requirement, a full-car model can be decoupled into either *pitch* oriented or *roll* oriented Four-Degree-Of-Freedom (4DOF) half-car model. A pitch oriented half-car model of active suspension system is illustrated in figure 1.1. Terms m_b and I_ϕ represent the vehicle's body mass and pitch moment of inertia, respectively. ϕ represents pitch angle, and l_f and l_r denote the distances of the front and rear axles from the centre of mass, respectively. The stiffnesses of the front and rear suspension springs are expressed by k_{sf} and k_{sr} , respectively. The damping coefficients of the front and rear suspensions are represented by b_{sf} and b_{sr} , respectively. u_f and u_r represent the front and rear actuator force components, respectively. The unsprung mass on the front and rear wheels is denoted by m_{wf} and m_{wr} , respectively. The tire is represented as a combination of a spring and a damper, with k_{tf} and b_{tf} representing the front tire stiffness and damping coefficients, respectively, and k_{tr} and b_{tr} representing the rear tire stiffness and damping coefficients. Variables x_c , x_{bf} ,

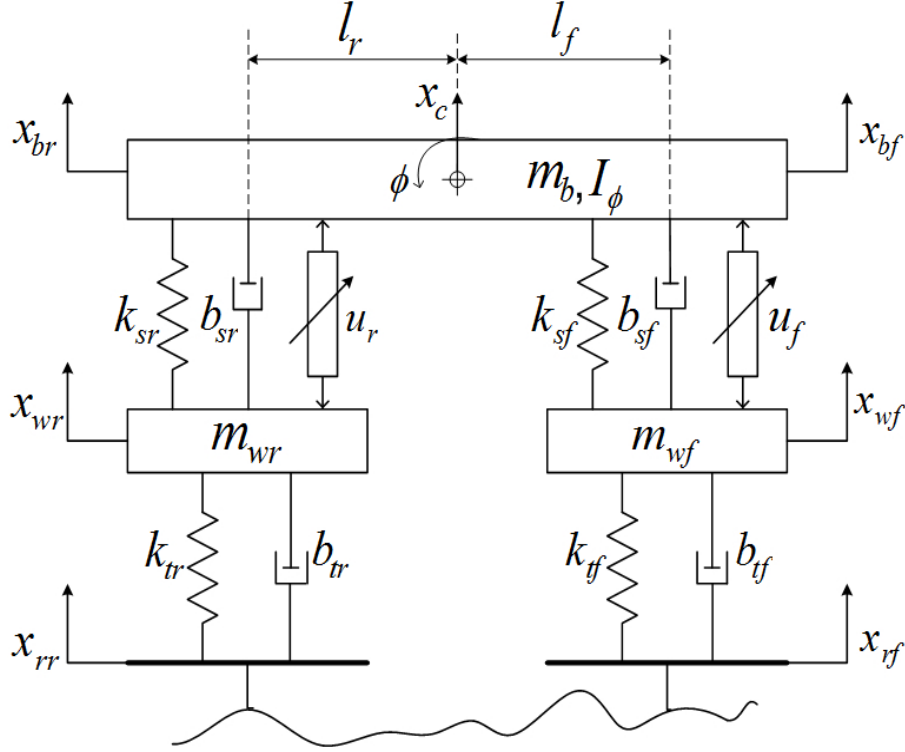


Figure 1.1: Pitch oriented Model of half-car active suspension system

and x_{br} indicate the vertical displacements of the centre of mass, front and rear body displacements, about their respective mean locations. The vertical displacements of the front and rear tires around their equilibrium positions are denoted by the symbols x_{wf} and x_{wr} , respectively. The front and rear terrain height displacements are denoted by x_{rf} and x_{rr} , respectively. The above model consists of a single sprung mass representing vehicle body with heave (vertical) and pitch freedoms of motion and two unsprung masses denoting front and rear wheels with vertical freedom of motion. The vertical displacements of the sprung mass are related as follows:

$$\begin{aligned} x_{bf} &= x_c + l_f \sin \phi \\ x_{br} &= x_c - l_r \sin \phi \end{aligned} \tag{1.1}$$

and $l_f + l_r = l$. $\sin \phi$ can be approximated as $\sin \phi \approx \phi$ since the pitch angle is modest enough. Therefore, equation (1.1) becomes $x_{bf} = x_c + l_f \phi$ and $x_{br} = x_c - l_r \phi$.

1.2.3 Quarter-Car Active Suspension Model

The quarter-car model is a bench-scale model which represents one-quarter of a car. Although its scope is limited to study of vertical dynamics only, it can be used to study the effect of road disturbances on the sprung mass, and design the controller at the basic level. Quarter-car model has Two-Degree-Of-Freedom (2DOF): sprung and unsprung mass vertical motions.

Figure 1.2 depicts a model of a quarter-car active suspension system. Mass m_b rep-

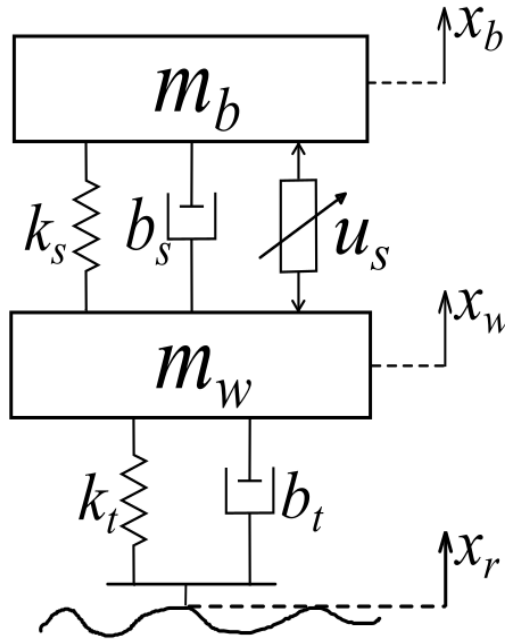


Figure 1.2: Quarter car model of active suspension system

resents one-fourth of the mass of the chassis which is supported by spring k_s , damper with damping coefficient b_s and an active force element u_s . The cumulative mass of the wheel, rim, brake and other linkage elements is represented by m_w . The road input x_r acts on the wheel whose stiffness and damping coefficients are represented by k_t and b_t respectively. x_b and x_w represent the displacements of chassis and wheel from their equilibrium points respectively.

1.3 Performance Requirements And Constraints Of Suspension System

1. **Ride Comfort:** Ideally, passengers must be isolated from the road disturbances to experience best ride. Practically, it is not possible to completely isolate the passengers from the effect of road disturbances. A good suspension system must be able to minimise the vibratory forces transmitted to the passengers. The vibratory forces on the sprung mass results in the acceleration of the sprung mass, which can be taken as the measure of ride comfort. The peak and RMS values of accelerations must be minimised to improve the ride comfort.

- For half-car suspension model, heave and pitch accelerations of sprung mass \ddot{x}_c and $\ddot{\phi}$ in Figure 1.1 are taken as a ride comfort performance indices.
- For quarter-car suspension model, vertical acceleration \ddot{x}_b in Figure 1.2 is taken as a ride comfort performance index.

2. **Good Road holding:** Unevenness of the road surface results in vertical displacement of the vehicle causing it to lose contact with the road surface. This causes vehicle to lose grip on road and deteriorates the stability. For good road holding, the dynamic tire load must always be less than the static tire load. Relative dynamic tire load (RDTL), which is a ratio of dynamic tire load to static tire load is taken as a measure of road holding.

- For half-car suspension model,

$$RDTL_f = \left| \frac{k_{tf}(x_{wf} - x_{rf}) + b_{tf}(\dot{x}_{wf} - \dot{x}_{rf})}{F_{wf}} \right| \leq 1 \quad (1.2a)$$

$$RDTL_r = \left| \frac{k_{tr}(x_{wr} - x_{rr}) + b_{tr}(\dot{x}_{wr} - \dot{x}_{rr})}{F_{wr}} \right| \leq 1 \quad (1.2b)$$

where F_{wf} and F_{wr} are the front and rear tire static loads, respectively.

$$F_{wf} + F_{wr} = (m_b + m_{wf} + m_{wr})g \quad (1.3a)$$

$$F_{wf}(l_f + l_r) = m_b g l_r + m_{wf} g (l_f + l_r) \quad (1.3b)$$

$$F_{wr}(l_f + l_r) = m_b g l_f + m_{wr} g (l_f + l_r) \quad (1.3c)$$

where g refers to the acceleration due to gravity.

- For quarter-car suspension model,

$$RDTL = \left| \frac{k_t(x_w - x_r) + b_t(\dot{x}_w - \dot{x}_r)}{F_w} \right| \leq 1 \quad (1.4)$$

where F_w is the tire static load.

$$F_w = (m_b + m_w)g \quad (1.5)$$

3. **Suspension stroke limits:** The suspension stroke (deflection between sprung and unsprung masses) must be maintained within the designed limits to prevent the damage of the mechanical structure.

- For a half-car system,

$$|x_{bf}(t) - x_{wf}(t)| \leq SS_{max} \quad (1.6a)$$

$$|x_{br}(t) - x_{wr}(t)| \leq SS_{max} \quad (1.6b)$$

- For a quarter-car suspension system,

$$|x_b(t) - x_w(t)| \leq SS_{max} \quad (1.7)$$

1.4 Port-Controlled Hamiltonian Systems

Dynamics of lumped-parameter physical systems can be represented by their Port-controlled Hamiltonian with Dissipation (PCHD) models where the system is represented in terms of their interconnection structure, damping structure and energy storage function called Hamiltonian (Ortega et al., 2002). A linear time invariant active suspension system can be represented as follows:

$$\dot{\mathbf{x}} = [\mathbf{J} - \mathbf{R}] \nabla \mathbf{H}(\mathbf{x}) + \mathbf{g} \mathbf{u} \quad (1.8a)$$

$$\mathbf{y} = \mathbf{g}^T \nabla \mathbf{H}(\mathbf{x}) \quad (1.8b)$$

where $\mathbf{x} \in \mathbb{R}^n$ is the state vector of the system which contains the energy variables, $H(\mathbf{x})$ known as Hamiltonian is the total energy stored in the system, $\mathbf{u}, \mathbf{y} \in \mathbb{R}^m$

are the input and output ports respectively, through which the power is exchanged to external inputs. The product $\langle \mathbf{u}, \mathbf{v} \rangle$ represents the power exchanged with the external input vector \mathbf{u} . The matrix $\mathbf{J} = -\mathbf{J}^T \in \mathbb{R}^{n \times n}$ is the interconnection matrix which represents the energy exchange between the storage elements in the system, $\mathbf{R} \in \mathbb{R}^{n \times n}$ defines the dissipative structure of the system, where $\mathbf{R} = \mathbf{R}^T \geq 0$, and $\mathbf{g} \in \mathbb{R}^{n \times m}$ is a full (column) rank matrix. The time derivative of the energy function can be written as,

$$\frac{d}{dt}H(\mathbf{x}) = \nabla^T H(\mathbf{x}) \cdot \dot{\mathbf{x}} \quad (1.9)$$

Substituting equation (1.8) in equation (1.9) results in

$$\frac{d}{dt}H(\mathbf{x}) = \nabla^T H(\mathbf{x}) \left\{ [\mathbf{J} - \mathbf{R}] \nabla H(\mathbf{x}) + \mathbf{g}\mathbf{u} \right\} \quad (1.10a)$$

$$= \nabla^T H(x) J \nabla H(x) - \nabla^T H(x) R \nabla H(x) + \nabla^T H(x) g u \quad (1.10b)$$

$$= -\nabla^T H(x) R \nabla H(x) + y^T u \quad (1.10c)$$

Integrating equation (1.10) gives,

$$\underbrace{[H(x(t)) - H(x(0))]}_{\text{Energy stored}} = - \underbrace{\int_0^t \nabla^T H(x(s)) R \nabla H(x(s)) ds}_{\text{Energy dissipated}} + \underbrace{\int_0^t u^T(s) y(s) ds}_{\text{Energy supplied}} \quad (1.11)$$

Equation (1.11) represents the energy balance, which says that a *passive* system (system with no active inputs) cannot store more energy than supplied to it by the external environment, and the difference between the supplied and stored energies is the dissipated energy. Typical example of passive systems are electrical systems where energy is dissipated as heat in resistors and mechanical systems where the energy is dissipated by friction.

1.4.1 Example: 1DOF Mass Spring Damper System With Base Excitation

Figure 1.3 illustrates a one-degree-of-freedom mass-spring-damper system with actuator. A base excitation is considered for analysis of the system, since vehicle suspension system is a base excited mechanical system. If we define $q \triangleq x - x_r(t)$, q describes the deflection of the spring. The kinetic and potential energies $\tau(\dot{q})$ and $\nu(q)$ can be

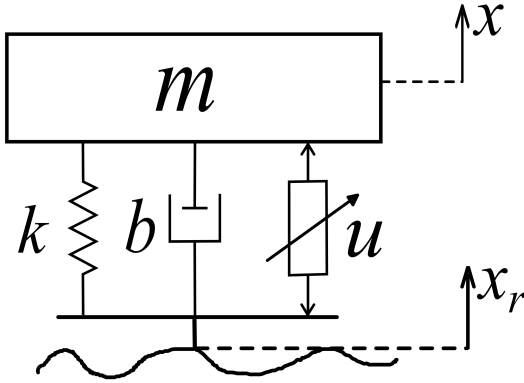


Figure 1.3: 1DOF Mass Spring Damper System

written as

$$\tau(\dot{q}) = \frac{1}{2}m(\dot{q} + \dot{x}_r)^2 \quad \text{and} \quad \nu(q) = \frac{1}{2}kq^2 \quad (1.12)$$

The Lagrangian of the system, in this case is a difference between kinetic and potential energies can be written as,

$$L(q, \dot{q}) = \tau(\dot{q}) - \nu(q) \quad (1.13a)$$

$$= \frac{1}{2}m(\dot{q} + \dot{x}_r)^2 - \frac{1}{2}kq^2 \quad (1.13b)$$

Taking the derivative with respect to \dot{q} ,

$$\nabla_q L = m(\dot{q} + \dot{x}_r) = m\dot{x} = p \quad (1.14)$$

If we define a function H which describes the total energy stored in terms of the displacement and velocity states p and q respectively,

$$H(p, q) = \tau(p) + \nu(q) \quad (1.15a)$$

$$= \frac{1}{2} \frac{p^2}{m} + \frac{1}{2} kq^2 \quad (1.15b)$$

$$= \frac{1}{2} p^T m^{-1} p + \frac{1}{2} q^T k q \quad (1.15c)$$

where $\tau(p)$ corresponds to the kinetic energy and $\nu(q)$ corresponds to the potential energy of the system. The force experienced by the mass is \dot{p} ,

$$\dot{p} = -kq - b\dot{q} + u \quad (1.16)$$

rate of change of spring displacement \dot{q} can be deduced from equation (1.14) as,

$$\dot{q} = m^{-1}p - \dot{x}_r(t) \quad (1.17a)$$

$$= \nabla_p H - \dot{x}_r(t) \quad (1.17b)$$

Substituting above equation in force equation,

$$\dot{p} = -kq - b(m^{-1}p - \dot{x}_r(t)) + u \quad (1.18a)$$

$$= -\nabla_q H - b\nabla_p H + b\dot{x}_r(t) + u \quad (1.18b)$$

Rewriting equations in state-space form,

$$\begin{bmatrix} \dot{p} \\ \dot{q} \end{bmatrix} = \begin{bmatrix} -b & -1 \\ 1 & 0 \end{bmatrix} \begin{bmatrix} \nabla_p H \\ \nabla_q H \end{bmatrix} + \begin{bmatrix} b & 1 \\ -1 & 0 \end{bmatrix} \begin{bmatrix} \dot{x}_r(t) \\ u \end{bmatrix} \quad (1.19)$$

The vertical velocity $\dot{x}_r(t)$ and actuator force u act as external inputs to the system. Input due to actuator and road disturbance can be written separately, which leads to the representation of the form

$$\underbrace{\begin{bmatrix} \dot{p} \\ \dot{q} \end{bmatrix}}_{\dot{\mathbf{x}}} = \left\{ \underbrace{\begin{bmatrix} 0 & -1 \\ 1 & 0 \end{bmatrix}}_{\mathbf{J}} - \underbrace{\begin{bmatrix} b & 0 \\ 0 & 0 \end{bmatrix}}_{\mathbf{R}} \right\} \underbrace{\begin{bmatrix} \nabla_p H \\ \nabla_q H \end{bmatrix}}_{\nabla H(\mathbf{x})} + \underbrace{\begin{bmatrix} 1 \\ 0 \end{bmatrix}}_{\mathbf{g}} u + \underbrace{\begin{bmatrix} b \\ -1 \end{bmatrix}}_{\mathbf{d}} \dot{x}_r(t) \quad (1.20)$$

The above equation can be written in generalised form as:

$$\dot{\mathbf{x}} = [\mathbf{J} - \mathbf{R}]\nabla H(\mathbf{x}) + \mathbf{g}u + \mathbf{d}f \quad (1.21)$$

where $f = \dot{x}_r(t)$ is the input from the road, and u is the input from actuator.

1.4.1.1 Case (i): Conservative System

We first consider an undamped case with external inputs set to zero. In this case, the system is assumed to be initially excited. Then the PCH form reduces to

$$\begin{bmatrix} \dot{p} \\ \dot{q} \end{bmatrix} = \underbrace{\begin{bmatrix} 0 & -1 \\ 1 & 0 \end{bmatrix}}_{\mathbf{J}} \begin{bmatrix} \nabla_p H \\ \nabla_q H \end{bmatrix} \quad (1.22)$$

The change in systems energy can be found by taking time derivative of H , which is

$$\dot{H} = (\nabla_p H)\dot{p} + (\nabla_q H)\dot{q} = \begin{bmatrix} \nabla_p H & \nabla_q H \end{bmatrix} \begin{bmatrix} \dot{p} \\ \dot{q} \end{bmatrix} \quad (1.23)$$

$$\dot{H} = \begin{bmatrix} \nabla_p H & \nabla_q H \end{bmatrix} \underbrace{\begin{bmatrix} 0 & -1 \\ 1 & 0 \end{bmatrix}}_{\mathbf{J}} \begin{bmatrix} \nabla_p H \\ \nabla_q H \end{bmatrix} = 0 \quad (1.24)$$

The above equation suggests that the change in the system energy is zero, which means that the energy present in the system is exchanged between the storage elements mass and spring, whose energy exchange is captured by the interconnection matrix \mathbf{J} .

1.4.1.2 Case (ii): System With Damping

The dynamics are given by,

$$\begin{bmatrix} \dot{p} \\ \dot{q} \end{bmatrix} = \underbrace{\begin{bmatrix} -b & -1 \\ 1 & 0 \end{bmatrix}}_{\mathbf{J-R}} \begin{bmatrix} \nabla_p H \\ \nabla_q H \end{bmatrix} \quad (1.25)$$

If we see the change in the systems energy,

$$\dot{H} = \begin{bmatrix} \nabla_p H & \nabla_q H \end{bmatrix} \begin{bmatrix} \dot{p} \\ \dot{q} \end{bmatrix} \quad (1.26a)$$

$$= \begin{bmatrix} \nabla_p H & \nabla_q H \end{bmatrix} \left\{ \underbrace{\begin{bmatrix} 0 & -1 \\ 1 & 0 \end{bmatrix}}_{\mathbf{J}} - \underbrace{\begin{bmatrix} b & 0 \\ 0 & 0 \end{bmatrix}}_{\mathbf{R}} \right\} \begin{bmatrix} \nabla_p H \\ \nabla_q H \end{bmatrix} \quad (1.26b)$$

$$= -(\nabla_p H)b(\nabla_p H) \quad (1.26c)$$

The change in the systems energy is negative, which means that the damping element dissipates the systems energy. The resistive/ damping properties of the system are captured by the resistive matrix \mathbf{R} , where $\mathbf{R} \geq 0$.

1.4.1.3 Case (ii): System With External Inputs

The system equations are given by,

$$\begin{bmatrix} \dot{p} \\ \dot{q} \end{bmatrix} = \begin{bmatrix} -b & -1 \\ 1 & 0 \end{bmatrix} \begin{bmatrix} \nabla_p H \\ \nabla_q H \end{bmatrix} + \begin{bmatrix} 1 \\ 0 \end{bmatrix} u + \begin{bmatrix} b \\ -1 \end{bmatrix} \dot{x}_r(t) \quad (1.27)$$

The change in the systems energy is given by,

$$\begin{aligned} \dot{H} = & \underbrace{-(\nabla_p H)b(\nabla_p H)}_{\text{power dissipated by damper}} + \underbrace{(\nabla_p H)u}_{\text{Power input by actuator}} \\ & + \underbrace{(\nabla_p H)b\dot{x}_r(t) - (\nabla_q H)\dot{x}_r(t)}_{\text{power input due to road excitation}} \quad (1.28) \end{aligned}$$

For the system to be stable in presence of the road disturbance, the change in energy $\dot{H}(t)$ must be negative. This can be done by adding active damping (actuator generating force similar to damper). Additionally, the systems characteristics can be shaped using actuator force to get the desired response and meet the performance requirements.

1.5 Interconnection And Damping Assignment Passivity Based Control

Interconnection and Damping Assignment Passivity Based Control (IDA-PBC) is one of the the popularly used passivity based control (PBC) techniques to design the control law for PCH systems. The control law is designed based on the physical properties of the system where the state feedback is chosen by shaping the kinetic and potential energies while assigning the desired damping such that the closed-loop port-Hamiltonian structure is preserved. The closed-loop dynamics of the system are described below:

$$\dot{\mathbf{x}} = (\mathbf{J}_d - \mathbf{R}_d)\nabla H_d(\mathbf{x}) \quad (1.29)$$

where $\mathbf{J}_d \in \mathbb{R}^{n \times n}$ is the desired or closed-loop interconnection and $\mathbf{R}_d \in \mathbb{R}^{n \times n}$ is the desired dissipative matrix, such that $\mathbf{J}_d = -\mathbf{J}_d^T$ and $\mathbf{R}_d = \mathbf{R}_d^T \geq 0$. The function $H_d(\mathbf{x}) : \mathbb{R}^n \rightarrow \mathbb{R}_+$ is the desired energy function which must be continuously differentiable. It must be noted that $H_d(\mathbf{x}^*) = 0$ with \mathbf{x}^* strict (local) minimizer of H_d . If $\mathbf{g}^\perp : \mathbb{R}^n \rightarrow \mathbb{R}^{(n-m) \times n}$ represents the full rank left annihilator of the matrix \mathbf{g} , i.e., $\mathbf{g}^\perp \mathbf{g} = \mathbf{0}$ for all $\mathbf{x} \in \mathbb{R}^n$ and $\text{rank}(\mathbf{g}^\perp) = (n - m)$, the classical solution of the IDA-PBC design problem depends upon the solution $\mathbb{K} : \mathbb{R}^n \rightarrow \mathbb{R}^n$ of the so-called *matching equation*, namely the system of equations

$$\mathbf{g}^\perp [(\mathbf{J} - \mathbf{R})\nabla H(\mathbf{x}) - (\mathbf{J}_d - \mathbf{R}_d)(\nabla H(\mathbf{x}) + \mathbb{K}(\mathbf{x}))] = \mathbf{0} \quad (1.30)$$

where $\nabla H_d(\mathbf{x}) = \nabla H(\mathbf{x}) + \mathbb{K}(\mathbf{x})$ denotes the gradient vector of the desired energy function H_d . Note that the mapping \mathbb{K} must satisfy the condition $\partial \mathbb{K} / \partial \mathbf{x} = (\partial \mathbb{K} / \partial \mathbf{x})^T$, thus ensuring integrability of \mathbb{K} (Nunna et al., 2015).

1.5.1 Example: Control Of 1DOF Mass Spring Damper System With Base Excitation Using IDA-PBC

The closed-loop kinetic and potential energies of the system can be *shaped* by modifying the inertia and stiffness terms. If the desired total energy of the system is considered as,

$$H_d(p, q) = \tau_d(p) + \nu_d(q) \quad (1.31a)$$

$$= \frac{1}{2} p^T m_d^{-1} p + \frac{1}{2} q^T k_d q \quad (1.31b)$$

where $m_d > 0$ is the desired inertia (mass) to shape the desired kinetic energy $\tau_d(p)$ and $k_d > 0$ is the desired stiffness coefficient used to shape the potential energy $\nu_d(q)$. The velocity term \dot{q} in equation (1.17) can be now rewritten as,

$$\dot{q} = m^{-1} p - \dot{x}_r(t) \quad (1.32a)$$

$$= m^{-1} m_d m_d^{-1} p - \dot{x}_r(t) \quad (1.32b)$$

$$= m^{-1} m_d \nabla_p H_d - \dot{x}_r(t) \quad (1.32c)$$

To maintain the skew-symmetric nature of \mathbf{J}_d and $\mathbf{R}_d = \mathbf{R}_d^T \geq 0$, they are chosen as,

$$\mathbf{J}_d = \begin{bmatrix} 0 & -m_d m^{-1} \\ m^{-1} m_d & 0 \end{bmatrix}, \quad \mathbf{R}_d = \begin{bmatrix} d_d & 0 \\ 0 & 0 \end{bmatrix} \quad (1.33)$$

Therefore, the closed-loop dynamics of the system can be written as,

$$\begin{bmatrix} \dot{p} \\ \dot{q} \end{bmatrix} = \begin{bmatrix} -d_d & -m_d m^{-1} \\ m^{-1} m_d & 0 \end{bmatrix} \begin{bmatrix} \nabla_p H_d \\ \nabla_q H_d \end{bmatrix} + \begin{bmatrix} b \\ -1 \end{bmatrix} \dot{x}_r(t) \quad (1.34)$$

The corresponding state feedback law is given by,

$$u = -d_d \nabla_p H_d - m_d m^{-1} \nabla_q H_d + b \nabla_p H + \nabla_q H \quad (1.35a)$$

$$= -(d_d m_d^{-1} - b m^{-1}) p - (m_d m^{-1} k_d - k) q \quad (1.35b)$$

From the above equations (1.31), (1.34) and (1.35), it can be seen that the closed-loop dynamics can be modified by shaping the kinetic energy using m_d , potential energy by choice of k_d , and dissipation can be modified by using d_d . From the perspective of the closed-loop physical system, m_d can be understood as the desired mass, while k_d can be assumed as the stiffness, and d_d the damping coefficient of the closed-loop system. From equation (1.34), it can be noted that the change in the desired inertia modifies the interconnection structure \mathbf{J}_d , which effects the overall system properties.

1.5.2 Effect Of Control Parameters On The Performance Indices And Constraints

From the closed-loop dynamics of the system, it is obvious that the desired characteristics of the system can be obtained by proper choice of closed-loop inertia, stiffness and damping coefficients m_d , k_d and d_d , respectively. Therefore, it is necessary to study the effect of these parameters on the performance indices, namely acceleration of the sprung mass, suspension deflection and dynamic load.

Figure 1.4 illustrates the frequency responses of the acceleration \ddot{x} with respect to the road displacement x_r , for change in k_d , d_d and the uncontrolled (passive) cases of 1DOF system respectively. The passive system has a resonant frequency of $\approx 3Hz$. The desired stiffness and damping of the system can be modified by adjusting the values of gains corresponding to the states q and p , respectively, in

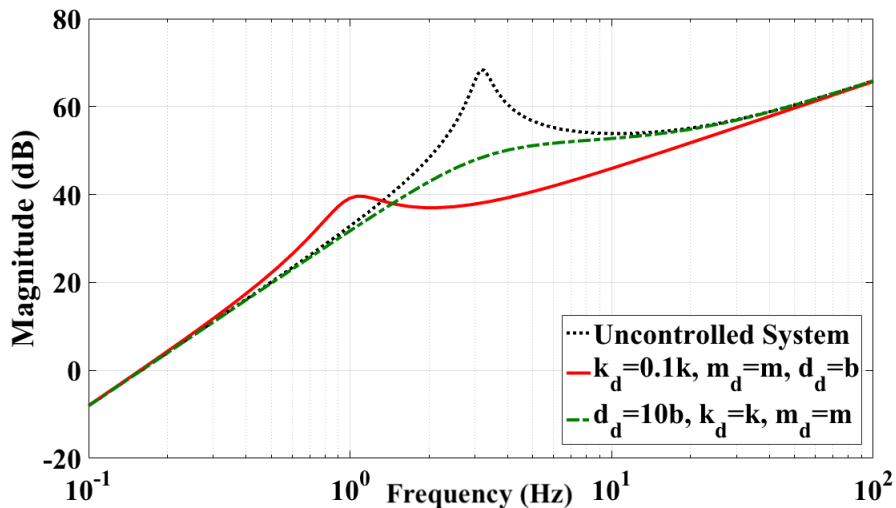


Figure 1.4: Frequency response of Sprung mass acceleration to road displacement

the feedback law (1.35). With reduction in the desired stiffness of the system, the resonant frequency shifts to the left side and attenuation in the gain at the resonant frequency, and in the frequency range $\approx (1 - 10Hz)$ is observed. Increase of the closed-loop damping coefficient d_d reduces the gain around the resonant frequencies. Thus, by modifying the closed-loop stiffness and damping coefficient k_d and d_d , the reduction in acceleration can be observed over a range of frequencies indicating overall improvement in the ride comfort.

1.6 Research Motivation

Results of 1DOF active suspension system suggest that by suitable choice of closed loop energy function parameters k_d, m_d , and damping coefficient d_d , the performance of the closed-loop system can be altered. However, 1DOF is a fully actuated mechanical system. Quarter-car and half-car active suspension systems are under-actuated mechanical systems with more than one degree-of-freedom. The design and choice of the control parameters for quarter and half-car models is a challenging task since improvement of one control objective may lead to deterioration the other performances. Moreover, incase of quarter-car and half-car systems, which happen to be under-actuated mechanical systems, solving PDEs to obtain closed-loop energy function and state feedback law is a difficult task. The choice of the desired inertia matrix

changes the control structure and behaviour of the closed-loop system.

1.7 Thesis Organization

The whole thesis is organized into six chapters as follows,

Chapter 1: This chapter includes quarter-car and half-car active suspension system models, Port-Controlled Hamiltonian (PCH) Framework, Interconnection and Damping Assignment Passivity Based Control (IDA-PBC).

Chapter 2: State-of-the-art related various popular active suspension control techniques, Passivity Based Control methods, identified research gaps and research objectives are discussed in this chapter.

Chapter 3: Design and analysis of an IDA-PBC controller for quarter-car active suspension system is presented in this chapter. Various cases of the controller arising from the choice of desired inertia matrix are discussed in detail. Experimental results of the control implemented on a bench scale model of active suspension system are presented.

Chapter 4: Design of an observer for estimating the states of the quarter-car active suspension system modelled in port-Hamiltonian form for implementing IDA-PBC full-state feedback law is presented in this chapter. Experimental results of the IDA-PBC control law implemented on the bench scale model of active suspension system using state estimates resulting from observer design are detailed.

Chapter 5: This chapter presents the design and analysis of an algebraic IDA-PBC controller for half-car active suspension system. Various cases of the control arising from the choice of the desired inertia matrix, and their effect on the performance indices is analysed with the help of simulation results.

Chapter 6: This chapter concludes the contributions of the proposed research work and also discusses about scope for the possible future works.

1.8 Summary

This chapter presents a brief introduction to vehicle suspension systems, and different models of vehicle suspension systems relevant to the control of vertical dynamics. Performance requirements of suspension system are presented for half-car and quarter-car models of active suspension systems. PCH framework and IDA-PBC are introduced with the help of a 1DOF active suspension system.

Chapter 2

LITERATURE

Contents

2.1	Control Of Active Suspension Systems	21
2.1.1	Sliding Mode Control	21
2.1.2	H_∞ Control	23
2.1.3	Backstepping Control	24
2.1.4	Linear Quadratic Regulator	25
2.2	Port-Hamiltonian Systems And Passivity Based Control Methods	26
2.2.1	Interconnection And Damping Assignment Passivity Based Control	27
2.2.2	Recent Trends In IDA-PBC	28
2.2.3	On The Obstacle Of Solving Matching Equation	29
2.3	Observer Methods For PCH Systems	30
2.4	Summary Of Literature Survey	31
2.5	Identified Research Areas	32
2.6	Research Objectives	32
2.7	Summary	33

An good suspension system must improve the ride quality of the system while ensuring the ride stability and maintaining rattle space requirements. These multiple

requirements are often contradictory. Active suspension systems consist of an electronically controlled actuator whose characteristics can be modified by designing a control law using the feedback from several sensors present on the system. Therefore, active suspension control is a control engineering problem.

Numerous control strategies have been proposed to address the problem of performance improvement of active suspension systems in the literature. Depending on the perception of the control engineer, the problem has been addressed in multiple formats.

Some of the major contributions and ideas to this application are discussed in this chapter.

2.1 Control Of Active Suspension Systems

2.1.1 Sliding Mode Control

Sliding mode control (SMC) is a model based control law which is characterised by a discontinuous feedback control structure that switches as the system crosses certain manifold in the state space to force the system states to reach, and subsequently to remain on a specified surface within the state space called sliding surface. It is a model based control law which can guarantee the invariance for matched uncertainties and disturbances having a known bound (Deshpande et al., 2014). Active suspension control using SMC has been explored vastly in literature.

A disturbance observer based SMC intended to reduce the sprung mass acceleration is proposed in (Deshpande et al., 2014), where the effect of road disturbance, nonlinearities of spring and damper are estimated and negated using the control law. Further, the control law is designed to obviate the need of unsprung mass sensor.

SMC in combination of inertial delay observer and controller is designed and experimentally validated in (Gupta et al., 2016). In this method, all the states of the system are estimated along with uncertainties, and control law is designed to address the uncertainties and reduce the sprung mass acceleration with only sprung mass position measurement.

The disadvantage of SMC is that it suffers from chattering (high frequency switching). A higher order SMC using Super Twisting Algorithm (STA) is applied and experimentally evaluated to improve the performance characteristics of Active suspension

system in (Ozer et al., 2018). The results obtained are observed to be superior than conventional SMC.

Presence of delay in data acquisition would lead to deterioration of the system performance, sometimes even making it unstable if the delay is very high. An SMC is designed considering data acquisition delay and input control disturbance in (Alves et al., 2014). This work also addresses and compares the SMC design in discrete and continuous time modes.

Different physical structures of active suspension models are available in vehicles. One such structure is double-wishbone structure. An equivalent 2DOF model of double wishbone active suspension system considering suspension kinematic structure and rubber properties, is derived, and the equivalent 2DOF model parameters are estimated. SMC is designed for the system and the control law is compensated for double wishbone structure variables. The results are experimentally validated on a bench scale model (Qin et al., 2020a).

SMC with disturbance observer for nonlinear 2DOF system combined with skyhook model is proposed on active suspension in (Qin et al., 2020b). A skyhook model is considered as reference for the sprung mass displacement to improve the convergence of suspension deflection to zero in finite time.

Terminal SMC is proposed and experimented on 2DOF prototype in (Pan et al., 2015) to improve the convergence rate of the system while considering the hard constraints such as dynamic tire load and suspension spaces. A second-order sliding mode algorithm is designed to address the problem of chattering and designing smooth switching control law.

A hydraulic actuator is generally used in the vehicle active suspensions which is controlled by an input voltage or current signal generated using feedback control law. The dynamics of the actuator play an important role in the design of control law. Output feedback based Terminal SMC is proposed on quarter-car active suspension systems in (Rath et al., 2016) where the actuator dynamics are also considered in the control law design. Using only suspension deflection as the measurable output, a high gain observer is designed to estimate the remaining states, thus addressing the complexity of sensor placement in unsprung mass, and the control law is designed using the state estimates.

SMC in combination with Fuzzy logic control (FLC) has been studied in recent literature for control of active suspension system in (Lian, 2012) and (Pang et al., 2020)

to minimise the dependence on the accuracy of the model, designing a better sliding surface with lower control gains, and designing fault tolerant control methods.

2.1.2 H_∞ Control

H_∞ Control is a method where the objective is expressed as a mathematical optimisation problem and solved. These methods have been widely explored for design of active suspension since it can be treated as a optimisation problem. Controlling multiple states and outputs whose performances are contradictory can be formulated as an optimisation problem.

Constrained H_∞ control design for active suspension control of quarter-car (2DOF) and half-car models (4DOF) is proposed in (Chen and Guo, 2005) and (Chen et al., 2005), respectively. The state feedback control law is designed for the constrained H_∞ problem by formulating the problem in linear matrix inequality (LMI) optimisation framework and multi-objective control. The sprung mass acceleration which defines the ride comfort is measured in terms of H_∞ performance for an assumed bounded value of maximum disturbance energy, while the remaining outputs (suspension stroke and road holding) and inputs (actuator forces) are analysed in terms of time domain signal responses. The design of constrained H_∞ control for half-car active suspension system where the non-linear dynamics of the actuator are considered in (Ma and Chen, 2011). In this work, first a state feedback H_∞ control law is designed for linear subsystem to improve the ride performance in terms of H_∞ norm and considering the time domain constraints of suspension stroke and dynamic tire load, and then backstepping technique is applied to deal with the non-linear actuator dynamics.

In (Sun et al., 2011), a finite frequency H_∞ control design is proposed for quarter-car active suspension system, where the designed is targeted to improve the ride comfort in a fixed frequency range (4-8Hz) where the response of the human body to vibrations is more sensitive. Further, the design also considers a fixed delay in the actuator input to improve the performance of the designed control law.

Multi-objective H_∞ control for quarter-car active suspension with time-varying actuator delay is proposed in (Li et al., 2012). In this work, a probability distributed actuator delay is considered, and the system is converted into a stochastic system to design the control law using stochastic stability theory. Controller design using H_∞ method for half-car active suspension system is presented in (Du and Zhang, 2008)

where both the actuators suffer from a time delay which is bounded and equal. The validity of the proposed method is verified using simulation results, and the proposed method gives better results compared to the conventional method for the systems which possess delay in the control input.

An output feedback H_∞ control design is presented in (Li et al., 2013a) where the control design considers a variable, bounded delay in actuator. The output feedback controller was designed to minimise the H_∞ norm of sprung mass acceleration to disturbance transfer function mainly in the frequency range of 4-8Hz.

A problem of uncertainties in the actuators is addressed in (Li et al., 2013b) where a non-fragile H_∞ control design which is insensitive to the gain changes in the feedback control is proposed for a half-car active suspension system. A non-fragile H_∞ control design for quarter-car system is designed considering uncertainties in time varying actuator delay and experimental validation of the proposed method is presented in (Li et al., 2019), which showed a better performance compared to the conventional H_∞ design.

A memory state feedback H_∞ controller is proposed to improve the H_∞ performance of the quarter-car and half-car active suspensions suffering from input-control delay in (Afshar et al., 2018) and (Karim Afshar and Javadi, 2019). The authors present a new formula to obtain a prediction vector from the dynamics of the system, and the controller is designed using prediction vector such that the effect of time-delay on the system performance of the closed-loop system is minimised.

H_∞ controller integrated with PID controller is designed and tested on a quarter-car experimental set-up by (Erol and Delibaşı, 2018). In this work, the H_∞ norm of the transfer function between vertical acceleration and input disturbance is minimised. In this work, a non convex solution region is reduced to a convex region by an inner LMI approximation technique.

2.1.3 Backstepping Control

Backstepping control is a popular technique to design controllers to stabilise dynamical systems based on the idea of Lyapunov function. This design can be applicable to a special class of dynamical systems with strict feedback form or lower triangular form. Backstepping control of active suspension systems has been widely explored in literature.

Adaptive backstepping controller design is presented for quarter-car and half-car active suspension models in (Sun et al., 2014) and (Sun et al., 2012). The controller design considers nonlinearities in the spring and damping coefficients of the suspension system, and a virtual control law is design for a lower order subsystem to stabilise asymptotically. Then, an adaptive control law is designed such that the error between the actual control signal tracks the desired or virtual control signal in presence of the uncertain parameters. Controller design presented in (Sun et al., 2012) is extended in (Sun et al., 2015) where the dynamics of electrohydraulic actuator are considered in the controller design. Backstepping controller design often requires calculating derivatives of the lower order terms in the virtual control law, which is difficult to obtain. This paper uses proposes a filter design to estimate the derivatives without the need to differentiate the terms.

The problem of actuator delay in quarter-car active suspension is addressed in (Pang et al., 2019a), where, first estimate of uncertainty in sprung mass is done using a projector-operator based adaptive control law, and the control law is design using backstepping control technique.

A disturbance observer based output feedback backstepping control law is proposed in (Yilmaz and Basturk, 2019) where an observer is designed to estimate the disturbance and the unknown states, assuming that only the knowledge of sprung mass states is known. However, this work assumes that the sprung mass velocity is measurable, which is generally difficult.

Backstepping controller in combination with neural networks is proposed in (Al Aela et al., 2022) for nonlinear quarter-car system, and an adaptive control law is used to estimate the uncertainties in the actuator parameters. The results presented show overall improvement in the frequency response of the sprung mass acceleration against the road frequency, when compared to that of passive system.

2.1.4 Linear Quadratic Regulator

Linear Quadratic Regulator (LQR) is an optimal control approach aimed to design a closed-loop control system by generating optimal feedback control gains to improve the performance of the dynamical system at minimum cost. The state feedback gains are obtained by minimising a quadratic function known as cost function. The cost function is a function of system states and input weighted appropriately to maximise

the performance and minimise the cost or input.

Active suspension control using LQR has been vastly explored in literature. Design and control of LQR for half-car active suspension system is presented in (Taghirad and Esmailzadeh, 1998). A detailed analysis of LQR method for quarter-car active suspension system, and the effect of the weighting functions on the performance indices is compared in (Rajamani, 2011) using the frequency responses of the performance indices. The results suggest that the performance of the closed-loop system completely depends on the choice of the weights in the quadratic function.

2.2 Port-Hamiltonian Systems And Passivity Based Control Methods

Classical control design approaches are mainly based on the signal processing viewpoint, where the plant and controller are viewed as signal processing devices which transform certain inputs to outputs. Many a times, complex dynamical systems may be studied by decomposing them into simpler subsystems and treating them as energy transformation devices. These subsystems, upon interconnection, add up their energies and define the behaviour of overall system. Further, the controller can also be considered as another energy transformation device, whose actions can be interpreted in terms of additional interconnection to the system and its contribution to the energy and behaviour of the system. This perspective allows the control problem to be recast as finding a closed loop dynamical system whose overall energy function is modified by the controller to take the desired form. Passivity-based control (PBC), a well-known controller design method in mechanical systems, is based on this “energy-shaping” approach. Passivity-based control (PBC) is a form of system control that involves shaping the physical energy of the system with the help of a feedback structure Ortega et al. (2001). Several variations in the concept of PBC have evolved with the advancement of control theory and modelling techniques, leading to various control techniques in this direction. Application of PBC to electrical, mechanical and electromechanical systems modelled in Euler-Lagrangian formulation have been discussed in detail manner in Ortega et al. (2013). A vision based three dimensional target tracking based on PBC is discussed in Fujita et al. (2006), which is one of the noted works in PBC for tracking systems. Interested readers can refer to

Pare Jr (2001), (Venkatraman, 2010), Van Der Schaft and Jeltsema (2014), (Ryalat, 2015), and other references.

When designing a controller based on the energy and physical properties of the system, incorporating the prior information in terms of its energy parameters makes it easier to design the closed-loop system and control law. Modelling of dynamical systems in terms of their interconnection structure, resistive structure, and energy storage (Hamiltonian) function is well defined by port-controlled Hamiltonian (PCH) framework, which makes it suited for carrying out basic steps of PBC, i.e, modifying the energy function and adding dissipation (SCHAFT, 2000). This structure is well-established formulation, and it has been used to build many PBC techniques (Ortega et al., 2002), Van Der Schaft and Jeltsema (2014), Ortega et al. (2008), (Nagesh Rao et al., 2015), (Zhang et al., 2017), (Alkrunz and Yalçın, 2019).

2.2.1 Interconnection And Damping Assignment Passivity Based Control

Interconnection and damping assignment passivity based control (IDA-PBC) is one of the eminent control techniques of PBC which was introduced to control physical systems modelled in PCH structure (Ortega et al., 2002). The design process of IDA-PBC consists of assigning energy function to the closed-loop system, and modifying the interconnection and damping structures while preserving the PCH structure of the controlled system. The design procedure comprises of designating desired interconnection and damping structures, and solving a set of partial differential equations (PDE) known as matching equation to obtain the closed-loop energy function and static state-feedback law. This approach is appealing in that the system can be interpreted in terms of its physical parameters such as spring stiffnesses, dampers, and inertias, and the control structure can be realised in terms of adjusting the physical structure of the system by incorporating virtual springs and dampers to achieve the desired behaviour (Nunna et al., 2015).

Numerous applications of IDA-PBC in various fields including electrical, mechanical, aerospace and other branches have been reported in the literature since its introduction. Few recent works in electrical engineering applications include control of PMSM (Yu et al., 2013), Suppression of low frequency oscillations in traction net-

works(Liu et al., 2018),control of grid connected inverter interfacing a photovoltaic system,(Barman et al., 2018),control of DC/DC converters (Pang et al., 2019b), control of dual active bridge converter for microgrid applications (Cupelli et al., 2019), three phase rectifier control for stable interfacing of AC and DC microgrids (Lapique et al., 2022), to name a few.

Few recent noted applications of IDA-PBC for mechanical systems include control of quadrotor unmanned aerial vehicle (Yüksel et al., 2019), motion control of 2DOF self-balancing robot(Gandarilla et al., 2019), vibration suppression of mechanical systems (Cornejo and Alvarez-Icaza, 2012), (Aoki et al., 2016), control of vehicle suspension systems (Renton et al., 2012), (Xiao and Zhu, 2014) and (Hao et al., 2022).

2.2.2 Recent Trends In IDA-PBC

Several developments in IDA-PBC have been proposed in the literature, sometimes combining it with other control procedures. Model reference adaptive control based IDA-PBC is proposed to improve the robustness of under-actuated mechanical systems suffering from matched disturbances (Haddad et al., 2018). The proposed method, when demonstrated to stabilise on an inertia wheel pendulum shows improved results when compared to the preliminary design. An adaptive IDA-PBC is designed for underactuated mechanical systems with constant matched and unmatched disturbances in (Franco, 2019). In this method, an estimate of disturbance is found out, and an additional term is added in the IDA-PBC design to compensate the disturbance. An integral action is added to the IDA-PBC design (Ferguson et al., 2017) to improve the robustness of IDA-PBC for systems which preserves the PCH structures and rejects the unknown disturbances for large class of systems. An IDA-PBC design along with an integral action is used for output voltage reference tracking of boost converter in micro-grid application (Montoya et al., 2021), and micro-grid connected inverter control to deal with the uncertain system dynamics in (Khefifi et al., 2019) .

A relation between IDA-PBC and LQR is for LTI systems is studied in (Vu and Lefèvre, 2018), showing how the optimal design can be used in the design of IDA-PBC. The problem of time delay in the actuator while designing IDA-PBC for linear time invariant systems is addressed in (Mattioni et al., 2020). The design is proposed assuming that the solution of the IDA-PBC exists without time-delay, and the results

suggest improved performance when compared to the controller designed without the time delay in the actuator.

2.2.3 On The Obstacle Of Solving Matching Equation

The design of IDA-PBC involves shaping the closed-loop energy function to find the feedback control law, requires solves a set of PDEs known generally known as matching equation. Solving matching equation is a barrier in the design procedure, and has attracted lot of attention of the researchers. Various methods have been suggested in the recent past to overcome this obstacle.

A coordinate transformation method is proposed in (Viola et al., 2007) to simplify the solution of PDE for mechanical systems in IDA-PBC design, where the need for positive definiteness of the kinetic energy of inertia matrix is obviated. This method is verified on a pendulum on a cart system where the inertia matrix is a function of displacement coordinates. A new constructive procedure for shaping the energy of port-Hamiltonian systems is proposed in (Borja et al., 2016) which obviates the need to solve the PDEs. However, the closed-loop structure does not preserve the PCH structure in closed-loop. Nunna et al. (2015) propose a constructive IDA-PBC method for PCH systems, by using algebraic method. In this method, first a dynamic control law is used to stabilise the desired equilibrium of the closed-loop system, which does not preserve the closed-loop structure. Then, an additional dynamic control law which allows the preservation of PCH structure of closed-loop extended system corresponding to an auxiliary energy function, interconnection and damping matrices is designed.

Stabilisation of a roll balancing system is presented using IDA-PBC in (Donaire et al., 2016), where the need to solve PDEs is eliminated by using a two stage procedure. In the first stage, a partial feedback linearisation is performed, which preserves the Hamiltonian structure, and then an energy function like Lyapunov energy-like candidate function is designed to stabilise the system. An algebraic IDA-PBC is proposed for a class of systems in (Cieza and Reger, 2018) where there is no need to solve PDEs. The conditions are solve using semi-definite programming. A newly developed method to solve the matching equations is proposed in (Harandi and Taghirad, 2021b), where the matching equations are transformed into what are called Pfaffian

differential equations. The effectiveness of the proposed method is demonstrated by designing controller to standard systems like magnetic levitation system and a cable driven robot system. A procedure for shaping the kinetic energy of an underactuated mechanical systems is proposed to simplify the solution of PDEs in (Harandi and Taghirad, 2021a). This is applicable to large class of nonlinear mechanical systems where the inertia matrix is nonlinear, and the degree of underactuation is one.

2.3 Observer Methods For PCH Systems

State observers or estimators are important for many reasons. Many a times, controller requires a full state feedback control law for achieving best results. However, full state feedback may not always be possible due to unavailability of the sensors, complexity in the placement of sensors, noise entering into the sensors etc,. Numerous techniques are available in literature for state estimation.

Most of the control techniques available in literature for control of active suspension systems demand full states for implementing the state feedback. However, measurement of all the state, especially unsprung mass states may not be easy due to placement of sensors. In case of mechanical systems, measurement of velocities or momenta states is a long standing problem Astolfi et al. (2010). Implementing state-observers can help solve this problem. Using observers to implement the control algorithm provides the added benefit of reducing measurement noise entering into the controller Yaghmaei and Yazdanpanah (2018). This state-of-art related to the observer design in port-Hamiltonian systems is presented in this section.

An augmented and feedback observer is proposed in (Wang et al., 2005) for a large class of PCH systems, which is adaptive with respect to perturbations in the parameters. This observer design is integrated to implement a H_∞ controller for a power system application. However, this observer design is based on measurable passive output, which may not always be possible. An observer design for a class of underactuated mechanical systems is presented in (Venkatraman et al., 2008), where the well known immersion and invariance method is used to estimate the momenta states under the assumption that the displacement states are measurable. This may not be well suited for suspension system state estimation, since measurement of tire displacement is difficult due to complexity in placement of sensors. A full order observer design is designed for a more general class of system modelled in PCH form in (Venkatraman

and Van der Schaft, 2010). This work proposes a globally stable full order observers designed based on passivity property. (Biedermann et al., 2018) proposed a passivity based observer design which resembles feedback stabilization of systems by IDA-PBC for PCH systems. This method is applicable for large class of state affine systems. Yaghmaei and Yazdanpanah (2018) proposed an observer design for large class of port-Hamiltonian systems based on the contraction analysis., which is applicable to large class of electromechanical and mechanical systems. The observer design process involves solving matching equation which is similar to the controller design process of IDA-PBC. This method can be considered as a equivalent of IDA-PBC for state estimator design. One of the major advantages of this method is that the output of the system is not equal to the passive output, which represents velocity in mechanical systems, while the measurable outputs would be displacements and velocities.

2.4 Summary Of Literature Survey

The prospect for designing a controller to improve the performance of active suspension systems has been a line of research since the introduction of automotive systems. Several methods have been proposed and analysed using simulation and experimental results. Based on the technique used, the approaches addressed in the literature can be classified into different categories. H_∞ control improves performance by minimising system norms while confining time domain signals, whereas LQR reduces the cost function of the desired performance indices. Recursive methods like backstepping have been intensively examined, as have robust control methods like SMC, which are built based on variable structure to approach the equilibrium point. Most of the control techniques discussed in the literature for active suspension control are based on signal conditioning properties or asymptotic stabilisation or error dynamics.

Due to its essential notion of altering the energy and physical properties of the closed-loop system, passivity-based control, a control approach based on the passivity properties of the systems, has found diverse applications. Because the design is based on the physical properties of the system, the structure-preserving properties of IDA-PBC for PCH systems have received a lot of attention. The control law can be designed and investigated for mechanical systems such as active suspension systems by shaping the total energy of the closed-loop system and designing and tweaking the control parameters in terms of physical qualities such as stiffness and damping coefficients.

2.5 Identified Research Areas

Although IDA-PBC has been a great topic of research, and explored on variety of systems including electrical, mechanical and electromechanical systems, the effectiveness and advantages of the control technique in improving the performance of active suspension system properties have not been explored in detail. Based on the priorities of the performance requirements, the control design can be chosen by changing the modifying the structure of the closed-loop energy function.

It is observed that to achieve the desired performance characteristics of the active suspension system, control law demands a full state feedback, which is often not possible due to inability to measure or sense all the states. In case of active suspension systems, measuring the tire and unsprung mass states is difficult due to complexity in placement of sensors. Several observer design have been proposed and used in the literature in this regard. However, implementation of IDA-PBC for active suspension systems modelled in port-Hamiltonian form remains incomplete.

The IDA-PBC design technique entails determining the necessary interconnection and damping structures, as well as solving a set of partial differential equations (PDEs) known as the matching equation to synthesise the closed-loop energy function and static state-feedback rule. PDE solutions are notoriously difficult to find, which has been a research difficulty in the development of the IDA-PBC approach. Half-car active suspension is a higher-order, underactuated complicated mechanical system that requires solving multiple (two) PDEs with a bigger number of states (four) to obtain a solution for closed-loop or desired potential energy. The difficulty can be simplified by selecting the appropriate inertia matrix. However, selecting the desired inertia matrix is a challenging task that has a significant impact on the closed-loop system's behaviour. A decision of inertia matrix can be made based on the notion of quarter-car controller design. According to the author's knowledge, no half-car active suspension system control employing IDA-PBC has been attempted in the literature.

2.6 Research Objectives

After thorough literature survey on Active suspension system control, this work aims to design and analyse static feedback control law for quarter-car and half-car models of active suspension systems using IDA-PBC. The proposed research objectives of

this work are:

1. Design a state feedback control law using IDA-PBC for a quarter-car model of active suspension system. Modifying the structure of the inertia matrix and its effect on the stiffness and damping coefficients will be used to analyse the performance of the closed-loop system. Experimental evaluation and comparison of the results produced by choosing different control topologies on a bench size model of a quarter car active suspension system.
2. Design of an observer for quarter-car active suspension system assuming that only suspension stroke as the measurement available. Implementation of a full state IDA-PBC control law on the system using state estimates acquired with observer, and comparison of performance to a design with all states available for feedback.
3. Design a state feedback IDA-PBC control law for half-car model of active suspension system. Based on the choice of inertia matrix, derive the closed-loop potential energy function, and the corresponding state-feedback law. Analyse and compare the performance of the closed-loop system with the derived control topologies.

2.7 Summary

A detailed literature review of numerous methods for control of quarter-car and half-car active suspension systems is presented in this chapter. Recent developments in IDA-PBC and its applications to various systems are briefed to show its versatility. Major contributions in the literature to solve the problem of matching equation in IDA-PBC design are highlighted. A brief discussion on the observer design methods available in literature for PCH systems are presented.

Chapter 3

Design and performance comparison of IDA-PBC for vibration suppression in Active suspension systems

Contents

3.1	System Description	35
3.1.1	Port-Hamiltonian Model Of Active Suspension System	36
3.1.2	Control Objectives	37
3.2	Controller Design	37
3.3	Simulation And Discussion	41
3.3.1	Controller 1: Active Damping Injection (ADI)	42
3.3.2	Controller 2: Potential Energy Shaping And Damping Injection (PESADI)	44
3.3.3	Controller 3: Energy shaping and damping injection with coupled stiffness (ESDICS)	45
3.3.4	Controller 4: Energy shaping and damping injection with inertial decoupling (ESDIID)	47
3.3.5	Linear Quadratic Regulator (LQR)	51
3.4	Experimental Validation	53

3.4.1	Hardware Description	53
3.4.2	Experimental Results	54
3.5	Summary	65

In this chapter, design of an IDA-PBC controller is presented for a quarter-car active suspension system. The control law is designed considering an arbitrary bounded disturbance in acceptable limits. Four cases of the controller are chosen based on the structure of the desired inertia matrix, and simulation and experimental results for these cases are presented in terms of time and frequency responses.

3.1 System Description

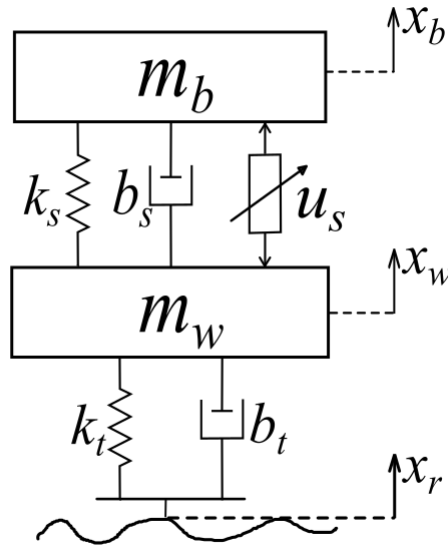


Figure 3.1: Double mass-spring damper used to model active suspension experiment

Figure 3.1 depicts a model of a quarter-car active suspension system. Mass m_b represents one-fourth of the mass of the chassis which is supported by spring k_s , damper with damping coefficient b_s and an active force element u_s . The cumulative mass of the wheel, rim, brake and other linkage elements is represented by m_w . The road input x_r acts on the wheel whose stiffness and damping coefficients are represented

by k_t and b_t respectively. x_b and x_w represent the displacements of chassis and wheel from their equilibrium points respectively.

3.1.1 Port-Hamiltonian Model Of Active Suspension System

This section presents a port-controlled Hamiltonian model of a quarter-car active suspension system. Detailed derivation of the model is given in Appendix A. The displacement coordinates of the system are defined as $q_1 = (x_w - x_r)$ and $q_2 = (x_b - x_w)$. The momenta coordinates are derived as $p_1 = m_w \dot{x}_w + m_b \dot{x}_b$ and $p_2 = m_b \dot{x}_b$. Defining $\mathbf{x}^T = [\mathbf{p}^T \quad \mathbf{q}^T]$, where $\mathbf{p}^T = [p_1 \quad p_2]$ and $\mathbf{q}^T = [q_1 \quad q_2]$, the port-Hamiltonian model of the active suspension system in Figure 3.1 is given by:

$$\dot{\mathbf{x}} = [\mathbf{J} - \mathbf{R}] \nabla H(\mathbf{x}) + \mathbf{g}u_s + \mathbf{d}f \quad (3.1)$$

where $\mathbf{J} = \begin{bmatrix} \mathbf{0} & -\mathbf{I} \\ \mathbf{I} & \mathbf{0} \end{bmatrix}$, $\mathbf{R} = \begin{bmatrix} \mathbf{D} & \mathbf{0} \\ \mathbf{0} & \mathbf{0} \end{bmatrix}$, and \mathbf{I} represents the identity matrix. The energy function $H(\mathbf{x})$ is defined as

$$H(\mathbf{x}) = \tau(\mathbf{p}) + \nu(\mathbf{q}) = \frac{1}{2} \mathbf{p}^T \mathbf{M}^{-1} \mathbf{p} + \frac{1}{2} \mathbf{q}^T \mathbf{K} \mathbf{q} \quad (3.2)$$

where $\tau(\mathbf{p})$ and $\nu(\mathbf{q})$ denote the kinetic and potential energies of the system, respectively. The matrices \mathbf{M} and \mathbf{K} are the inertia and stiffness matrices of the system given by

$$\mathbf{M} = \begin{bmatrix} m_w + m_b & m_b \\ m_b & m_b \end{bmatrix} \quad \mathbf{K} = \begin{bmatrix} k_t & 0 \\ 0 & k_s \end{bmatrix} \quad (3.3)$$

The Hamiltonian $H(\mathbf{x})$ can be written as a quadratic function in terms of a positive definite matrix \mathbf{Q} as,

$$H(\mathbf{x}) = \frac{1}{2} \mathbf{x}^T \mathbf{Q} \mathbf{x} \quad (3.4)$$

where

$$\mathbf{Q} = \begin{bmatrix} \mathbf{M} & \mathbf{0} \\ \mathbf{0} & \mathbf{K} \end{bmatrix} \quad (3.5)$$

The term \mathbf{D} represents the damping matrix consisting of the damping coefficients of the system

$$\mathbf{D} = \begin{bmatrix} b_t & 0 \\ 0 & b_s \end{bmatrix} \quad (3.6)$$

The remaining matrices are defined as $g = [\mathbf{G}^T \ \mathbf{0}]^T$ where $\mathbf{G}^T = [0 \ 1]$, $\mathbf{d}^T = [b_t \ 0 \ -1 \ 0]$ and $f = \dot{x}_r(t)$. The performance requirements of the closed-loop system can then be written in terms of state variables as:

3.1.2 Control Objectives

- Minimising the force \dot{p}_2 , which is a function of sprung mass acceleration \ddot{x}_b to improve the passenger ride comfort.
- Minimising the tire deflection and velocity q_1 and \dot{q}_1 , respectively, which are the main factors contributing to dynamic tire load, to improve the contact forces between tire and road, resulting in improved road holding and stability.
- Restricting the suspension deflection q_2 within the allowable maximum limits, that is, $|q_2| \leq |q_{2max}|$.

In addition, the control design must be such that the amplitude of the actuator force u_s lies within the feasible actuator limits, that is, $|u_s| \leq |u_{smax}|$.

3.2 Controller Design

In this section, the control law u_s is designed such that the system properties are modified using the desired energy function while maintaining the PCH structure of the closed-loop system. The desired energy function $H_d(\mathbf{x})$ is chosen as

$$H_d(\mathbf{x}) = \tau_d(\mathbf{p}) + \nu_d(\mathbf{q}) = \frac{1}{2} \mathbf{p}^T \mathbf{M}_d^{-1} \mathbf{p} + \nu_d(\mathbf{q}) \quad (3.7)$$

where $\tau_d(\mathbf{p})$ is the desired closed-loop kinetic energy profile, which can be modified using the desired inertia matrix $\mathbf{M}_d = \mathbf{M}_d^T$, and $\nu_d(\mathbf{q})$ is the desired potential energy function. The closed-loop dynamic system is defined as

$$\dot{\mathbf{x}} = [\mathbf{J}_d - \mathbf{R}_d] \nabla H_d(\mathbf{x}) + \mathbf{d}f \quad (3.8)$$

where \mathbf{J}_d and \mathbf{R}_d are defined as,

$$\mathbf{J}_d = \begin{bmatrix} \mathbf{J}_a & -\mathbf{M}_d \mathbf{M}^{-1} \\ \mathbf{M}^{-1} \mathbf{M}_d & \mathbf{0} \end{bmatrix}, \mathbf{R}_d = \begin{bmatrix} \mathbf{D}_d & \mathbf{0} \\ \mathbf{0} & \mathbf{0} \end{bmatrix} \quad (3.9)$$

Equating the open-loop and closed-loop system dynamics, we obtain

$$[\mathbf{J} - \mathbf{R}] \nabla H(\mathbf{x}) + \mathbf{g}u_s + \mathbf{d}f = [\mathbf{J}_d - \mathbf{R}_d] \nabla H_d(\mathbf{x}) + \mathbf{d}f \quad (3.10)$$

From equation (3.10), we can find that the disturbance term f is present on both sides, implying that the control law modifies the closed-loop system properties based on the desired energy function $H_d(\mathbf{x})$, and renders the closed-loop system tight to bounded arbitrary disturbance f . Rearranging equation (3.10),

$$\mathbf{g}u_s = [\mathbf{J}_d - \mathbf{R}_d] \nabla H_d(\mathbf{x}) - [\mathbf{J} - \mathbf{R}] \nabla H(\mathbf{x}) \quad (3.11)$$

The fourth order quarter-car active suspension system is controlled by a single actuator, resulting in the following constraint:

$$\mathbf{g}^\perp ([\mathbf{J}_d - \mathbf{R}_d] \nabla H_d(\mathbf{x}) - [\mathbf{J} - \mathbf{R}] \nabla H(\mathbf{x})) = \mathbf{0} \quad (3.12)$$

where \mathbf{g}^\perp is the left annihilator of \mathbf{g} , that is $\mathbf{g}^\perp \mathbf{g} = \mathbf{0}$, and $rank(\mathbf{g}^\perp) = 3$. If the condition (equation (3.12)) is satisfied, the control force u_s can then be calculated by:

$$u_s = (\mathbf{g}^\top \mathbf{g})^{-1} \mathbf{g}^\top ([\mathbf{J}_d - \mathbf{R}_d] \nabla H_d(\mathbf{x}) - [\mathbf{J} - \mathbf{R}] \nabla H(\mathbf{x})) \quad (3.13)$$

Substituting for $\mathbf{J}, \mathbf{R}, \mathbf{J}_d, \mathbf{R}_d, \mathbf{H}_d, \mathbf{H}$ and \mathbf{g} , equation (3.12) reduces to

$$\mathbf{G}^\perp (\mathbf{D} \nabla_{\mathbf{p}} H + (\mathbf{J}_a - \mathbf{D}_d) \nabla_{\mathbf{p}} H_d + \nabla_{\mathbf{q}} H - \mathbf{M}_d \mathbf{M}^{-1} \nabla_{\mathbf{q}} H_d) = 0 \quad (3.14)$$

where \mathbf{G}^\perp is the left annihilator of \mathbf{G} , i.e., $\mathbf{G}^\perp \mathbf{G} = 0$, and $rank(\mathbf{G}^\perp) = 1$. Because the two-degree-of-freedom (2DOF) quarter vehicle system is controlled by a single actuator, the constraint (equation(3.14)) emerges as a result of the system being under-actuated. Choosing the structure of $\nu_d(\mathbf{q})$ to be

$$\nu_d(\mathbf{q}) = \frac{1}{2} \mathbf{q}^\top \mathbf{K}_d \mathbf{q} \quad (3.15)$$

where \mathbf{K}_d is the stiffness matrix used to shape the desired potential energy $\nu_d(\mathbf{q})$ of the closed-loop system. Equation (3.12) can be split into terms independent on powers of \mathbf{p} , terms dependent on \mathbf{D} and \mathbf{D}_d , and terms dependent on power of \mathbf{p} ,

respectively.

$$\mathbf{G}^\perp(\mathbf{K}\mathbf{q} - \mathbf{M}_d\mathbf{M}^{-1}\mathbf{K}_d\mathbf{q}) = 0 \quad (3.16)$$

$$\mathbf{G}^\perp(\mathbf{J}_a\mathbf{M}_d^{-1}\mathbf{p}) = 0 \quad (3.17)$$

$$\mathbf{G}^\perp(\mathbf{D}\mathbf{M}^{-1}\mathbf{p} - \mathbf{D}_d\mathbf{M}_d^{-1}\mathbf{p}) = 0 \quad (3.18)$$

The control objective is to choose $\mathbf{K}_d = \mathbf{K}_d^\mathbf{T} > 0$, $\mathbf{M}_d = \mathbf{M}_d^\mathbf{T} > 0$, $\mathbf{D}_d = \mathbf{D}_d^\mathbf{T} > 0$, and $\mathbf{J}_a = -\mathbf{J}_a^\mathbf{T}$ such that equation (3.16), equation (3.17) and equation (3.18) are satisfied. In this work, additional interconnection matrix \mathbf{J}_a is chosen as zero to simplify the control design. Parameterising \mathbf{M}_d and \mathbf{D}_d as

$$\mathbf{M}_d = \begin{bmatrix} a_1 & a_2 \\ a_2 & a_3 \end{bmatrix}, \quad \mathbf{D}_d = \begin{bmatrix} b_1 & 0 \\ 0 & b_2 \end{bmatrix} \quad (3.19)$$

Solving equation (3.16), the desired potential energy function is obtained as (Renton et al., 2012),

$$\nu_d(\mathbf{q}) = \frac{1}{2}\mathbf{q}^\mathbf{T}\mathbf{K}_d\mathbf{q} = \frac{1}{2}\mathbf{q}^\mathbf{T} \begin{bmatrix} \frac{k_t m_w}{a_1 - a_2} + \alpha^2 k_z & \alpha k_z \\ \alpha k_z & k_z \end{bmatrix} \mathbf{q} \quad (3.20)$$

where $\alpha = \frac{a_1 m_b - a_2(m_w + m_b)}{m_b(a_1 - a_2)}$, and k_z is a free parameter used to modify the desired potential energy function. Solving equation (3.17) and equation (3.18), coefficients of \mathbf{D}_d are

$$b_1 = \frac{b_t}{m_w}(a_1 - a_2) \quad (3.21)$$

and b_2 is a free parameter representing suspension damping coefficient in the closed-loop. The closed-loop energy function $H_d(\mathbf{x})$ can be written as a quadratic storage function

$$H_d(\mathbf{x}) = \frac{1}{2}\mathbf{x}^\mathbf{T}\mathbf{Q}_d\mathbf{x} \quad (3.22)$$

where \mathbf{Q}_d is given by

$$\mathbf{Q}_d = \begin{bmatrix} \mathbf{M}_d & \mathbf{0} \\ \mathbf{0} & \mathbf{K}_d \end{bmatrix} \quad (3.23)$$

The closed-loop Hamiltonian $H_d(\mathbf{x})$ is chosen as the Lyapunov function for stability analysis. Taking the time-derivative of $H_d(\mathbf{x})$, we obtain

$$\dot{H}_d = (\nabla H_d(\mathbf{x}))^T \dot{\mathbf{x}} \quad (3.24)$$

Substituting equation (3.8) in equation (3.24) we get,

$$\dot{H}_d = \mathbf{x}^T \mathbf{Q}_d \mathbf{J}_d \mathbf{Q}_d \mathbf{x} - \mathbf{x}^T \mathbf{Q}_d \mathbf{R}_d \mathbf{Q}_d \mathbf{x} + \mathbf{x}^T \mathbf{Q}_d \mathbf{d} f \quad (3.25)$$

Due to the skew-symmetric property of \mathbf{J}_d , \dot{H}_d is reduced to

$$\dot{H}_d = -\mathbf{x}^T \mathbf{Q}_d \mathbf{R}_d \mathbf{Q}_d \mathbf{x} + \mathbf{x}^T \mathbf{Q}_d \mathbf{d} f \quad (3.26)$$

Now consider the term $N = (\mathbf{x}^T \mathbf{Q}_d \mathbf{d} - f^T)$. Then we can write,

$$NN^T = (\mathbf{x}^T \mathbf{Q}_d \mathbf{d})(\mathbf{d}^T \mathbf{Q}_d \mathbf{x}) - \mathbf{x}^T \mathbf{Q}_d \mathbf{d} f - f^T \mathbf{d}^T \mathbf{Q}_d \mathbf{x} + f^T f \quad (3.27)$$

Rearranging the terms in equation (3.27),

$$\mathbf{x}^T \mathbf{Q}_d \mathbf{d} f + f^T \mathbf{d}^T \mathbf{Q}_d \mathbf{x} = (\mathbf{x}^T \mathbf{Q}_d \mathbf{d})(\mathbf{d}^T \mathbf{Q}_d \mathbf{x}) + f^T f - NN^T \quad (3.28a)$$

$$2\mathbf{x}^T \mathbf{Q}_d \mathbf{d} f = (\mathbf{x}^T \mathbf{Q}_d \mathbf{d})(\mathbf{d}^T \mathbf{Q}_d \mathbf{x}) + f^T f - NN^T \quad (3.28b)$$

$$\implies \mathbf{x}^T \mathbf{Q}_d \mathbf{d} f \leq (\mathbf{x}^T \mathbf{Q}_d \mathbf{d})(\mathbf{d}^T \mathbf{Q}_d \mathbf{x}) + f^T f \quad (3.28c)$$

Substituting equation (3.28c) in equation (3.26), we get the inequality

$$\dot{H}_d \leq -\mathbf{x}^T \mathbf{Q}_d \mathbf{R}_d \mathbf{Q}_d \mathbf{x} + (\mathbf{x}^T \mathbf{Q}_d \mathbf{d})(\mathbf{d}^T \mathbf{Q}_d \mathbf{x}) + f^T f \quad (3.29)$$

which can be written as,

$$\dot{H}_d \leq -\mathbf{x}^T \mathbf{Q}_d^{1/2} (\mathbf{Q}_d^{1/2} \mathbf{R}_d \mathbf{Q}_d^{1/2}) \mathbf{Q}_d^{1/2} \mathbf{x} + \mathbf{x}^T \mathbf{Q}_d^{1/2} (\mathbf{Q}_d^{1/2} \mathbf{d} \mathbf{d}^T \mathbf{Q}_d^{1/2}) \mathbf{Q}_d^{1/2} \mathbf{x} + f^T f \quad (3.30)$$

If the disturbance f is assumed to be bounded such that $f^T f \leq f_{max}$, and defining $\varepsilon = (2\lambda_{1min} - 2\lambda_{2max})$ where λ_{1min} corresponds to minimum eigen value of $(\mathbf{Q}_d^{1/2} \mathbf{R}_d \mathbf{Q}_d^{1/2})$ and λ_{2max} corresponds to maximum eigen value of $(\mathbf{Q}_d^{1/2} \mathbf{d} \mathbf{d}^T \mathbf{Q}_d^{1/2})$, the equation (3.30) can be written as

$$\dot{H}_d \leq -\varepsilon H_d + f_{max} \quad (3.31)$$

If \mathbf{Q}_d , and \mathbf{R}_d are chosen such that $\varepsilon > 0$, then the decay of $H_d(t)$ can be guaranteed, and solution of equation (3.31) is given by

$$H_d(t) \leq \left\{ \left(H_d(0) - \frac{f_{max}}{\varepsilon} \right) e^{-\varepsilon t} + \frac{f_{max}}{\varepsilon} \right\} = \kappa(t) \quad (3.32)$$

Therefore, trajectories of states with initial conditions $\mathbf{x}(\mathbf{0})$ in the region defined by,

$$\mathbf{x}(\mathbf{t}) = \{ \mathbf{x}(\mathbf{0}) \in \mathbb{R}^n | H_d(t) \leq \kappa(t) \} \quad (3.33)$$

will stay inside the ellipsoid, which is the region of attraction, which proves the stability of the closed-loop system (equation(3.8)).

3.3 Simulation And Discussion

In this section, the validity of the proposed control law is tested on a bench-scale model of quarter-car suspension system. The specifications of the active suspension experimental setup are listed in Table 3.1.

Based on the choice of the control variables a_1, a_2, a_3, k_z and b_2 , four cases of the control law are presented in the following sections. Desired inertia matrix \mathbf{M}_d is chosen by varying the value α from 0 to 1 using parameter a_2 . The free parameters a_1 and a_3 are set as $a_1 = m_w + m_b$ and $a_3 = m_b$, which are same as that of open-loop inertia matrix \mathbf{M} . Simulation results for these different cases are shown when the system is excited by a road profile shown in Figure 3.2.

Table 3.1: Quarter-Car Active Suspension System System Parameters

Parameter	Value
Body mass (m_b)	2.45 kg
Suspension stiffness (k_s)	980 N/m
Inherent suspension damping constant (b_s)	7.5 N.s/m
Tire mass (m_w)	1 kg
Tire stiffness (k_t)	2500 N/m
Inherent tire damping constant (b_t)	5 N.s/m
Suspension travel range q_{2max}	3.8×10^{-2} m
Maximum disturbance $x_{r_{p-p}}$	3×10^{-2} m

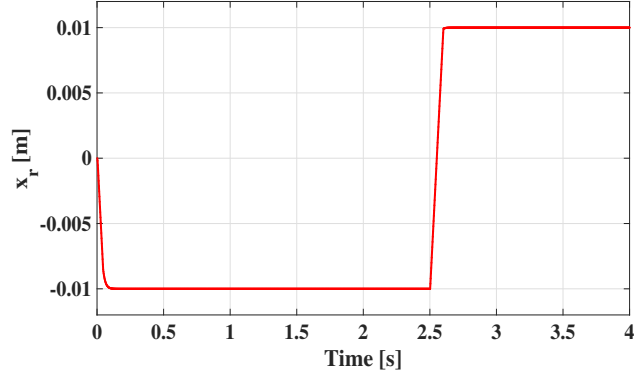


Figure 3.2: Road profile for simulation analysis

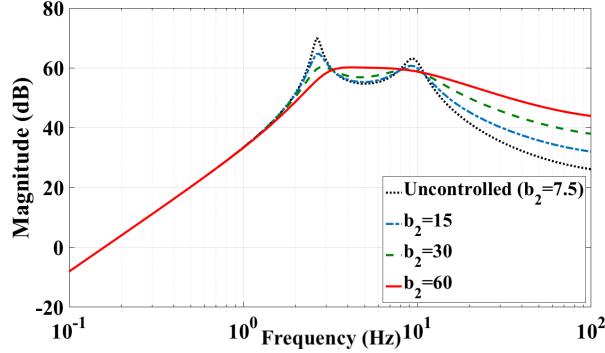


Figure 3.3: Frequency response of $\ddot{x}_b(s)/x_r(s)$ with varying b_2

3.3.1 Controller 1: Active Damping Injection (ADI)

In this case, the kinetic and potential energy functions are chosen to be same as that of the open-loop system, and only closed-loop damping is varied using free parameter b_2 . This is obtained by choosing $\mathbf{M}_d = \mathbf{M}$ and $k_z = k_s$. By choosing k_z equal to k_s , the resulting stiffness matrix becomes $\mathbf{K}_d = \mathbf{K}$. The closed-loop desired damping matrix \mathbf{D}_d takes the form,

$$\mathbf{D}_d = \begin{bmatrix} b_t & 0 \\ 0 & b_2 \end{bmatrix} \quad (3.34)$$

Comparing the open-loop damping matrix \mathbf{D} (3.6) with the closed-loop damping matrix \mathbf{D}_d (3.34), it can be seen that the free variable b_2 represents the closed-loop suspension damping coefficient. The actuator acts like an additional damper connected between x_b and x_w with the damping coefficient $(b_2 - b_s)$. By varying the

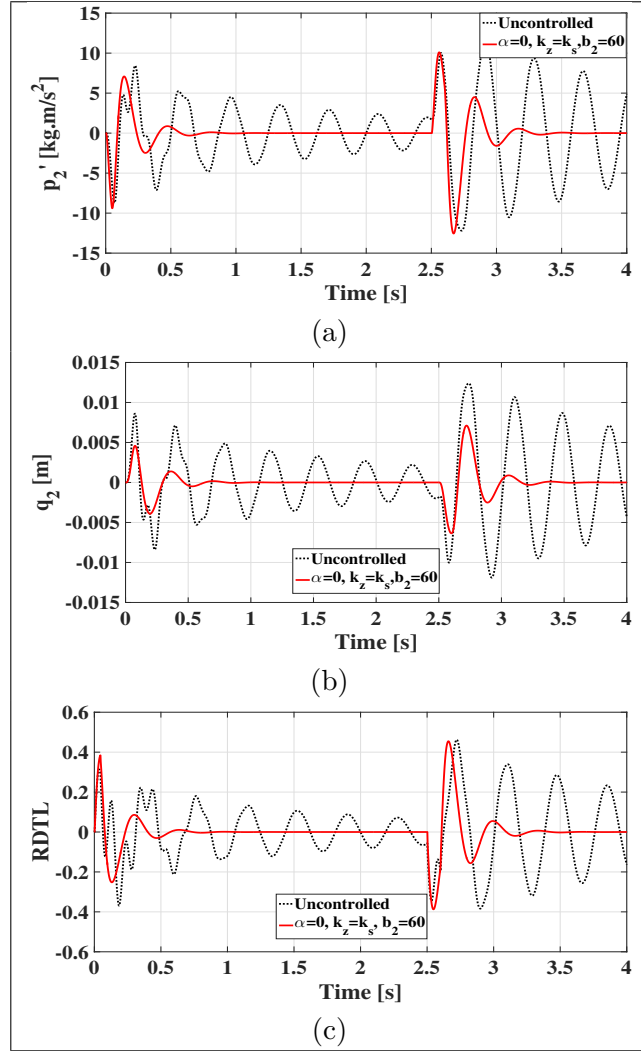


Figure 3.4: Time responses of ADI Controller design: (a) Sprung mass force, (b) Suspension deflection, (c) RDTL

value of b_2 , power dissipation in the system can be controlled. For higher value of b_2 , the power dissipation increases and the system settles faster, but the suspension becomes hard as the controller tries to minimise the suspension deflection q_2 , and the propagation of vibrations from the road to the passenger increases thus reducing the ride comfort. In contrast, choosing very low value of b_2 would make the suspension softer and improve the ride comfort. But this makes the suspension deflection very high. Frequency response of the body acceleration for different values of b_2 is shown in figure 3.3. The frequency response of the body acceleration \ddot{x}_b for different values of b_2 is shown in figure 3.3. Increasing the value of b_2 reduces the gain at the resonant

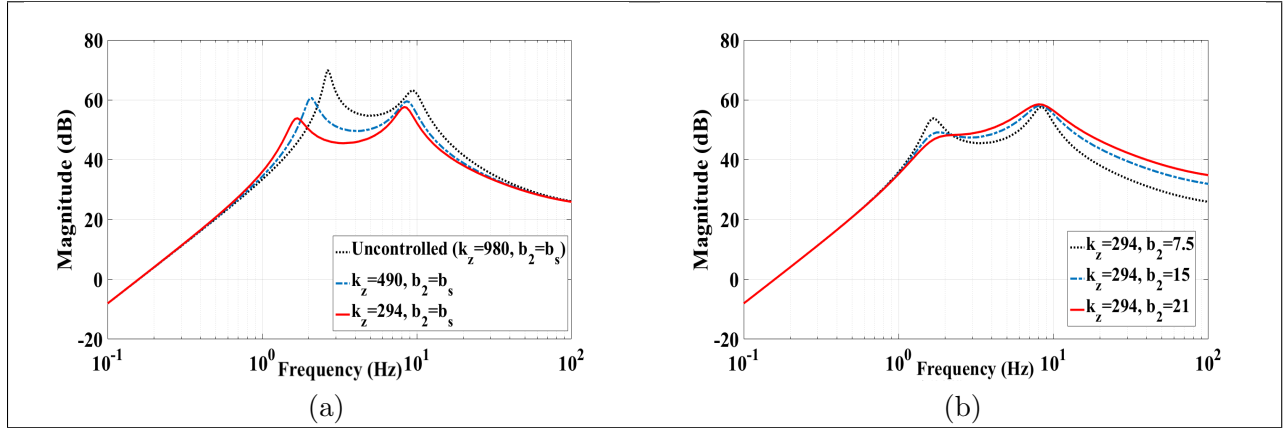


Figure 3.5: Frequency response of $\ddot{x}_b(s)/x_r(s)$ for PESADI

peaks, but increases the gain at higher frequencies. Therefore, with Active damping injection, improvement in the ride comfort is limited. For very high values of b_2 , the performance of the system degrades compared to the uncontrolled system. Time responses of the sprung mass force \dot{p}_2 , suspension deflection q_2 and $RDTL$ are shown in figure 3.4 for $b_2 = 60$. The response of the closed-loop system shows considerable reduction in peak value of suspension deflection when compared to the uncontrolled system, whereas there is no improvement in peak values of sprung mass force \dot{p}_2 and $RDTL$.

3.3.2 Controller 2: Potential Energy Shaping And Damping Injection (PESADI)

In this case, the closed-loop system is controlled by shaping the desired potential energy function via free parameter k_z in the closed-loop stiffness matrix \mathbf{K}_d and power dissipation is shaped using free parameter b_2 in the closed-loop damping matrix \mathbf{D}_d . Desired inertia matrix is chosen as $\mathbf{M}_d = \mathbf{M}$. The resulting closed-loop stiffness matrix is given by,

$$\mathbf{K}_d = \begin{bmatrix} k_t & 0 \\ 0 & k_z \end{bmatrix} \quad (3.35)$$

Comparing open-loop and closed-loop stiffness matrices (3.3) and (3.35), the term k_z represents the closed-loop suspension stiffness of the system. The closed-loop desired

damping matrix \mathbf{D}_d takes the form

$$\mathbf{D}_d = \begin{bmatrix} b_t & 0 \\ 0 & b_2 \end{bmatrix} \quad (3.36)$$

where b_2 is a free variable which represents closed-loop suspension damping coefficient.

The frequency response of the body acceleration for variation in k_z and b_2 is shown in figure 3.5. Lower values of k_z shift the resonant frequencies to lower frequencies and reduces the gain as seen in figure 3.5(a). To isolate the sprung mass from road disturbances, lower values of k_z must be chosen, which improves the ride comfort, as seen in the time response of the sprung mass force \dot{p}_2 in figure 3.6(a). However, reducing the suspension stiffness increases the suspension stroke, which is controlled by increasing b_2 . Figure 3.6(b) illustrates the time response of suspension stroke with PESADI. In this control scenario, a good improvement can be seen in the RDTL of the system in figure 3.6(c). However, improvement in the dynamic tire load cannot be directly achieved using this case, and the improvement is an indirect consequence. PESADI controller behaves like a PD controller with suspension deflection as the feedback, proportional gain $(k_s - k_z)$, and derivative gain $(b_s - b_2)$.

3.3.3 Controller 3: Energy shaping and damping injection with coupled stiffness (ESDICS)

This is a general case where closed-loop kinetic energy function $\tau_d(\mathbf{p})$ using the desired inertia matrix \mathbf{M}_d . The variable a_2 can be written as a function of α as

$$a_2 = \frac{(m_w + m_b)m_b(1 - \alpha)}{m_w + m_b(1 - \alpha)} \quad (3.37)$$

The closed-loop stiffness matrix in this case is given by,

$$\mathbf{K}_d = \begin{bmatrix} k_t \frac{m_w + m_b(1 - \alpha)}{(m_w + m_b)} + \alpha^2 k_z & \alpha k_z \\ \alpha k_z & k_z \end{bmatrix} \quad (3.38)$$

From matrix \mathbf{K}_d in (3.38), it can be seen that a coupling is created between the spring elements due to kinetic energy shaping, which is a function of α . The desired

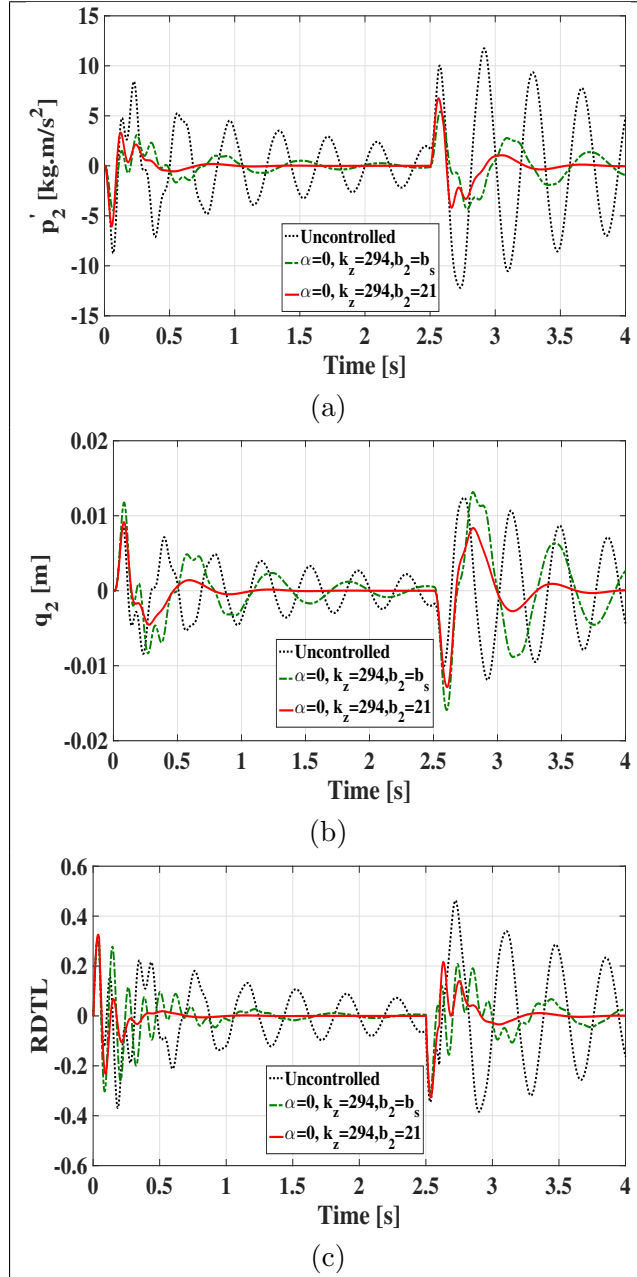


Figure 3.6: Time responses of PESADI Controller design: (a) Sprung mass force,(b) Suspension deflection, (c) RDTL

damping matrix is given by,

$$\mathbf{D}_d = \begin{bmatrix} b_t \frac{(m_w + m_b)}{m_w + m_b(1-\alpha)} & 0 \\ 0 & b_2 \end{bmatrix} \quad (3.39)$$

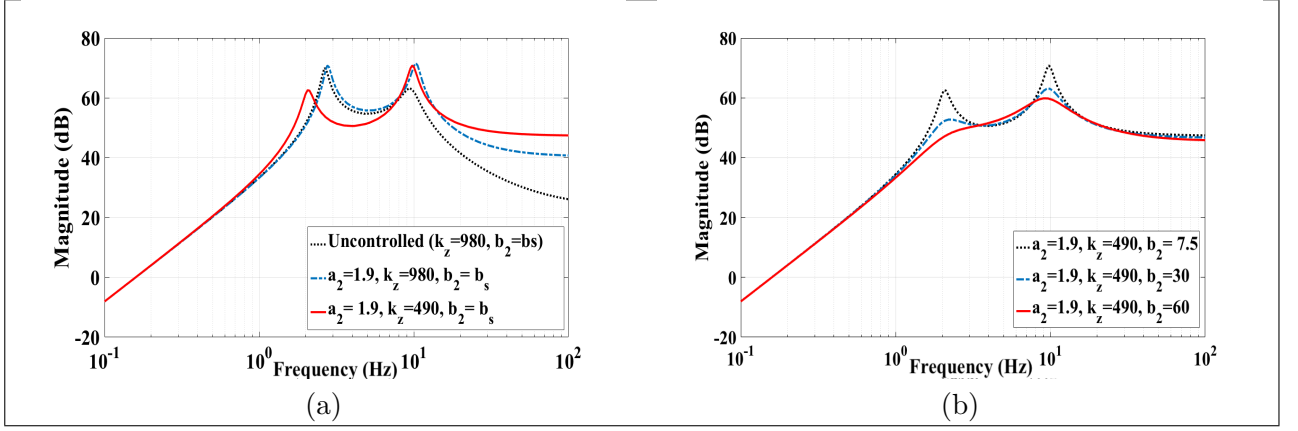


Figure 3.7: Frequency response of $\ddot{x}_b(s)/x_r(s)$ for ESDICS

From the closed-loop damping matrix \mathbf{D}_d in (3.39), it can be observed that the effective tire stiffness is increased when α is varied from zero to one. Figure 3.7 illustrates the frequency responses of the closed-loop system with $\alpha = 0.5$ for varying k_z and b_2 . This case modifies the overall structure of the system and requires a full-state feedback law to be implemented. The time responses of the ESDICS controller for square wave input are shown in figure 3.8.

3.3.4 Controller 4: Energy shaping and damping injection with inertial decoupling (ESDIID)

Inertial decoupling corresponds to a case where $\alpha = 1$, resulting in a diagonal inertial matrix \mathbf{M}_d given by,

$$\mathbf{M}_d = \begin{bmatrix} m_w + m_b & 0 \\ 0 & m_b \end{bmatrix} \quad (3.40)$$

The matrix \mathbf{K}_d is given by

$$\mathbf{K}_d = \begin{bmatrix} k_t \frac{m_w}{m_w + m_b} + k_z & k_z \\ k_z & k_z \end{bmatrix} \quad (3.41)$$

The free variable k_z represents the suspension stiffness in the closed-loop system. The damping matrix \mathbf{D}_d

$$\mathbf{D}_d = \begin{bmatrix} b_t \frac{m_w + m_b}{m_w} & 0 \\ 0 & b_2 \end{bmatrix} \quad (3.42)$$

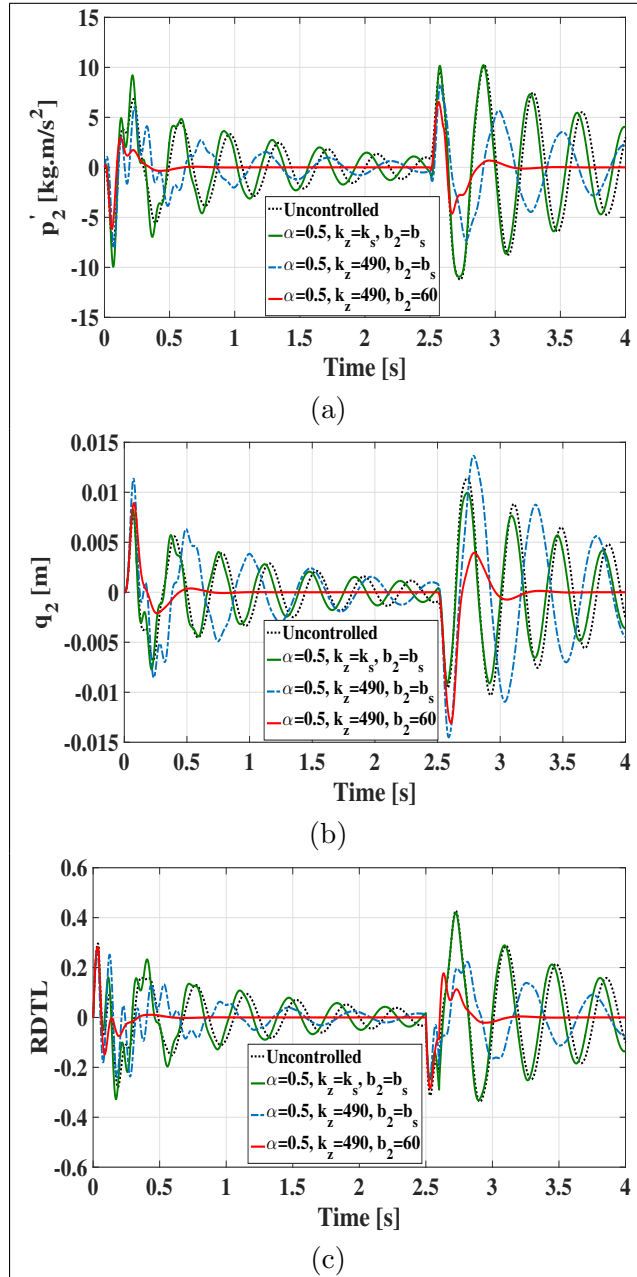


Figure 3.8: Time responses of ESDICS Controller design: (a) Sprung mass force,(b) Suspension deflection, (c) RDTL

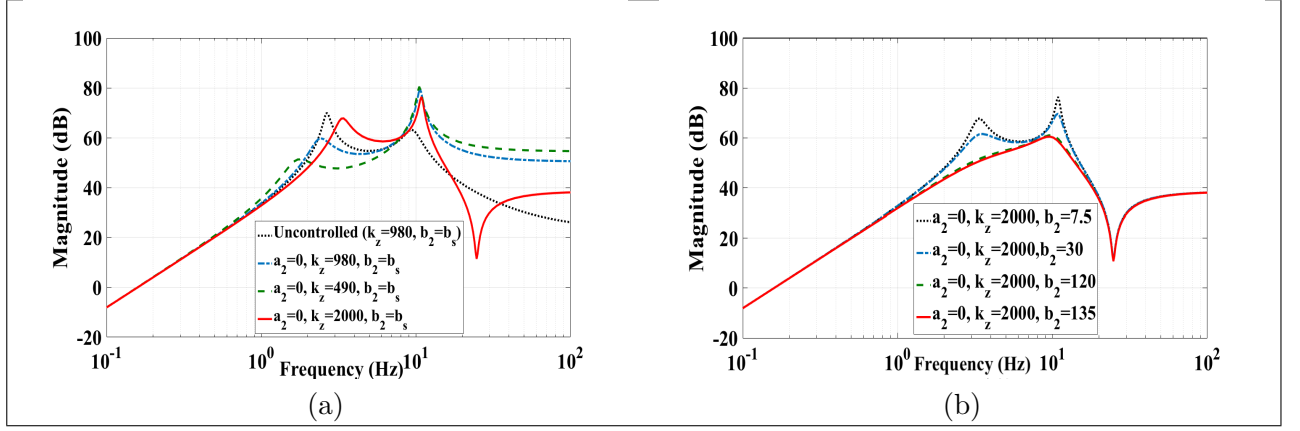


Figure 3.9: Frequency response of $\ddot{x}_b(s)/x_r(s)$ for ESDIID

Table 3.2: Values of control variables for different cases of IDA-PBC

Controller	a_1	a_2	a_3	α	b_1	b_2	k_z
Uncontrolled (equivalent)	3.45	2.45	2.45	0	5	7.5	980
ADI	3.45	2.45	2.45	0	5	60	980
PESADI	3.45	2.45	2.45	0	5	21	294
ESDICS	3.45	1.9	2.45	0.5	7.75	60	490
ESDIID	3.45	0	2.45	1	17.25	135	2000

The values of k_z and b_2 must be chosen very high to make the suspension harder to isolate the road disturbance from the body. The frequency responses of the system with varying k_z and b_2 for ($\alpha = 1$) are shown in figure 3.9. From the frequency response, it can be seen that gain at both the resonant frequencies is reduced considerably, and ride comfort is improved over a wide range of frequencies.

From the time responses of ESDIID controller with $k_z = k_s$ and $b_2 = b_s$, considerable improvement in the RDTL is observed in this case due to increased effective tire stiffness and damping (see figure 3.10). This choice of kinetic energy shaping directly effects the road holding ability of the system. This also improves the ride comfort by isolating the sprung mass from the road disturbance and restricting the disturbance at the tire itself. To improve the suspension deflection and settling time, k_z and b_2 are tuned accordingly.

Table 3.2 lists various control parameters chosen for different cases discussed. The results of the proposed controller are compared with that of Linear Quadratic Regulator.

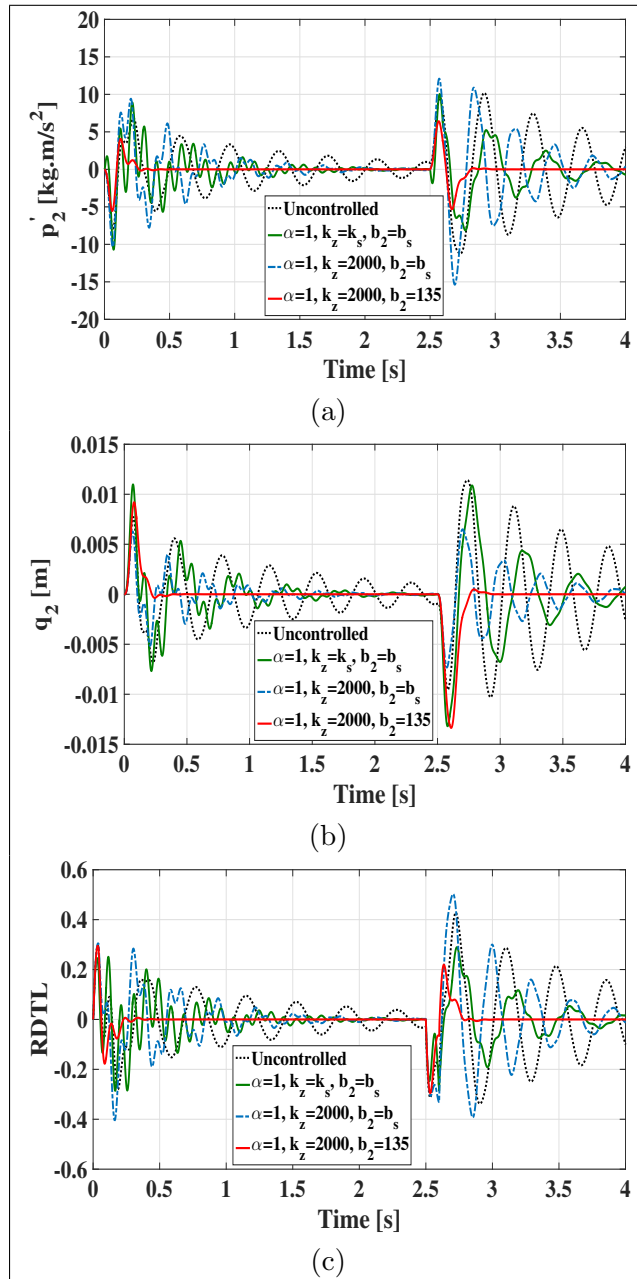


Figure 3.10: Time responses of ESDIID Controller design: (a) Sprung mass force,(b) Suspension deflection, (c) RDTRL

3.3.5 Linear Quadratic Regulator (LQR)

The state space model of the system can be written as

$$\dot{\mathbf{x}}_t = \mathbf{A}\mathbf{x}_t + \mathbf{B}u + \mathbf{w}f \quad (3.43)$$

where

$$\mathbf{x}_t = \begin{bmatrix} \dot{x}_w \\ \dot{x}_b \\ q_1 \\ q_2 \end{bmatrix} \quad \mathbf{B} = \begin{bmatrix} -\frac{1}{m_w} \\ \frac{1}{m_b} \\ 0 \\ 0 \end{bmatrix} \quad \mathbf{w} = \begin{bmatrix} \frac{b_t}{m_w} \\ 0 \\ -1 \\ 0 \end{bmatrix}$$

$$\mathbf{A} = \begin{bmatrix} -\frac{b_t + b_s}{m_w} & \frac{b_s}{m_w} & -\frac{k_t}{m_w} & \frac{k_s}{m_w} \\ \frac{b_s}{m_b} & -\frac{b_s}{m_b} & 0 & -\frac{k_s}{m_b} \\ 1 & 0 & 0 & 0 \\ -1 & 1 & 0 & 0 \end{bmatrix}$$

The matrix \mathbf{B} is related to the control input $u = u_s$, and the matrix \mathbf{w} relates to road disturbance acting on the system $f = \dot{x}_r(t)$.

Linear Quadratic Regulator (LQR) is an optimization method used to find the state feedback controller gains. The main idea of the LQR is that it calculates the optimum gains by minimizing the quadratic cost function J given below.

$$J = \int_0^{\infty} \mathbf{x}_t^T \mathbf{Q}_c \mathbf{x}_t + \mathbf{u}^T \mathbf{R} \mathbf{u} \quad (3.44)$$

where $\mathbf{Q}_c = \mathbf{Q}_c^T \in \mathbb{R}^{n \times n}$ is a positive semi-definite matrix, which is a cost structure that determines the importance of the states and $\mathbf{R} = \mathbf{R}^T \in \mathbb{R}^{m \times m}$ weighing gain for the control input \mathbf{u} . The cost function J minimises the suspension deflection q_2 , tire deflection q_1 , tire velocity \dot{x}_w and body velocity \dot{x}_b which are the system states through the weighing matrix \mathbf{Q}_c . The control input u_s is penalised through R . The weighing matrix \mathbf{Q}_c is given by

$$\mathbf{Q}_c = \begin{bmatrix} c_1 & 0 & 0 & 0 \\ 0 & c_2 & 0 & 0 \\ 0 & 0 & c_3 & 0 \\ 0 & 0 & 0 & c_4 \end{bmatrix} \quad (3.45)$$

The gains are chosen as $c_1 = 0.01$, $c_2 = 30$, $c_3 = 5$, $c_4 = 450$ and $R = 0.01$ (Alves et al., 2014). The state feedback equation for LQR is given by

$$u_s = -\mathbf{K}_g \mathbf{x}_t \quad (3.46)$$

where $\mathbf{K}_g = [k_1 \ k_2 \ k_3 \ k_4]$, and the corresponding feedback gains are given in Table 3.3.

Table 3.3: Controller gains

Control law	k1	k2	k3	k4
LQR	3.85	48.71	3.79	22.70
ADI	-52.50	52.50	0	0
PESADI	-13.50	13.50	0	-686
ESDICS	-16.04	39.55	-574.88	-355.16
ESDIID	7.50	127.50	224.64	1020

The performance of different cases of controllers arising from the choice of various control parameters in IDA-PBC control law are presented in terms of their peak and

Table 3.4: Performance comparison of simulation results

Type of suspension	Acceleration in m/s^2		Suspension deflection in m	RDTL	
	peak	rms		peak	rms
Uncontrolled	5.3728	2.1531	0.0139	0.4541	0.1462
LQR	2.4542	0.4761	0.0134	0.2894	0.0470
ADI	4.5187	0.9235	0.0071	0.4324	0.0895
PESADI	2.4023	0.4697	0.0125	0.3082	0.0508
ESDICS	2.4233	0.4657	0.0128	0.2838	0.0459
ESDIID	2.3856	0.4381	0.01297	0.2953	0.0471

RMS values is tabulated in Table 3.4. Validity of the proposed controllers is tested experimentally on a bench-scale model for three different road profiles, and the results are presented in the next section.

3.4 Experimental Validation

3.4.1 Hardware Description

The proposed IDA-PBC control is tested on a bench-scale model of quarter-car active suspension system from Quanser. The model consists of a quarter-car test rig, data acquisition and output modules, and a power amplifier. This quarter-car test rig comprises of three plates which can move independently in the vertical direction. The bottom plate represents the road and can be moved using a servomotor, which generates different road profiles for the system. The middle plate represents the unsprung mass m_w of the vehicle and linked to the bottom plate through a linear spring k_t representing tire stiffness. The friction between the bearing connected provides inherent damping, which is considered as tire damping b_t . The top plate m_b represents the vehicle body, which is connected to the middle plate through spring with suspension stiffness k_s and a linear motor through a capstan which acts as an actuator. The inherent damping due to bearing of the sprung mass represents suspension damping b_s . The bottom plate displacement $x_r(t)$, suspension deflection $(x_b - x_w)$ and top plate displacement x_b are measured using three optical encoders. Acceleration of the vehicle body is measured using a dual-axis accelerometer mounted underneath the top plate. The data acquisition board consists of Quanser¹ Q1-cRIO NI-9024, which acquires the data from the optical encodes and accelerometer through Q1-cRIO data acquisition module and sends it to the computer. Quanser rapid control prototyping toolkit using LabVIEW² software was used for implementing the control algorithm. The control output and road input signals obtained from the computer through CRIO are amplified by a power amplifier fed and to the actuator and road simulation Brushed servomotor. The experimental setup is shown in Figure 3.11 and the Implementation scheme of hardware setup is shown in Figure 3.12.

¹Quanser Consulting Inc, 119 Spy Court, Markham, ON L3R 5H6 Canada

²LabVIEW, National Instruments, 11500 N Mopac Expwy, Austin, USA.

3.4.2 Experimental Results

To verify the effectiveness of the designed controller, experiments have been performed on the quarter-car test rig and three road profiles shown in Figure 3.13 have been considered for trials.

3.4.2.1 Case 1: Square Wave Input

A square wave of frequency 0.2 Hz and a peak value of 0.01 m shown in Figure 3.13(a) is applied as the road profile, and the responses of the system are shown in Figures 3.14(a) and 3.14(b). The performance indices of the controllers in terms of peak and RMS values are tabulated in Table 3.5. In case of ADI, peak and RMS values of body acceleration are almost the same as those of the uncontrolled system. However, ADI gives the best performance in terms of minimising the suspension deflection. PESADI improves ride comfort, but increases the suspension deflection of the system. ESDICS delivers better performance in terms of control objectives, that is reducing the body acceleration, suspension deflection, and tire deflection when compared with ADI and ESDI. ESDICS is tuned in such a way that it has a comparable control effort to that of LQR. It can be observed that in case of ESDIID, the body acceleration is reduced and there is a considerable improvement in minimising the suspension deflection as well as RMS value of dynamic tire load.

From the time responses for step input, it can be observed that the settling time of the system reduces as α is varied from zero (ADI) to one (ESDIID). The body acceleration

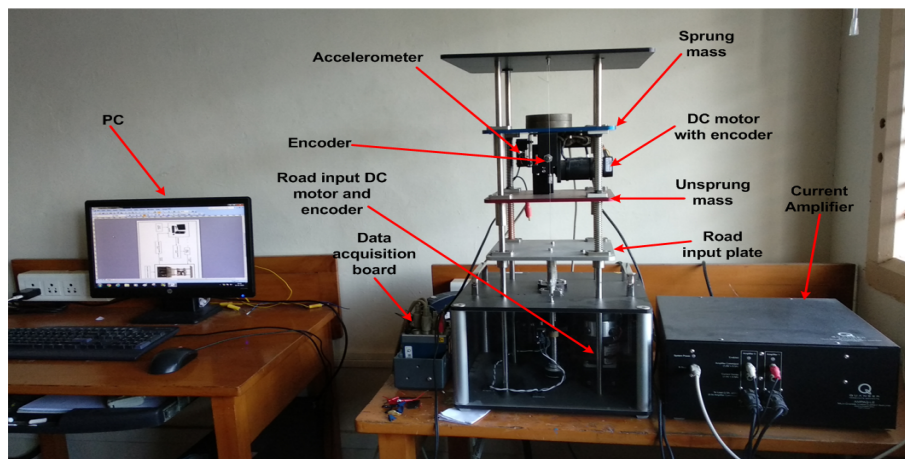


Figure 3.11: Experimental setup

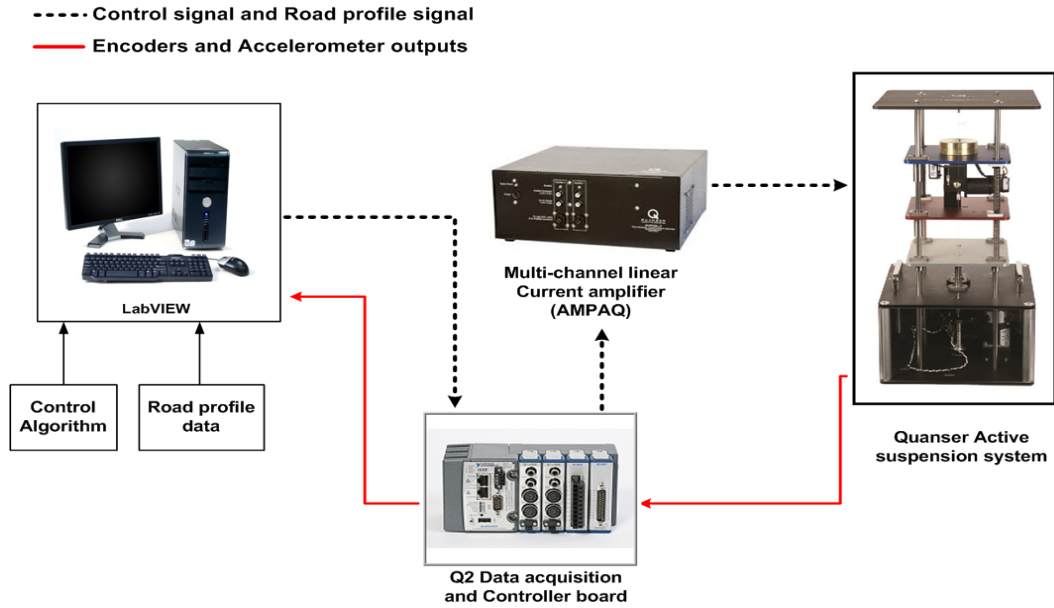


Figure 3.12: Implementation scheme of hardware setup.

reduces and the vibrations die out faster as α is increased from zero to one, which can be observed from Figures 3.14(a) and 3.14(b). The peak value of suspension deflection is minimum in ADI compared with all the cases, and with the increase in α , it can be seen that the peak value is increased at the instant of occurrence of disturbance but settles faster, as seen in 3.14(c) and 3.14(d). Dynamic tire load is higher and more oscillatory with two overshoots in ADI, implying poor road holding capacity of the vehicle, which can be observed from Figure 3.14(e), whereas in ESDICS, the peak value of tire deflection is less and settles faster than other cases, which shows that the road holding capacity improves as α is increased. The time responses of tire deflection for PESADI, ESDICS, and ESDIID can be seen in Figure 3.14(f).

From Figures 3.15(a) and 3.15(b), it can be easily observed that as we go from $\alpha = 0$ (ADI) to $\alpha = 1$ (ESDIID), the overshoot in the body deflection is clearly reduced, and in case of ESDIID, x_b follows the road disturbance input $x_r(t)$. This clearly shows that the increase in α attenuates the disturbance near the tire itself.

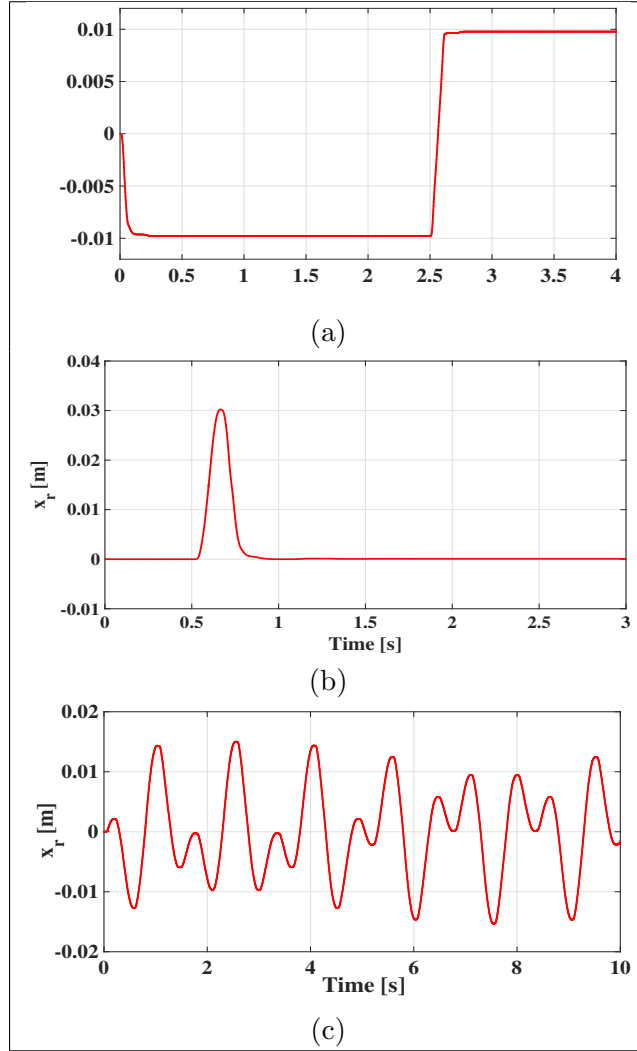


Figure 3.13: Road profiles: (a) Square wave ,(b) Bump and (c) Random disturbance

3.4.2.2 Case 2: Bump Input

The road profile is given by

$$x_r(t) = \begin{cases} 0.015(1 - \cos 8\pi t); & 0.5 \leq t < 0.75 \\ 0 & \text{else} \end{cases} \quad (3.47)$$

This profile mimics a realistic case of transient bump disturbance which can occur on the road. This profile is taken similar to that of a profile used in (Li et al., 2019) and (Alves et al., 2014). A peak value of $0.03m$, which is the maximum value of disturbance $x_r(t)$ considered for the design of the controller, is considered as the input

to test the performance of the controller. Figures 3.16 and 3.17 shows acceleration, body displacement, suspension deflection, tire deflection, and actuator force plots for the uncontrolled system, with LQR and IDA-PBC. The comparison of peak and RMS values of \ddot{x}_b , $(x_b - x_w)$, and u_s for all the controllers is given in Table 3.6. From Figure 3.16(c) and (d), the suspension deflection is the least with ADI, but the improvement in ride comfort is minimal compared with other cases, which is evident from the peak and RMS values of \ddot{x}_b . Peak and RMS values of \ddot{x}_b for PESADI are comparable to those of LQR, but the suspension deflection in PESADI is the highest compared with all the cases. Suspension deflection and RMS values of \ddot{x}_b of ESDICS are comparable to those of LQR. ESDIID gives the best performance in terms of minimising the sprung mass acceleration \ddot{x}_b as well as reducing the suspension deflection, and a good improvement in road holding compared to uncontrolled system.

Table 3.5: Performance comparison of experimental results for square wave input

Type of suspension	Acceleration (m/s^2)		Suspension deflection(m)	Control effort (N)		RDTL	
	peak	rms		peak	rms	peak	rms
Uncontrolled	3.2824	0.8332	0.0107	-	-	0.4028	0.1083
LQR	1.9435	0.4041	0.0139	8.2545	1.3781	0.3790	0.0837
ADI	3.6147	0.7289	0.0070	9.1510	1.4934	0.4197	0.1001
PESADI	2.5578	0.4068	0.0133	9.6791	1.4854	0.3802	0.0767
ESDICS	1.9067	0.3815	0.0139	9.9886	1.7011	0.3420	0.0780
ESDIID	2.4895	0.4136	0.0123	14.2624	1.9344	0.4043	0.0811

Table 3.6: Performance comparison of experimental results for bump input

Type of suspension	Acceleration (m/s^2)		Suspension deflection(m)	Control effort (N)		RDTL	
	peak	rms		peak	rms	peak	rms
Uncontrolled	10.6249	1.6834	0.0263	-	-	0.7450	0.2684
LQR	3.9336	0.6889	0.0247	14.8346	1.9338	0.6402	0.1502
ADI	7.4752	1.2193	0.0197	19.5971	2.4600	1.1006	0.2221
PESADI	3.3368	0.5862	0.0309	21.8412	2.4698	0.5226	0.1208
ESDICS	6.6551	0.6715	0.0252	18.1963	2.0355	0.6429	0.1139
ESDIID	3.3176	0.6587	0.0198	23.5119	2.4374	0.6598	0.1292

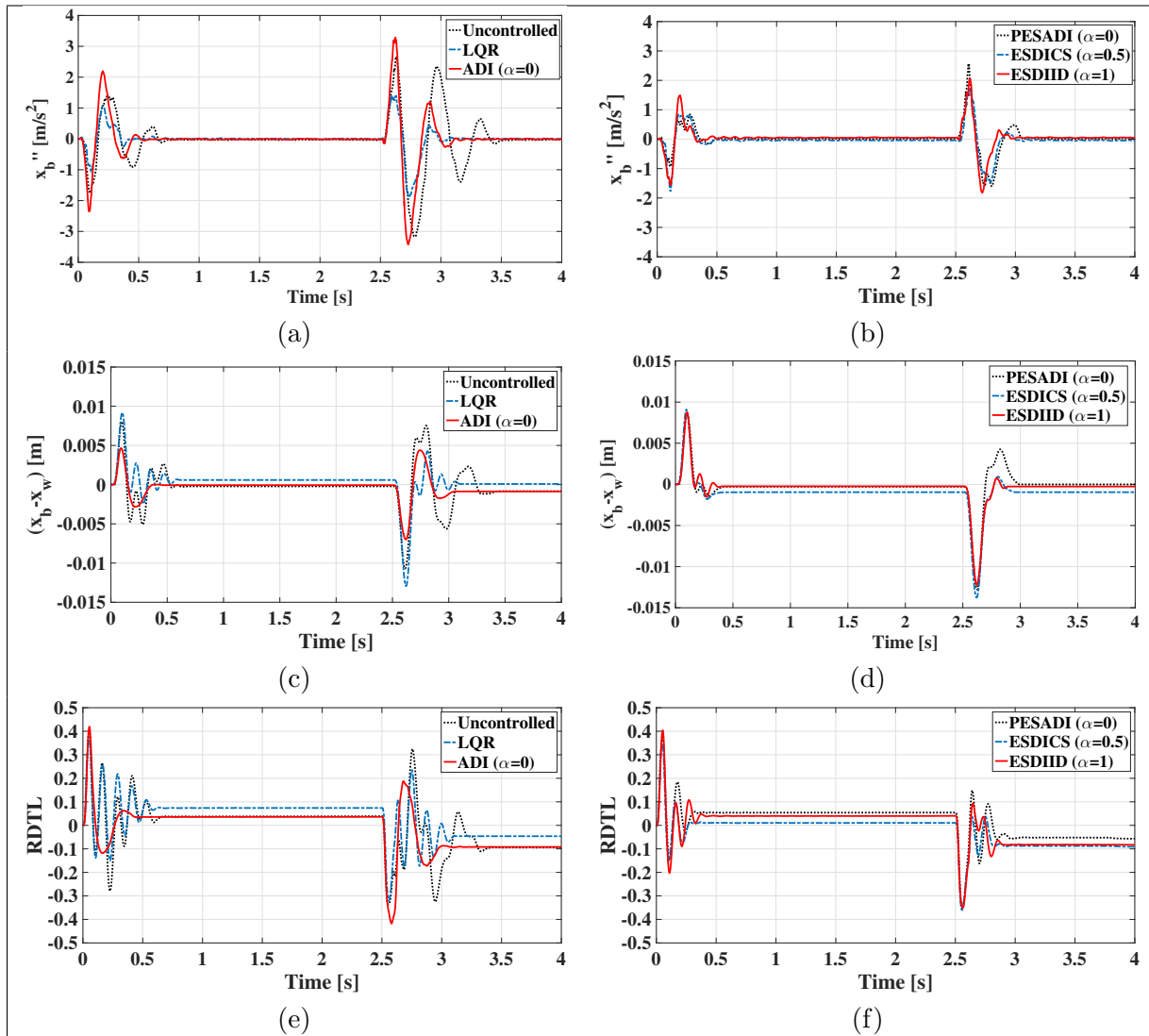


Figure 3.14: Experimental results for square wave input: (a, b) Body acceleration, (c, d) Suspension deflection, (e, f) Relative Dynamic Tire Load

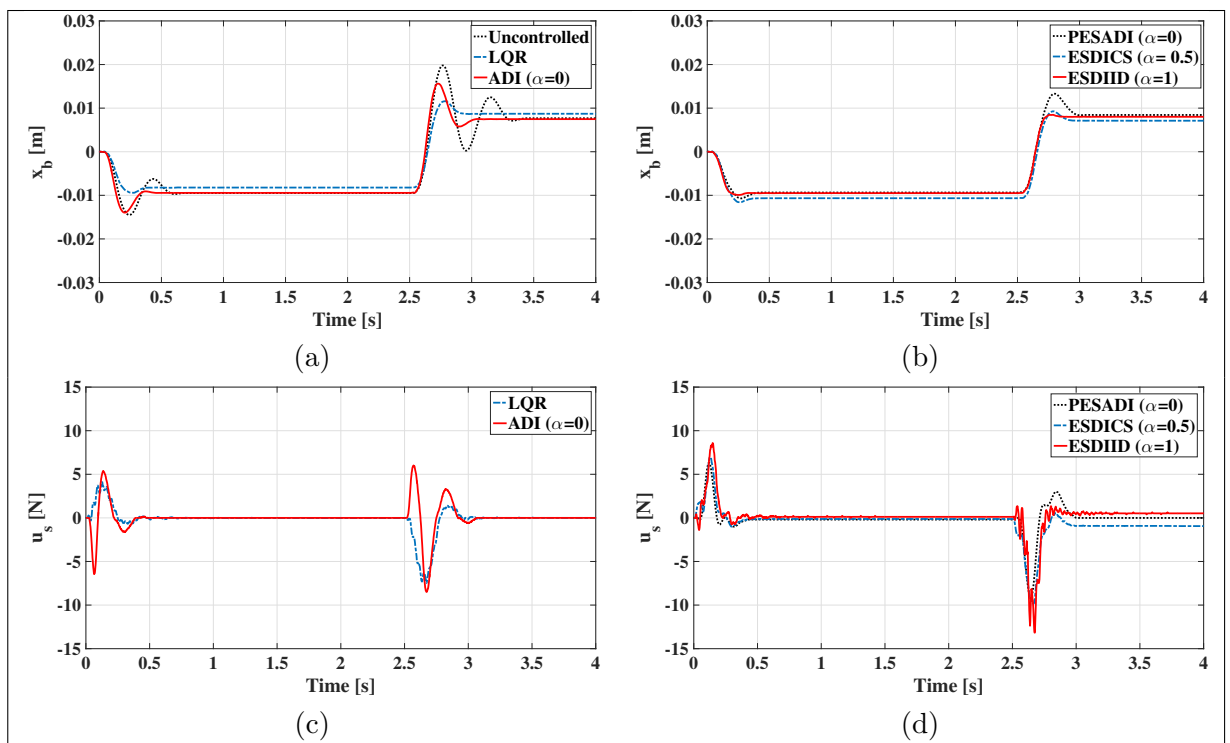


Figure 3.15: Experimental results for square wave input: (a, b) body displacement and (c, d) actuator force

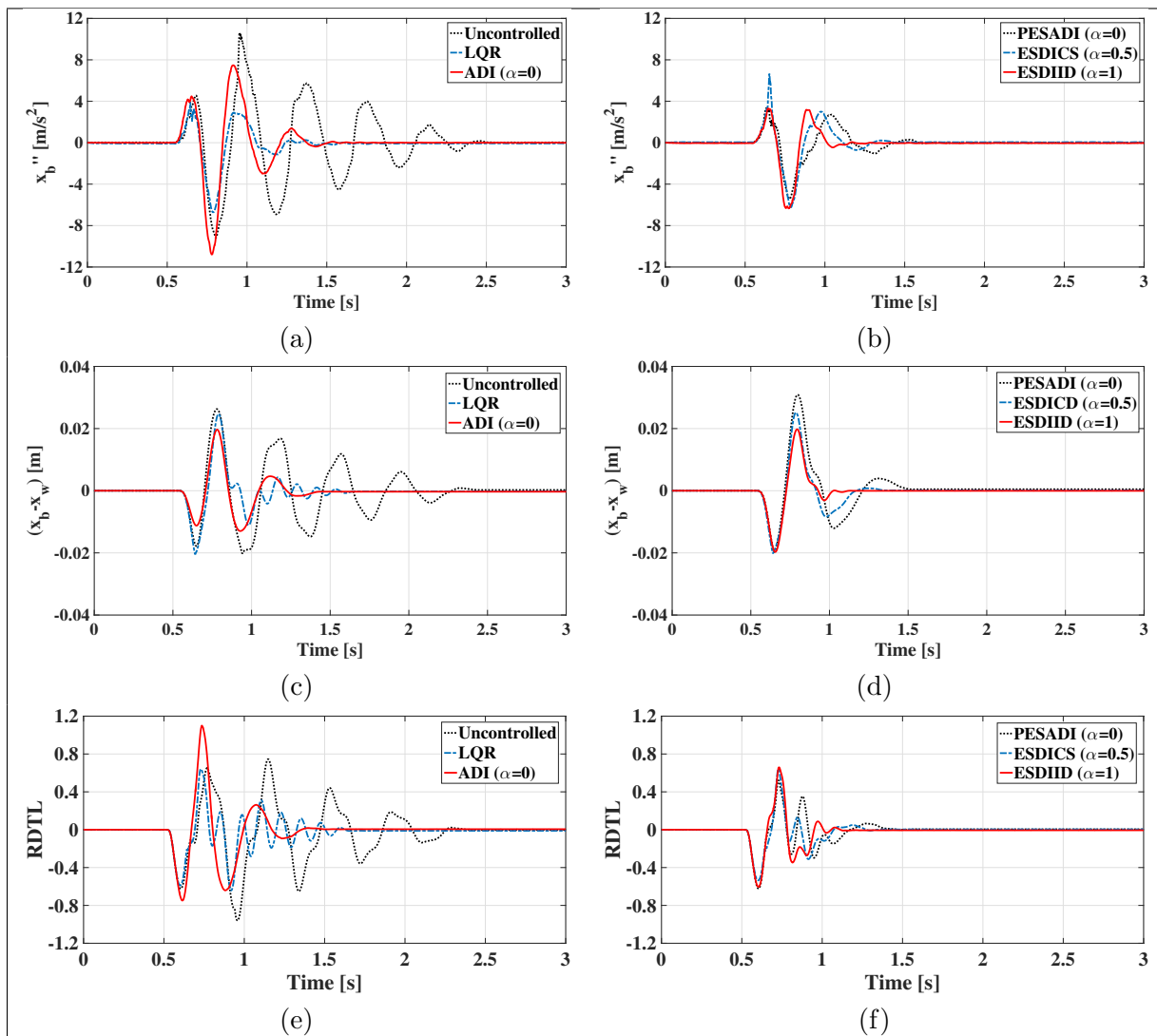


Figure 3.16: Experimental results for bump input: (a, b) Body acceleration, (c, d) Suspension deflection, (e, f) Relative Dynamic Tire Load

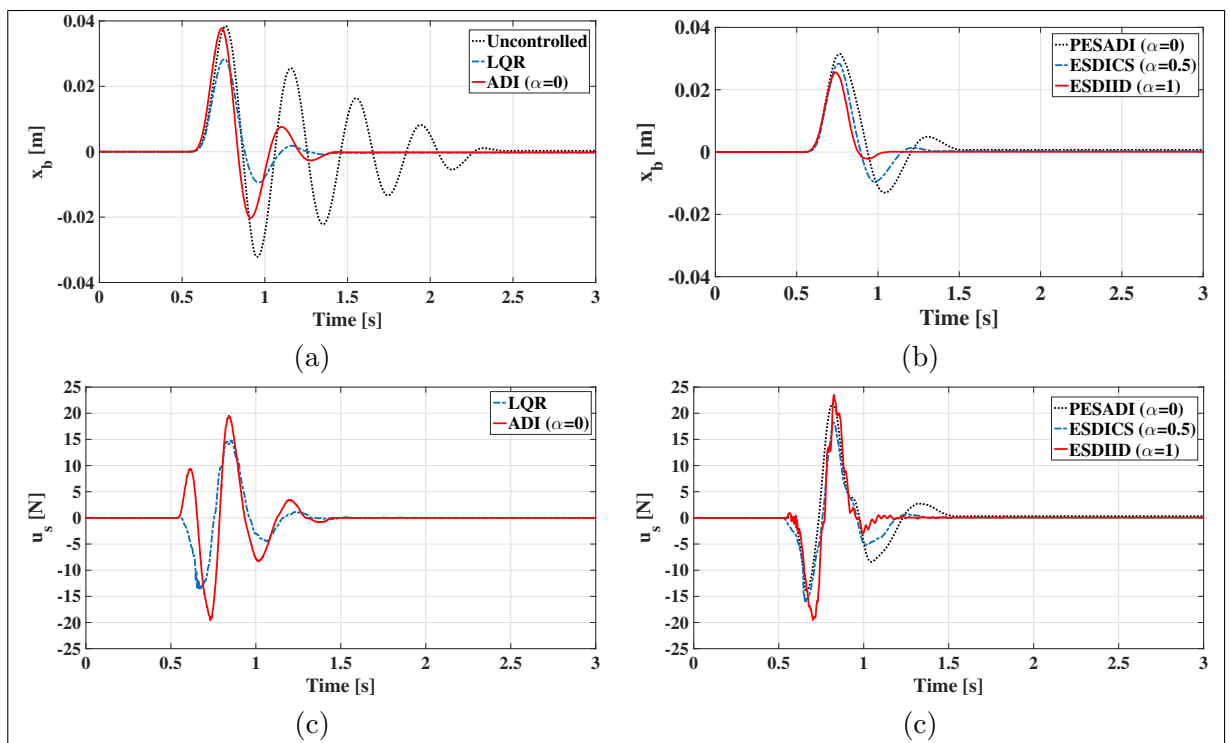


Figure 3.17: Experimental results for bump input: (a, b) body displacement and (c, d) actuator force

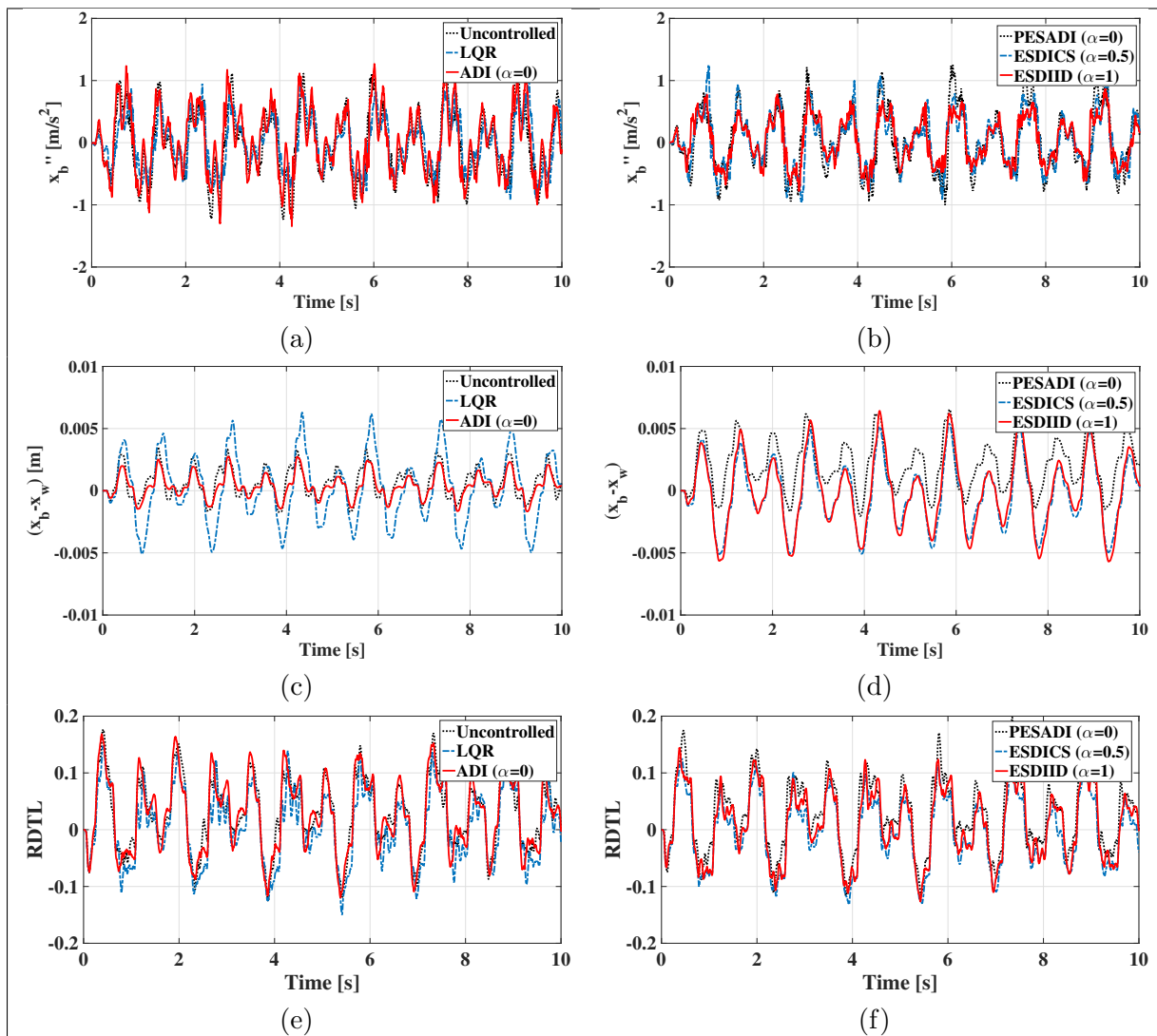


Figure 3.18: Experimental results for Continuously varying input: (a, b) Body acceleration, (c, d) Suspension deflection, (e, f) Relative Dynamic Tire Load

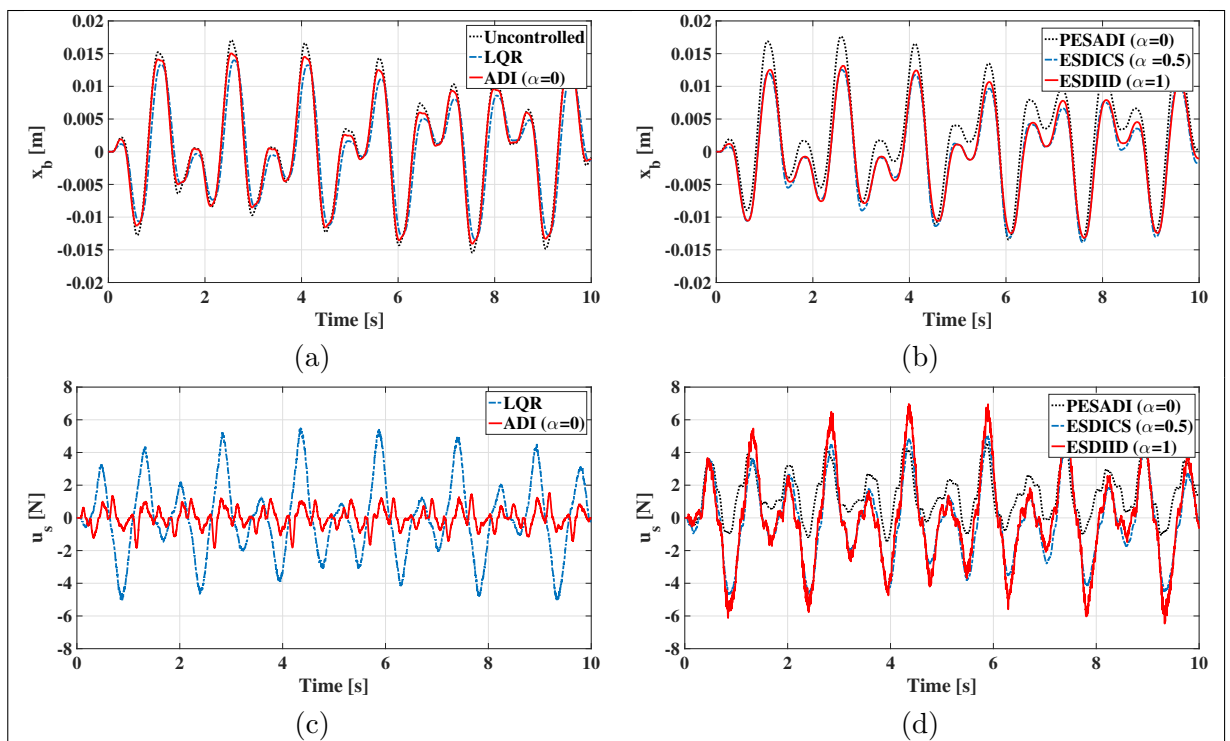


Figure 3.19: Experimental results for Continuously varying input: (a, b) body displacement and (c, d) actuator force

3.4.2.3 Case 3: Continuously Varying Input

The road profile is given by Gupta et al. (2016).

$$x_r(t) = 0.015 \cos(2\pi t) \sin(0.6\pi t) \quad (3.48)$$

This profile represents a rough and continuously varying road disturbance with a peak value of $0.015m$. Responses of the system for the disturbance are shown in Figures 3.18 and 3.19. The performance indices for the same are listed in Table 3.7. Comparing the peak and RMS values of \ddot{x}_b , ESDIID gives the best performance in terms of reduction in acceleration, thus improving the ride comfort and minimising the suspension deflection. Similar to case 1 and case 2, it is observed that the suspension deflection is minimum in ADI compared with all the cases. PESADI improves the ride comfort, that is reduces the acceleration \ddot{x}_b considerably but increases the suspension deflection. From the discussions, it is evident that based on the choice of desired damping, stiffness, and inertia matrices, which effectively shape the dissipation, potential, and kinetic energy profiles of the system respectively, the general control law of IDA-PBC in equation (3.13) assumes a different structure. ADI shapes the dissipative structure of the system and controls the system's damping, and the controller tries to minimise the suspension deflection but does not contribute much in the improvement of ride comfort, that is reduction in \ddot{x}_b . The structure of ADI is similar to that of a derivative controller and can be implemented with suspension deflection as the feedback term. On the other hand, PESADI shapes the potential energy and damping of the system. This improves the ride comfort by reducing the

Table 3.7: Performance comparison of experimental results for continuously varying input

Type of suspension	Acceleration (m/s^2)		Suspension deflection(m)	Control effort (N)		RDTL	
	peak	rms		peak	rms	peak	rms
Uncontrolled	1.5181	0.5314	0.0035	-	-	0.1759	0.0690
LQR	1.0549	0.4273	0.0063	5.4896	2.3317	0.1479	0.0633
ADI	1.2692	0.5277	0.0027	1.8435	0.5984	0.1684	0.0717
PESADI	1.2479	0.4918	0.0065	4.5457	2.0007	0.1982	0.0685
ESDICS	1.3937	0.4342	0.0054	5.0013	3.3462	0.1287	0.0602
ESDIID	0.8887	0.3682	0.0064	6.9692	2.7421	0.1442	0.0628

body acceleration \ddot{x}_b but increases the suspension deflection due to soft closed-loop stiffness characteristics. PESADI is a PD controller with suspension stiffness as the state feedback term. To reduce the suspension deflection in the PESADI, more control effort is needed. From the practical implementation point of view, ADI and PESADI are easy to implement as they do not require the information of the tire deflection, which is generally not easy to measure. ESDICS and ESDIID are full-state feedback controllers which require all the four states for implementation. From the results, it is apparent that ESDICS and ESDIID give better results in terms of reduction in acceleration, tire deflection, and minimising the suspension deflection. The disadvantage of ESDICS and ESDIID is that they require tire deflection measurement, and vertical velocities of sprung and unsprung masses for feedback to the control law, which increase the complexity in implementation. However, because of their advantages, these can be used for controlling the system, and state estimation methods can be used for their implementation. It can be concluded from the discussion that, to obtain best results in terms of control objectives, that is improving the ride comfort, road holding, and keeping the suspension deflection within the limits for the maximum bounded disturbance, apart from shaping the damping and potential energy profiles, kinetic energy must also be shaped, which can be achieved by modifying the inertia matrix \mathbf{M}_d .

3.5 Summary

In this chapter, interconnection and damping assignment passivity-based control was designed for control of a quarter-car active suspension system. Detailed analysis of the controller is performed by varying the desired damping, stiffness, and inertia matrices \mathbf{D}_d , \mathbf{K}_d , and \mathbf{M}_d respectively. Based on the choice of the structure of these matrices, different control configurations were obtained, and their performance comparison is demonstrated in terms of their time and frequency responses to give better clarity on the choice of variables. The proposed controllers were validated experimentally on a bench-scale model of a quarter-car system with different road profiles. The performance indices of the controller for different conditions ensure that the controller is able to improve the ride comfort and road holding effectively while constraining the suspension deflection within the allowable limits. The study describes ways to tune the different controller parameters based on their physical meaning. Finally, the

study gives a detailed discussion on the relative merits and demerits of the proposed control configurations in terms of control and implementation issues.

Chapter 4

Design and Implementation of Port-Hamiltonian Observer for Active Suspension System

Contents

4.1	Observer Design	68
4.1.1	Choice Of Observer Parameters For Active Suspension Observer Design	70
4.2	Results and Discussion	71
4.3	Summary	74

This chapter presents an observer design for active suspension system modelled in port-Hamiltonian form, which estimates the states of the system directly in port-Hamiltonian form for the purpose of controller implementation. A novel observer is designed using suspension stroke as the only measurable output and implemented for active suspension system to minimise the error dynamics in presence of a bounded disturbance input.

4.1 Observer Design

Port-Hamiltonian model of the active suspension system is defined in section 3.1.1 is given by:

$$\dot{\mathbf{x}} = [\mathbf{J} - \mathbf{R}]\nabla H(\mathbf{x}) + \mathbf{g}u_s + \mathbf{d}f \quad (4.1)$$

with $H(\mathbf{x})$ defined in terms of a positive definite matrix \mathbf{Q} as,

$$H(\mathbf{x}) = \frac{1}{2}\mathbf{x}^T\mathbf{Q}\mathbf{x} \quad (4.2)$$

The measurable output are defined as

$$\mathbf{y} = \mathbf{C}\mathbf{x} \quad (4.3)$$

where $\mathbf{x} \in \mathbb{R}^n$, $\mathbf{y} \in \mathbb{R}^r$ and $\mathbf{C} \in \mathbb{R}^{r \times n}$ is a full rank (row) constant matrix. The following theorem from Yaghmaei and Yazdanpanah (2018) is used for observer design. *Theorem* Yaghmaei and Yazdanpanah (2018): Consider the port-Hamiltonian system (equation (4.1), equation (4.2)) with $f = 0$, the pair $(\mathbf{C}, (\mathbf{J} - \mathbf{R})\mathbf{Q})$ detectable (Observable), and there exist $\mathbf{J}_o = -\mathbf{J}_o^T$, $\mathbf{R}_o = \mathbf{R}_o^T \geq \mathbf{0}$, $\mathbf{Q}_o > \mathbf{0}$ and \mathbf{C}_\perp such that the condition (equation (4.4)) is satisfied:

$$(\mathbf{J}_o - \mathbf{R}_o)\mathbf{Q}_o\mathbf{C}_\perp = (\mathbf{J} - \mathbf{R})\mathbf{Q}\mathbf{C}_\perp \quad (4.4)$$

where \mathbf{C}_\perp is a right annihilator matrix of \mathbf{C} , i.e., $\mathbf{C}\mathbf{C}_\perp = \mathbf{0}$, and $rank(\mathbf{C}_\perp) = (n - r)$. Then the observer dynamics are given by

$$\dot{\hat{\mathbf{x}}} = (\mathbf{J}_o - \mathbf{R}_o)\mathbf{Q}_o(\hat{\mathbf{x}} - \mathbf{C}^\perp\mathbf{y}) + (\mathbf{J} - \mathbf{R})\mathbf{Q}\mathbf{C}^\perp\mathbf{y} + \mathbf{g}u_s \quad (4.5)$$

where \mathbf{C}^\perp is defined as Yaghmaei and Yazdanpanah (2018),

$$\mathbf{C}^\perp = \mathbf{C}^T(\mathbf{C}\mathbf{C}^T)^{-1} \quad (4.6)$$

Proof: To prove this theorem, *Lemma 10* is used from Yaghmaei and Yazdanpanah (2018) which states that any asymptotically stable linear system $\dot{\mathbf{x}} = \mathbf{A}\mathbf{x} + \mathbf{B}\mathbf{u}$ can be written as $\dot{\mathbf{x}} = (\mathbf{J}_o - \mathbf{R}_o)\mathbf{Q}_o\mathbf{x} + \mathbf{B}\mathbf{u}$ where $\mathbf{J}_o = -\mathbf{J}_o^T$, $\mathbf{R}_o = \mathbf{R}_o^T \geq \mathbf{0}$ and $\mathbf{Q}_o = \mathbf{Q}_o^T > \mathbf{0}$.

Consider the observer of the dynamical system to be a function of measurement \mathbf{y} as

$$\dot{\hat{\mathbf{x}}} = (\mathbf{J}_o - \mathbf{R}_o)\mathbf{Q}_o\hat{\mathbf{x}} + \hat{\mathbf{g}}u_s - \mathbf{L}\mathbf{y} \quad (4.7)$$

where $\hat{\mathbf{g}}$ is the input matrix of the observer. Defining the error between state and estimate:

$$\mathbf{e} = \mathbf{x} - \hat{\mathbf{x}} \quad (4.8)$$

Derivative of \mathbf{e} with respect to time can be written as:

$$\dot{\mathbf{e}} = \{(\mathbf{J} - \mathbf{R})\mathbf{Q}\mathbf{x} + \mathbf{g}u_s\} - \{(\mathbf{J}_o - \mathbf{R}_o)\mathbf{Q}_o\hat{\mathbf{x}} + \hat{\mathbf{g}}u_s - \mathbf{L}\mathbf{y}\} \quad (4.9)$$

rearranging equation (4.9) in terms of \mathbf{e} and x ,

$$\dot{\mathbf{e}} = (\mathbf{J}_o - \mathbf{R}_o)\mathbf{Q}_o\mathbf{e} + (\mathbf{g} - \hat{\mathbf{g}})u_s + ((\mathbf{J} - \mathbf{R})\mathbf{Q} - (\mathbf{J}_o - \mathbf{R}_o)\mathbf{Q}_o + \mathbf{L}\mathbf{C})\mathbf{x} \quad (4.10)$$

Now for the error to decay to zero asymptotically for any input and state,

$$\begin{aligned} \hat{\mathbf{g}} &= \mathbf{g} \\ (\mathbf{J}_o - \mathbf{R}_o)\mathbf{Q}_o &= (\mathbf{J} - \mathbf{R})\mathbf{Q} + \mathbf{L}\mathbf{C} \end{aligned} \quad (4.11)$$

multiplying by \mathbf{C}_\perp on both sides of equation (4.11), we get the relation (equation (4.4)). Now, equation (4.11) can be reframed as:

$$\mathbf{L}\mathbf{C} = (\mathbf{J}_o - \mathbf{R}_o)\mathbf{Q}_o - (\mathbf{J} - \mathbf{R})\mathbf{Q} \quad (4.12)$$

Multiplying (4.12) by \mathbf{C}^\top on both sides, \mathbf{L} can be written as

$$\mathbf{L} = \left((\mathbf{J}_o - \mathbf{R}_o)\mathbf{Q}_o - (\mathbf{J} - \mathbf{R})\mathbf{Q} \right) \mathbf{C}^\top \quad (4.13)$$

Substituting equation (4.13) in equation (4.7), the observer for system defined by equation (4.1) and equation (4.2) with $f = 0$ is obtained as equation (4.5), which proves the theorem. The error dynamics with road disturbance f can then be written as,

$$\dot{\mathbf{e}} = (\mathbf{J}_o - \mathbf{R}_o)\mathbf{Q}_o\mathbf{e} + \mathbf{d}f \quad (4.14)$$

The error dynamics decay asymptotically to zero with $f = 0$ if the matrix $(\mathbf{J}_o - \mathbf{R}_o)\mathbf{Q}_o$ is Hurwitz. In presence of disturbance f , the error dynamics are bounded by maximum value of disturbance Yaghmaei and Yazdanpanah (2018), and can be minimised by proper choice of \mathbf{J}_o , \mathbf{R}_o and \mathbf{Q}_o .

4.1.1 Choice Of Observer Parameters For Active Suspension Observer Design

Suspension deflection q_2 of the system is taken as the measurable state. The output (measurable) equation for the system (equation (4.1)) is given by,

$$\begin{aligned} y &= \mathbf{C}\mathbf{x} \\ \mathbf{C} &= \begin{bmatrix} 0 & 0 & 0 & 1 \end{bmatrix} \end{aligned} \quad (4.15)$$

The objective is to design an observer of the form given in equation (4.5). Choosing the $H_o(\mathbf{x})$ as:

$$H_o = H + \frac{1}{2}k_1q_1^2 + \frac{1}{2}k_2q_2^2 \quad (4.16)$$

The Quadratic function \mathbf{Q}_o given by

$$\mathbf{Q}_o = \begin{bmatrix} \frac{1}{m_w} & -\frac{1}{m_w} & 0 & 0 \\ -\frac{1}{m_w} & \frac{m_b+m_w}{m_b m_w} & 0 & 0 \\ 0 & 0 & (k_t + k_1) & \\ 0 & 0 & 0 & (k_s + k_2) \end{bmatrix} \quad (4.17)$$

Further, parameterising \mathbf{J}_o and \mathbf{R}_o as

$$\mathbf{J}_o = \mathbf{J}, \mathbf{R}_o = \begin{bmatrix} b_{1o} & 0 & 0 & 0 \\ 0 & b_{2o} & 0 & 0 \\ 0 & 0 & b_{3o} & 0 \\ 0 & 0 & 0 & b_{4o} \end{bmatrix} \quad (4.18)$$

Using the condition (4.4), we can obtain the constraints as $k_1 = 0$, $b_{1o} = b_t$, $b_{2o} = b_s$ and $b_{3o} = 0$. The observer is given in terms of suspension deflection and control input

by

$$\begin{bmatrix} \dot{\hat{p}}_1 \\ \dot{\hat{p}}_2 \\ \dot{\hat{q}}_1 \\ \dot{\hat{q}}_2 \end{bmatrix} = \begin{bmatrix} -\frac{b_t}{m_w} & \frac{b_t}{m_w} & -k_t & 0 \\ \frac{b_s}{m_w} & -b_s \frac{m_b+m_w}{m_b m_w} & 0 & -(k_s+k_2) \\ \frac{1}{m_w} & -\frac{1}{m_w} & 0 & 0 \\ -\frac{1}{m_w} & \frac{m_b+m_w}{m_b m_w} & 0 & -b_{4o}(k_s+k_2) \end{bmatrix} \begin{bmatrix} \hat{p}_1 \\ \hat{p}_2 \\ \hat{q}_1 \\ \hat{q}_2 \end{bmatrix} + \begin{bmatrix} 0 \\ k_2 \\ 0 \\ b_{4o}(k_s+k_2) \end{bmatrix} q_2 + \begin{bmatrix} 0 \\ 1 \\ 0 \\ 0 \end{bmatrix} u_s \quad (4.19)$$

where k_2 and b_{4o} are free parameters to tune the observer dynamics.

4.2 Results and Discussion

The observer design is tested on an active suspension laboratory scale setup from Quanser. The details of the experimental setup is given in Chapter 3. A road profile mimicking an isolated bump on a smooth surface is taken as a test input for analysis, which is mathematically defined as:

$$x_r(t) = \begin{cases} 0.0075(1 - \cos 8\pi t); & 0.5 \leq t < 0.75 \\ 0 & \text{else} \end{cases} \quad (4.20)$$

The observer gains are chosen as $k_2 = 1$ and $b_{4o} = 0.1$.

The time responses of the system when excited with road input signal in equation (4.20) without control input are presented in Figure 4.1. From the results, it can be observed that the measured and observed responses of the suspension deflection q_2 in Figure 4.1(a) are almost identical, indicating that the observer output is close to the measurement. The road disturbance input $f(t)$ directly effects the terms \dot{e}_1 and \dot{e}_3 in the error dynamic equation (4.14), which correspond to observer outputs \hat{p}_1 and \hat{q}_1 . Due to the unmodelled road input acting directly on these observer outputs, the error between the observed and actual states of q_1 and p_1 in Figure 4.1(b) and Figure 4.1(d) is slightly higher when compared to the errors of states q_2 and p_2 in Figure 4.1(a) and Figure 4.1(c). The momenta coordinates p_1 and p_2 are obtained by measuring the deflections using high resolution optical encoders and differentiating and filtering the signals. The error between \hat{p}_2 and p_2 is negligible, whereas \hat{p}_1 shows a delayed response compared to p_1 .

The proposed full-state observer is used to implement the IDA-PBC controller on

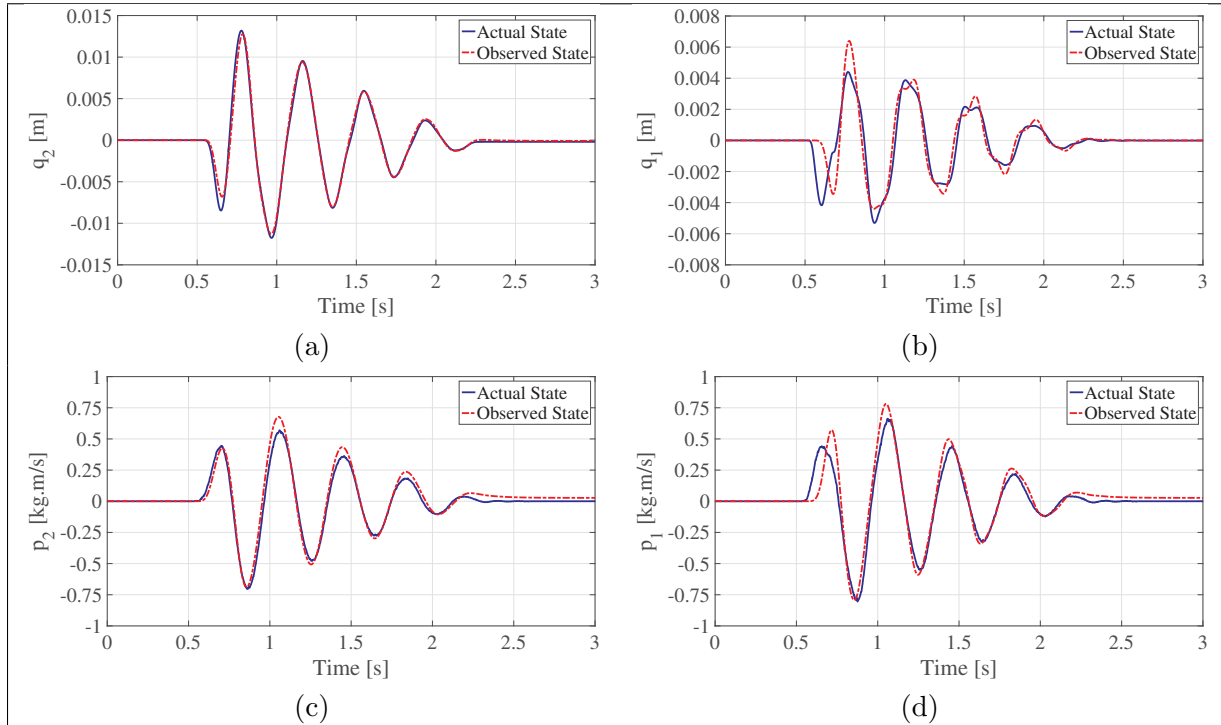


Figure 4.1: Experimental results of observer in open-loop

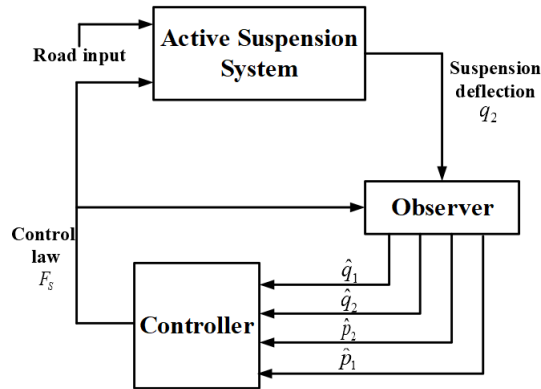


Figure 4.2: Configuration of proposed controller with observer

active suspension system. The configuration of the closed-loop system with proposed controller and observer is shown in Figure 4.2. Energy Shaping and Damping Injection with Inertial Decoupling controller (ESDIID) developed in Chapter 3 is used to test the closed-loop performance of the system with observer states in the feedback control law. The controller parameters are chosen as $a_1 = 3.45$, $a_2 = 0$, $a_3 = 1$, $\alpha = 1$, $b_1 = 17.25$, $b_2 = 135$, $k_z = 2000$. An observer with suspension deflection q_2 as the

measurable signal is designed using equation 4.19. Time responses of the system

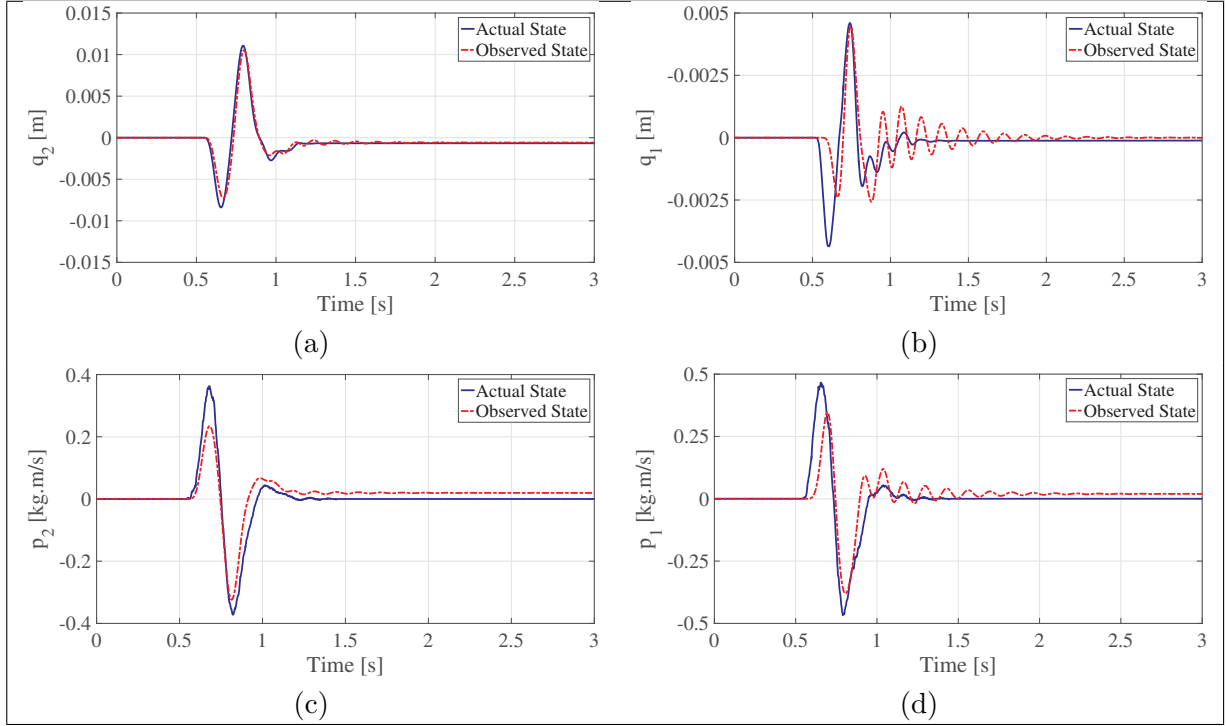


Figure 4.3: Experimental results of observer in closed-loop

when the state feedback law is implemented using the estimated states are shown in Figure 4.3. Similar to the case of the uncontrolled system, the error between q_2 and \hat{q}_2 in closed-loop is negligible, whereas the error between measured and observer states in case of q_1 and p_1 is high and oscillatory, which decays to zero after some time. The performance of the observer is tabulated in terms of Integral Square Error (ISE) and Integral Time Absolute Error (ITAE) in Table 4.1. From Figure 4.4, it is clear that with controller implemented using full state measurement improves the ride comfort more efficiently when compared to the control law implemented using observer in the feedback. However, implementation with help of full measurement requires accurate measurement of tire deflection and velocities of sprung and unsprung masses, which is not relatively easy on a real vehicle. Even with the observer on an IDA-PBC controller, the RMS value of the vehicle body acceleration is lowered by 54% compared an uncontrolled system, which is a considerable reduction. Table 4.2 gives the RMS values of \ddot{x}_b for all the three cases. The peak value of suspension deflection of the system in closed-loop is observed to be $\approx 0.01m$ in Figure 4.3(a), which is well within

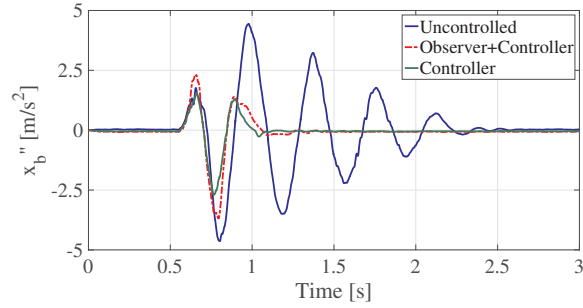


Figure 4.4: Experimental results of sprung mass acceleration

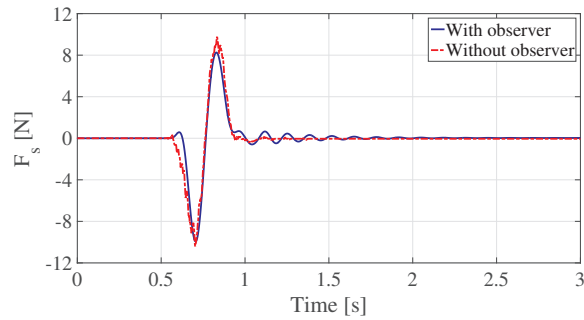


Figure 4.5: Experimental results of actuator force

the prescribed limits of the system. Comparing Figure 4.1(b) and Figure 4.3 (b), the peak value of tire deflection is reduced in closed-loop system and stabilises at a faster rate, which guarantees an improvement in ride stability of the closed-loop system when compared to uncontrolled system. The actuator force in Figure 4.5 is much less than the saturation limit of the actuator, which is 35N. From the above discussion and results, active suspension using IDA-PBC with observer performs effectively in terms of improving ride comfort and ride stability, which is verified using experimental results and performance indices.

4.3 Summary

In this chapter, an observer design for quarter car active suspension modelled in port-Hamiltonian form are presented. Suspension deflection, which is an easily measurable signal is used as the output in the design of the observer. Performance of the proposed observer is evaluated experimentally with road disturbance input mimicking a sudden bump, and proven to be effective in minimising the error dynamics in presence of road disturbance. Using the observer states in the feedback, a full-state IDA-PBC control

Table 4.1: Performance Indices of observer (Experimental Values)

Parameter	ISE	ITAE
\tilde{p}_1 (Uncontrolled)	1.85×10^{-2}	0.1895
\tilde{p}_1 (IDAPBC)	1.09×10^{-2}	0.1197
\tilde{p}_2 (Uncontrolled)	6.1×10^{-3}	0.1534
\tilde{p}_2 (IDAPBC)	3.6×10^{-3}	0.1028
\tilde{q}_1 (Uncontrolled)	1.76×10^{-6}	0.0012
\tilde{q}_1 (IDAPBC)	1.55×10^{-6}	0.0011
\tilde{q}_2 (Uncontrolled)	6.72×10^{-7}	0.0094
\tilde{q}_2 (IDAPBC)	6.82×10^{-7}	0.0071

$\tilde{p}_1 = (p_1 - \hat{p}_1), \tilde{p}_2 = (p_2 - \hat{p}_2), \tilde{q}_1 = (q_1 - \hat{q}_1), \tilde{q}_2 = (q_2 - \hat{q}_2)$

Table 4.2: RMS values of Acceleration (Experimental Values) \ddot{x}_b

Case	$\ddot{x}_b(m/s^2)$
Uncontrolled	1.4791
Controller	0.4748
Controller+Observer	0.6779

law is implemented, and compared with the case of control where all the states are available for measurement. Experimental results of the controller implemented using the designed state observer show good improvement in the ride comfort, ride stability and suspension stroke of the active suspension system, which proves the effectiveness of the proposed port-Hamiltonian observer in terms of minimising the error dynamics.

Chapter 5

Control Of Half-Car Active Suspension System Using Algebraic Interconnection And Damping Assignment Passivity Based Control

Contents

5.1	System Description: Half Car Active Suspension System	77
5.1.1	Port-Hamiltonian Model Of Half Car Active Suspension System	78
5.1.2	Control Objectives In Terms Of PCH Variables	81
5.2	Interconnection And Damping Assignment Passivity Based Control	81
5.2.1	Algebraic Solution Of Matching Equation	82
5.2.2	Controller Design For Half-Car Active Suspension System .	83
5.3	Case Studies	88
5.3.1	Controller-I: Potential Energy Shaping and Damping Injection (PESADI)	88
5.3.2	Controller-II: Inertial Decoupling	89

5.3.3	Quarter-Car IDA-PBC Method (QCAR IDA-PBC)	91
5.4	Simulation and Discussion	94
5.5	Summary	101

This chapter is purposed to design IDA-PBC controller for half-car active suspension system modelled in port-Hamiltonian framework. Half-car active suspension system is a *higher order, underactuated* complex mechanical system, which involves the challenge of solving multiple PDEs comprising of larger set of states to obtain a solution for closed-loop or *desired* potential energy. The novelty of this work lies in circumventing this problem by employing an algebraic method to construct the closed-loop energy function, and state-feedback law. First, the closed-loop kinetic energy function is shaped with the help of desired inertia matrix, and the associated closed-loop stiffness matrix which defines the closed-loop potential energy function is constructed with the help of matrix properties.

5.1 System Description: Half Car Active Suspension System

Figure 5.1 portrays a linear time invariant model of a half-car active suspension system. Terms m_b and I_ϕ represent the vehicle’s body mass and pitch moment of inertia, respectively. ϕ represents pitch angle, and l_f and l_r denote the distances of the front and rear axles from the centre of mass, respectively. The stiffnesses of the front and rear suspension springs are expressed by k_{sf} and k_{sr} , respectively. The damping coefficients of the front and rear suspensions are represented by b_{sf} and b_{sr} , respectively. u_f and u_r represent the front and rear actuator force components, respectively. The unsprung mass on the front and rear wheels is denoted by m_{wf} and m_{wr} , respectively. The tire is represented as a combination of a spring and a damper, with k_{tf} and b_{tf} representing the front tire stiffness and damping coefficients, respectively, and k_{tr} and b_{tr} representing the rear tire stiffness and damping coefficients. Variables x_c , x_{bf} , and x_{br} indicate the vertical displacements of the centre of mass, front and rear body displacements, about their respective mean locations. The vertical displacements of the front and rear tires around their equilibrium positions are denoted by the symbols x_{wf} and x_{wr} , respectively. The front and rear terrain height displacements are denoted by x_{rf} and x_{rr} , respectively. The above model consists of a single sprung

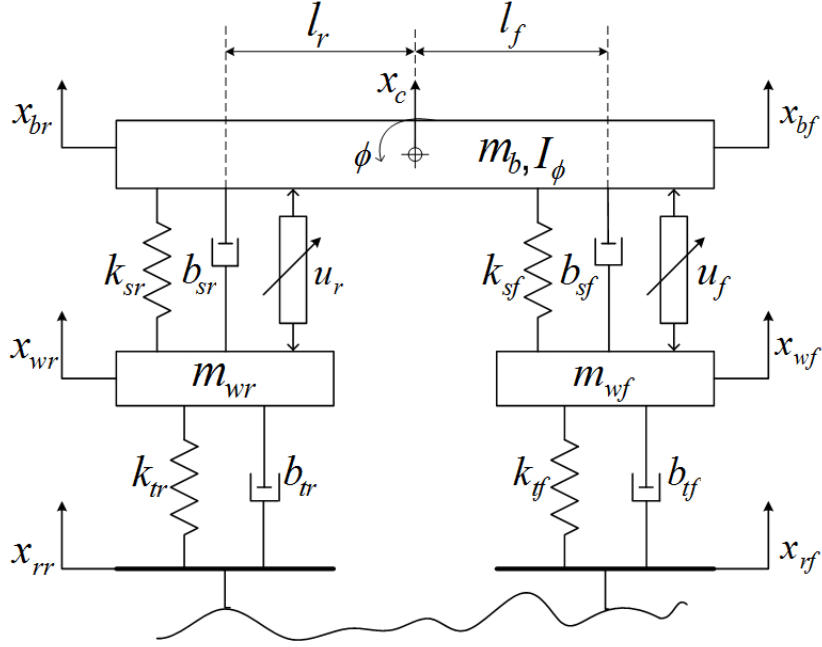


Figure 5.1: Model of half car active suspension system

mass representing vehicle body with vertical and pitch freedoms of motion and two unsprung masses denoting front and rear wheels with vertical freedom of motion. The vertical displacements of the sprung mass are related as follows:

$$\begin{aligned} x_{bf} &= x_c + l_f \sin \phi \\ x_{br} &= x_c - l_r \sin \phi \end{aligned} \quad (5.1)$$

and $l_f + l_r = l$. $\sin \phi$ can be approximated as $\sin \phi \approx \phi$ since the pitch angle is modest enough. Therefore, equation (5.1) becomes $x_{bf} = x_c + l_f \phi$ and $x_{br} = x_c - l_r \phi$.

5.1.1 Port-Hamiltonian Model Of Half Car Active Suspension System

The PCH model of half-car active suspension system shown in Figure 5.1 is derived in Appendix B. The model of the system is given by

$$\dot{\mathbf{x}} = [\mathbf{J} - \mathbf{R}] \nabla \mathbf{H}(\mathbf{x}) + \mathbf{g} \mathbf{u}_a + \mathbf{d} \mathbf{f} \quad (5.2)$$

where $\mathbf{x} = (\mathbf{p}, \mathbf{q}) \in \mathbb{R}^n$ ($n = 8$) is the state vector, and $\mathbf{u}_a = (u_f, u_r) \in \mathbb{R}^m$ ($m = 2$) is the actuator input vector. Road velocity input to the system is represented by $\mathbf{f} = (\dot{x}_{rf}(t), \dot{x}_{rr}(t)) \in \mathbb{R}^2$. Vectors $\mathbf{q} \in \mathbb{R}^4$ and $\mathbf{p} \in \mathbb{R}^4$ represent the generalised displacement and momenta coordinates, respectively, defined as

$$\mathbf{q} = \begin{bmatrix} q_1 \\ q_2 \\ q_3 \\ q_4 \end{bmatrix} = \begin{bmatrix} x_{bf} - x_{wf} \\ x_{br} - x_{wr} \\ x_{wf} - x_{rf} \\ x_{wr} - x_{rr} \end{bmatrix} \quad (5.3a)$$

$$(5.3b)$$

$$\mathbf{p} = \begin{bmatrix} p_1 \\ p_2 \\ p_3 \\ p_4 \end{bmatrix} = \begin{bmatrix} m_b \frac{l_r}{l} \dot{x}_c + \frac{I_\phi}{l} \dot{\phi} \\ m_b \frac{l_f}{l} \dot{x}_c - \frac{I_\phi}{l} \dot{\phi} \\ m_b \frac{l_r}{l} \dot{x}_c + \frac{I_\phi}{l} \dot{\phi} + m_{wf} \dot{x}_{wf} \\ m_b \frac{l_f}{l} \dot{x}_c - \frac{I_\phi}{l} \dot{\phi} + m_{wr} \dot{x}_{wr} \end{bmatrix} \quad (5.3c)$$

The Hamiltonian $H(\mathbf{x}) = H(\mathbf{p}, \mathbf{q})$ is the energy stored in the system, written in terms of its kinetic and potential energies, $\tau(\mathbf{p})$ and $\nu(\mathbf{q})$, respectively as,

$$H(\mathbf{x}) = \tau(\mathbf{p}) + \nu(\mathbf{q}) = \frac{1}{2} \mathbf{p}^T \mathbf{M}^{-1} \mathbf{p} + \frac{1}{2} \mathbf{q}^T \mathbf{K} \mathbf{q} \quad (5.4a)$$

$$= \frac{1}{2} \begin{bmatrix} \mathbf{p}^T & \mathbf{q}^T \end{bmatrix} \begin{bmatrix} \mathbf{M}^{-1} & \mathbf{0} \\ \mathbf{0} & \mathbf{K} \end{bmatrix} \begin{bmatrix} \mathbf{p} \\ \mathbf{q} \end{bmatrix} = \frac{1}{2} \mathbf{x}^T \bar{\mathbf{H}} \mathbf{x} \quad (5.4b)$$

From equation (5.4), it can be seen that the kinetic energy is a function of the inertia matrix \mathbf{M} , which is obtained as

$$\mathbf{M} = \begin{bmatrix} m_1 & m_3 & m_1 & m_3 \\ m_3 & m_2 & m_3 & m_2 \\ m_1 & m_3 & (m_1 + m_{uf}) & m_3 \\ m_3 & m_2 & m_3 & (m_2 + m_{ur}) \end{bmatrix} \quad (5.5)$$

where $m_1 = \frac{m_b l_r^2 + I_\phi}{l^2}$, $m_2 = \frac{m_b l_f^2 + I_\phi}{l^2}$ and $m_3 = \frac{m_b l_f l_r - I_\phi}{l^2}$. Potential energy $\nu(\mathbf{q})$ is a function of stiffness matrix \mathbf{K} , consisting of spring stiffness coefficients, given by,

$$\mathbf{K} = \begin{bmatrix} k_{sf} & 0 & 0 & 0 \\ 0 & k_{sr} & 0 & 0 \\ 0 & 0 & k_{tf} & 0 \\ 0 & 0 & 0 & k_{tr} \end{bmatrix} \quad (5.6)$$

Matrices \mathbf{J} and \mathbf{R} represent the interconnection and dissipative structures, respectively.

$$\mathbf{J} = \begin{bmatrix} \mathbf{0} & -\mathbf{I} \\ \mathbf{I} & \mathbf{0} \end{bmatrix} \quad \text{and} \quad \mathbf{R} = \begin{bmatrix} \mathbf{D} & \mathbf{0} \\ \mathbf{0} & \mathbf{0} \end{bmatrix} \quad (5.7)$$

The term \mathbf{D} is the damping matrix, consisting of damping coefficients of the system

$$\mathbf{D} = \begin{bmatrix} b_{sf} & 0 & 0 & 0 \\ 0 & b_{sr} & 0 & 0 \\ 0 & 0 & b_{tf} & 0 \\ 0 & 0 & 0 & b_{tr} \end{bmatrix} \quad (5.8)$$

The matrices \mathbf{g} and \mathbf{d} are defined as $\mathbf{g} = [\mathbf{G}^T \quad \mathbf{0}]^T$, and $\mathbf{d} = [\mathbf{G}_1^T \quad \mathbf{G}_2^T]^T$ where \mathbf{G}, \mathbf{G}_1 and \mathbf{G}_2 are given by

$$\mathbf{G}_1 = \begin{bmatrix} 0 & 0 \\ 0 & 0 \\ b_{tf} & 0 \\ 0 & b_{tr} \end{bmatrix}, \quad \mathbf{G}_2 = \begin{bmatrix} 0 & 0 \\ 0 & 0 \\ -1 & 0 \\ 0 & -1 \end{bmatrix}, \quad \mathbf{G} = \begin{bmatrix} 1 & 0 \\ 0 & 1 \\ 0 & 0 \\ 0 & 0 \end{bmatrix} \quad (5.9)$$

The term \dot{p}_1 represents the force on front portion of chassis $m_b(l_r/l)$ due to vertical acceleration \ddot{x}_c and angular acceleration $\ddot{\phi}$, whereas the force on rear component of chassis $m_b(l_f/l)$ due to vertical and angular accelerations is given by \dot{p}_2 . The front and rear suspension deflections are denoted by state variables q_1 and q_2 respectively. The tire deflections are represented by q_3 and q_4 , and their velocities are given by \dot{q}_3 and \dot{q}_4 respectively. Therefore, the performance requirements of active suspension in terms of the state variables can be written as follows:

5.1.2 Control Objectives In Terms Of PCH Variables

1. *Ride comfort*: Minimise the forces \dot{p}_1 and \dot{p}_2 by isolating road disturbance input from chassis m_b .
2. *Road holding*: Minimise q_3, q_4, \dot{q}_3 and \dot{q}_4 which are the components contributing to the dynamic tire loads $RDTL_f$ and $RDTL_r$.
3. *Suspension travel*: Controller must be tuned such that the state variables q_1 and q_2 must not exceed the maximum prescribed limits.

5.2 Interconnection And Damping Assignment Passivity Based Control

Consider the port-controlled Hamiltonian system with dissipation of the form,

$$\dot{\mathbf{x}} = [\mathbf{J} - \mathbf{R}] \nabla H(\mathbf{x}) + \mathbf{g} \mathbf{u} \quad (5.10)$$

where $\mathbf{x}(\mathbf{t}) \in \mathbb{R}^n$ is the state vector and $\mathbf{u}(\mathbf{t}) \in \mathbb{R}^m$ is the control input. $\mathbf{J}, \mathbf{R} \in \mathbb{R}^{n \times n}$ are the interconnection and dissipative matrices, respectively, where $\mathbf{J} = -\mathbf{J}^T$ and $\mathbf{R} = \mathbf{R}^T \geq 0$. $H(\mathbf{x}) : \mathbb{R}^n \rightarrow \mathbb{R}$ is a continuously differentiable Hamiltonian, and $\mathbf{g} \in \mathbb{R}^{n \times m}$ is a full (column) rank matrix. The objective of the IDA-PBC design is to find a control input \mathbf{u} such that a desired equilibrium point \mathbf{x}^* of the closed-loop system is (asymptotically) stable and the closed-loop system is characterised by

$$\dot{\mathbf{x}} = [\mathbf{J}_d - \mathbf{R}_d] \nabla H_d(\mathbf{x}) \quad (5.11)$$

where \mathbf{J}_d and \mathbf{R}_d are the desired interconnection and desired dissipative matrices belonging to $\mathbb{R}^{n \times n}$ such that $\mathbf{J}_d = -\mathbf{J}_d^T$, and $\mathbf{R}_d = \mathbf{R}_d^T \geq 0$, and $H_d(\mathbf{x}) : \mathbb{R}^n \rightarrow \mathbb{R}_+$ is the desired energy function. The desired energy must be continuously differentiable and such that $H_d(\mathbf{x}^*) = 0$ with \mathbf{x}^* a strict (local) minimizer of H_d . If $\mathbf{g}^\perp : \mathbb{R}^n \rightarrow \mathbb{R}^{(n-m) \times n}$ represents the full rank left annihilator of the matrix \mathbf{g} , i.e., $\mathbf{g}^\perp \mathbf{g} = \mathbf{0}$ for all $\mathbf{x} \in \mathbb{R}^n$ and $rank(\mathbf{g}^\perp) = (n - m)$, the classical solution of the IDA-PBC design problem depends upon the solution $\mathbb{K} : \mathbb{R}^n \rightarrow \mathbb{R}^n$ of the so-called *matching equation*,

namely the system of equations

$$\mathbf{g}^\perp[(\mathbf{J} - \mathbf{R})\nabla\mathbf{H}(\mathbf{x}) - (\mathbf{J}_d - \mathbf{R}_d)(\nabla\mathbf{H}(\mathbf{x}) + \mathbb{K}(\mathbf{x}))] = \mathbf{0} \quad (5.12)$$

where $\nabla\mathbf{H}_d(\mathbf{x}) = \nabla\mathbf{H}(\mathbf{x}) + \mathbb{K}(\mathbf{x})$ denotes the gradient vector of the desired energy function H_d . Note that the mapping \mathbb{K} must satisfy the condition $\partial\mathbb{K}/\partial x = (\partial\mathbb{K}/\partial x)^T$, thus ensuring integrability of \mathbb{K} .

5.2.1 Algebraic Solution Of Matching Equation

Consider the energy function $H(\mathbf{x})$ of the PCH system represented by equation (5.10). If the system is linear time invariant, then the Hamiltonian can be defined as

$$H(\mathbf{x}) = \frac{1}{2}\mathbf{x}^T\bar{\mathbf{H}}\mathbf{x} \quad (5.13)$$

Definition 1 Nunna et al. (2015): Consider the PCH system in equation (5.10) and fix $\mathbf{J}_d = -\mathbf{J}_d^T$ and $\mathbf{R}_d = \mathbf{R}_d^T \geq \mathbf{0}$. A matrix $\bar{\mathbf{P}} \in \mathbb{R}^{n \times n}$, $\bar{\mathbf{P}} = \bar{\mathbf{P}}^T$ for all $\mathbf{x} \in \mathbb{R}^n$ is said to be *algebraic solution* if

1. The matrix $\bar{\mathbf{H}} + \bar{\mathbf{P}}$ is positive definite
2. The condition

$$\mathbf{g}^\perp[(\mathbf{J} - \mathbf{R})\bar{\mathbf{H}}\mathbf{x} - (\mathbf{J}_d - \mathbf{R}_d)(\bar{\mathbf{H}} + \bar{\mathbf{P}})\mathbf{x}] = \mathbf{0} \quad (5.14)$$

holds for all $\mathbf{x} \in \mathbb{R}^n$. Then $\bar{\mathbf{P}}$ is said to be an *algebraic solution* of equation (5.12).

Definition 2 Nunna et al. (2015): Consider the PCH system defined in equation (5.10) and the function $H(\mathbf{x})$ in equation (5.13). Let $\mathbf{J}_d = -\mathbf{J}_d^T$, $\mathbf{R}_d = \mathbf{R}_d^T \geq \mathbf{0}$ be such that $\mathbf{J}_d - \mathbf{R}_d$ is invertible and a matrix $\lambda \in \mathbb{R}^{m \times n}$ be such that the following hold.

1. The matrix $(\mathbf{J}_d - \mathbf{R}_d)^{-1}[(\mathbf{J} - \mathbf{R})\bar{\mathbf{H}} - \mathbf{g}\lambda]$ is positive definite.
2. The matrix $(\mathbf{J}_d - \mathbf{R}_d)^{-1}[(\mathbf{J} - \mathbf{R})\bar{\mathbf{H}} - \mathbf{g}\lambda]$ is Symmetric provided $\bar{\mathbf{H}}$ is symmetric.

Then the matrix $\bar{\mathbf{P}}$ defined as

$$\bar{\mathbf{P}} = (\mathbf{J}_d - \mathbf{R}_d)^{-1}[(\mathbf{J} - \mathbf{J}_d - \mathbf{R} + \mathbf{R}_d)\bar{\mathbf{H}} - \mathbf{g}\lambda] \quad (5.15)$$

is the *algebraic solution* of equation (5.12), and $\mathbb{K}(\mathbf{x}) = \bar{\mathbf{P}}\mathbf{x}$.

5.2.2 Controller Design For Half-Car Active Suspension System

In this section, a general control law is designed using algebraic IDA-PBC method which can be used to modify the closed-loop system characteristics. The closed-loop structure is chosen to be in the form

$$\dot{\mathbf{x}} = [\mathbf{J}_d - \mathbf{R}_d]\nabla H_d(\mathbf{x}) + \mathbf{d}\mathbf{f} \quad (5.16)$$

where the structure of \mathbf{J}_d and \mathbf{R}_d is given by

$$\mathbf{J}_d = \begin{bmatrix} \mathbf{J}_a & -\mathbf{M}_d\mathbf{M}^{-1} \\ \mathbf{M}^{-1}\mathbf{M}_d & \mathbf{0} \end{bmatrix}, \mathbf{R}_d = \begin{bmatrix} \mathbf{D}_d & \mathbf{0} \\ \mathbf{0} & \mathbf{0} \end{bmatrix} \quad (5.17)$$

$\mathbf{J}_a = -\mathbf{J}_a^T$ is the additional interconnection matrix, and $\mathbf{M}_d = \mathbf{M}_d^T > 0$ is the desired inertia matrix used to shape the *desired kinetic energy* profile. The closed-loop energy function $H_d(\mathbf{x}) = H_d(\mathbf{p}, \mathbf{q})$ is desired to be

$$H_d(\mathbf{x}) = \tau_d(\mathbf{p}) + \nu_d(\mathbf{q}) = \frac{1}{2}\mathbf{p}^T\mathbf{M}_d^{-1}\mathbf{p} + \nu_d(\mathbf{q}) \quad (5.18)$$

where $\nu_d(\mathbf{q})$ is desired potential energy of the close-loop system. If we assume that the desired potential energy is in the form $\nu_d(\mathbf{q}) = \frac{1}{2}\mathbf{q}^T\mathbf{K}_d\mathbf{q}$, then $H_d(\mathbf{x})$ can be written as

$$H_d(\mathbf{x}) = \frac{1}{2} \begin{bmatrix} \mathbf{p}^T & \mathbf{q}^T \end{bmatrix} \begin{bmatrix} \mathbf{M}_d^{-1} & \mathbf{0} \\ \mathbf{0} & \mathbf{K}_d \end{bmatrix} \begin{bmatrix} \mathbf{p} \\ \mathbf{q} \end{bmatrix} = \frac{1}{2}\mathbf{x}^T\bar{\mathbf{H}}_d\mathbf{x} \quad (5.19)$$

Equating the open-loop (5.2) and closed-loop (5.16) to design the control law,

$$[\mathbf{J} - \mathbf{R}]\nabla H(\mathbf{x}) + \mathbf{g}\mathbf{u}_a + \mathbf{d}\mathbf{f} = [\mathbf{J}_d - \mathbf{R}_d]\nabla H_d(\mathbf{x}) + \mathbf{d}\mathbf{f} \quad (5.20)$$

The system is underactuated, i.e., $\text{rank}(\mathbf{g}) = m < n$, and the matching equation can be found by rearranging equation (5.20) as,

$$\mathbf{g}^\perp[(\mathbf{J} - \mathbf{R})\nabla\mathbf{H}(\mathbf{x}) - (\mathbf{J}_d - \mathbf{R}_d)\nabla\mathbf{H}_d(\mathbf{x})] = \mathbf{0} \quad (5.21)$$

$\nabla\mathbf{H}(\mathbf{x})$ and $\nabla\mathbf{H}_d(\mathbf{x})$ can be derived from equations (5.4) and (5.19), respectively, and substituted in equation (5.21)

$$\mathbf{g}^\perp[(\mathbf{J} - \mathbf{R})\bar{\mathbf{H}}\mathbf{x} - (\mathbf{J}_d - \mathbf{R}_d)\bar{\mathbf{H}}_d\mathbf{x}] = \mathbf{0} \quad (5.22)$$

Now, considering a real matrix $\bar{\mathbf{P}} = \bar{\mathbf{P}}^\mathbf{T}$ such that,

$$\bar{\mathbf{H}}_d = \bar{\mathbf{H}} + \bar{\mathbf{P}} \quad (5.23)$$

substituting for $\bar{\mathbf{H}}_d$ in equation (5.22),

$$\mathbf{g}^\perp[(\mathbf{J} - \mathbf{R})\bar{\mathbf{H}}\mathbf{x} - (\mathbf{J}_d - \mathbf{R}_d)(\bar{\mathbf{H}} + \bar{\mathbf{P}})\mathbf{x}] = \mathbf{0} \quad (5.24)$$

Equation (5.24) is the *matching equation* of the system free from partial differential terms, and the equation takes the form of equation (5.14). Since $\bar{\mathbf{H}}_d = \bar{\mathbf{H}}_d^\mathbf{T} > 0$, from *Definition 1*, $\bar{\mathbf{P}}$ is the solution of the matching equation, which is given by equation (5.15) in *Definition 2*. Rearranging terms in equation (5.15),

$$\bar{\mathbf{H}}_d = (\bar{\mathbf{H}} + \bar{\mathbf{P}}) = (\mathbf{J}_d - \mathbf{R}_d)^{-1}[(\mathbf{J} - \mathbf{R})\bar{\mathbf{H}} - \mathbf{g}\lambda] \quad (5.25)$$

In equation (5.25), $\lambda \in \mathbb{R}^{m \times n}$ is a matrix of static feedback gains, i.e., $\lambda \in \mathbb{R}^{2 \times 8}$. Parameterising λ as $\lambda = \begin{bmatrix} \lambda_p & \lambda_q \end{bmatrix}$ where,

$$\lambda_p = \begin{bmatrix} \lambda_{11} & \lambda_{12} & \lambda_{13} & \lambda_{14} \\ \lambda_{21} & \lambda_{22} & \lambda_{23} & \lambda_{24} \end{bmatrix} \quad (5.26a)$$

$$\lambda_q = \begin{bmatrix} \lambda_{15} & \lambda_{16} & \lambda_{17} & \lambda_{18} \\ \lambda_{25} & \lambda_{26} & \lambda_{27} & \lambda_{28} \end{bmatrix} \quad (5.26b)$$

where λ_p and λ_q are the state-feedback gains corresponding to states p and q , respectively, and the state-feedback law is given by,

$$\mathbf{u}_a = -\lambda \mathbf{x} = -\lambda_p \mathbf{p} - \lambda_q \mathbf{q} \quad (5.27)$$

Inverse of the matrix $(\mathbf{J}_d - \mathbf{R}_d)$ is computed using *Theorem 2.1.(i)* in Lu and Shiou (2002) as,

$$(\mathbf{J}_d - \mathbf{R}_d)^{-1} = \begin{bmatrix} \mathbf{0} & \mathbf{M}_d^{-1} \mathbf{M} \\ -\mathbf{M} \mathbf{M}_d^{-1} & (\mathbf{M} \mathbf{M}_d^{-1})(\mathbf{J}_a - \mathbf{D}_d)(\mathbf{M}_d^{-1} \mathbf{M}) \end{bmatrix} \quad (5.28)$$

Substituting for λ and $(\mathbf{J}_d - \mathbf{R}_d)^{-1}$ from equation (5.26) and equation (5.28), respectively, in equation (5.25), $\bar{\mathbf{H}}_d$ is derived as in equation (5.29).

$$\bar{\mathbf{H}}_d = \begin{bmatrix} \mathbf{M}_d^{-1} & \mathbf{0} \\ \mathbf{M} \mathbf{M}_d^{-1} (\mathbf{D} \mathbf{M}^{-1} + (\mathbf{J}_a - \mathbf{D}_d)(\mathbf{M}_d^{-1} \mathbf{M}) \mathbf{M}^{-1} + \mathbf{G} \lambda_p) & \mathbf{M} \mathbf{M}_d^{-1} \mathbf{K} + \mathbf{M} \mathbf{M}_d^{-1} \mathbf{G} \lambda_q \end{bmatrix} \quad (5.29)$$

Comparing equations (5.19) and (5.29), following conditions in (5.30) can be imposed for $\bar{\mathbf{H}}_d$ to be symmetric and positive definite,

$$\mathbf{M}_d = \mathbf{M}_d^T > 0 \quad (5.30a)$$

$$\mathbf{M} \mathbf{M}_d^{-1} (\mathbf{D} \mathbf{M}^{-1} + (\mathbf{J}_a - \mathbf{D}_d)(\mathbf{M}_d^{-1} \mathbf{M}) \mathbf{M}^{-1} + \mathbf{G} \lambda_p) = \mathbf{0} \quad (5.30b)$$

$$(\mathbf{M} \mathbf{M}_d^{-1} \mathbf{K} + \mathbf{M} \mathbf{M}_d^{-1} \mathbf{G} \lambda_q) = (\mathbf{M} \mathbf{M}_d^{-1} \mathbf{K} + \mathbf{M} \mathbf{M}_d^{-1} \mathbf{G} \lambda_q)^T > 0 \quad (5.30c)$$

Comparing equations (5.19) and (5.29), it can be found that the closed-loop stiffness matrix \mathbf{K}_d is

$$\mathbf{K}_d(\lambda_q) = \mathbf{M} \mathbf{M}_d^{-1} \mathbf{K} + \mathbf{M} \mathbf{M}_d^{-1} \mathbf{G} \lambda_q \quad (5.31)$$

Equation (5.30b) can be reduced and rewritten as

$$\mathbf{G} \lambda_p = -\mathbf{D} \mathbf{M}^{-1} - (\mathbf{J}_a - \mathbf{D}_d) \mathbf{M}_d^{-1} \quad (5.32)$$

The state-feedback gain matrix λ_p corresponding to states \mathbf{p} is obtained from equation (5.32)

$$\lambda_p = \mathbf{G}^\dagger (-\mathbf{D} \mathbf{M}^{-1} - (\mathbf{J}_a - \mathbf{D}_d) \mathbf{M}_d^{-1}) \quad (5.33)$$

where $\mathbf{G}^\dagger = (\mathbf{G}^T \mathbf{G})^{-1} \mathbf{G}^T$. The particular solution, which gives relation between \mathbf{D}_d , \mathbf{J}_a and \mathbf{M}_d can be obtained by solving

$$\mathbf{G}^\perp(-\mathbf{D}\mathbf{M}^{-1} - (\mathbf{J}_a - \mathbf{D}_d)\mathbf{M}_d^{-1}) = \mathbf{0} \quad (5.34)$$

According to equation (5.33), the state-feedback gains λ_p corresponding to momenta coordinates are a function of \mathbf{M}_d , \mathbf{J}_a and \mathbf{D}_d . Equation (5.34) gives the structure of the closed-loop damping matrix \mathbf{D}_d , which changes depending on the structure of \mathbf{M}_d . Equation (5.31) shows that the closed-loop stiffness matrix \mathbf{K}_d is a function of state-feedback gains λ_q , which correspond to displacement coordinates. As a result, after constructing the desired kinetic energy profile, which is a function of the desired inertia matrix \mathbf{M}_d , the closed-loop potential energy $\nu_d(\mathbf{q})$, which is a function of the closed-loop stiffness matrix, can be produced so that $\mathbf{K}_d = \mathbf{K}_d^T > 0$.

The desired storage function $H_d(\mathbf{p}, \mathbf{q})$ is considered as the candidate Lyapunov function for stability analysis. \dot{H}_d can be written down as,

$$\dot{H}_d = (\nabla \mathbf{H}_d(\mathbf{x}))^T \dot{\mathbf{x}} \quad (5.35)$$

Substituting equation (5.16) in equation (5.35) we get,

$$\dot{H}_d = \mathbf{x}^T \bar{\mathbf{H}}_d \mathbf{J}_d \bar{\mathbf{H}}_d \mathbf{x} - \mathbf{x}^T \bar{\mathbf{H}}_d \mathbf{R}_d \bar{\mathbf{H}}_d \mathbf{x} + \mathbf{x}^T \bar{\mathbf{H}}_d \mathbf{d} \mathbf{f} \quad (5.36)$$

Due to the skew-symmetric property of \mathbf{J}_d , \dot{H}_d is reduced to

$$\dot{H}_d = -\mathbf{x}^T \bar{\mathbf{H}}_d \mathbf{R}_d \bar{\mathbf{H}}_d \mathbf{x} + \mathbf{x}^T \bar{\mathbf{H}}_d \mathbf{d} \mathbf{f} \quad (5.37)$$

Now consider the term $\mathbf{N} = (\mathbf{x}^T \bar{\mathbf{H}}_d \mathbf{d} - \mathbf{f}^T)$. Then we can write,

$$\mathbf{N}\mathbf{N}^T = \mathbf{x}^T \bar{\mathbf{H}}_d \mathbf{d} \mathbf{d}^T \bar{\mathbf{H}}_d \mathbf{x} - \mathbf{x}^T \bar{\mathbf{H}}_d \mathbf{d} \mathbf{f} - \mathbf{f}^T \mathbf{d}^T \bar{\mathbf{H}}_d \mathbf{x} + \mathbf{f}^T \mathbf{f} \quad (5.38)$$

Rearranging the terms in equation (5.38),

$$\mathbf{x}^T \bar{\mathbf{H}}_d \mathbf{d} \mathbf{f} + \mathbf{f}^T \mathbf{d}^T \bar{\mathbf{H}}_d \mathbf{x} = \mathbf{x}^T \bar{\mathbf{H}}_d \mathbf{d} \mathbf{d}^T \bar{\mathbf{H}}_d \mathbf{x} + \mathbf{f}^T \mathbf{f} - \mathbf{N} \mathbf{N}^T \quad (5.39a)$$

$$2\mathbf{x}^T \bar{\mathbf{H}}_d \mathbf{d} \mathbf{f} = \mathbf{x}^T \bar{\mathbf{H}}_d \mathbf{d} \mathbf{d}^T \bar{\mathbf{H}}_d \mathbf{x} + \mathbf{f}^T \mathbf{f} - \mathbf{N} \mathbf{N}^T \quad (5.39b)$$

$$\implies \mathbf{x}^T \bar{\mathbf{H}}_d \mathbf{d} \mathbf{f} \leq \mathbf{x}^T \bar{\mathbf{H}}_d \mathbf{d} \mathbf{d}^T \bar{\mathbf{H}}_d \mathbf{x} + \mathbf{f}^T \mathbf{f} \quad (5.39c)$$

Substituting equation (5.39c) in equation (5.37), we get the inequality

$$\dot{H}_d \leq -\mathbf{x}^T \bar{\mathbf{H}}_d \mathbf{R}_d \bar{\mathbf{H}}_d \mathbf{x} + \mathbf{x}^T \bar{\mathbf{H}}_d \mathbf{d} \mathbf{d}^T \bar{\mathbf{H}}_d \mathbf{x} + \mathbf{f}^T \mathbf{f} \quad (5.40)$$

which can be written as,

$$\dot{H}_d \leq -\mathbf{x}^T \bar{\mathbf{H}}_d^{\frac{1}{2}} (\bar{\mathbf{H}}_d^{\frac{1}{2}} \mathbf{R}_d \bar{\mathbf{H}}_d^{\frac{1}{2}}) \bar{\mathbf{H}}_d^{\frac{1}{2}} \mathbf{x} + \mathbf{x}^T \bar{\mathbf{H}}_d^{\frac{1}{2}} (\bar{\mathbf{H}}_d^{\frac{1}{2}} \mathbf{d} \mathbf{d}^T \bar{\mathbf{H}}_d^{\frac{1}{2}}) \bar{\mathbf{H}}_d^{\frac{1}{2}} \mathbf{x} + \mathbf{f}^T \mathbf{f} \quad (5.41)$$

If the disturbance \mathbf{f} is assumed to be bounded such that $\mathbf{f}^T \mathbf{f} \leq f_{max}$, and defining $\varepsilon = (2\lambda_{1min} - 2\lambda_{2max})$ where λ_{1min} corresponds to minimum eigen value of $(\bar{\mathbf{H}}_d^{\frac{1}{2}} \mathbf{R}_d \bar{\mathbf{H}}_d^{\frac{1}{2}})$ and λ_{2max} corresponds to maximum eigen value of $(\bar{\mathbf{H}}_d^{\frac{1}{2}} \mathbf{d} \mathbf{d}^T \bar{\mathbf{H}}_d^{\frac{1}{2}})$, the equation (5.41) can be written as

$$\dot{H}_d \leq -\varepsilon H_d + f_{max} \quad (5.42)$$

If $\bar{\mathbf{H}}_d$, and \mathbf{R}_d are chosen such that $\varepsilon > 0$, then the decay of $H_d(\mathbf{x}(t))$ can be guaranteed, and solution of equation (5.42) is given by

$$H_d(\mathbf{x}(t)) \leq \left\{ \left(H_d(\mathbf{x}(0)) - \frac{f_{max}}{\varepsilon} \right) e^{-\varepsilon t} + \frac{f_{max}}{\varepsilon} \right\} = \kappa \quad (5.43)$$

Therefore, trajectories of states with initial conditions $\mathbf{x}(0)$ in the region defined by,

$$\mathbf{x}(t) = \{ \mathbf{x}(0) \in \mathbb{R}^n | H_d(t) \leq \kappa \} \quad (5.44)$$

will stay inside the ellipsoid, which is the region of attraction, which proves the stability of the closed-loop system (equation(5.16)).

5.3 Case Studies

Two controller scenarios are shown in this section to demonstrate the versatility of the proposed approach. In each scenario, a distinct \mathbf{M}_d is chosen, and the associated closed-loop stiffness matrix \mathbf{K}_d is built based on structure of \mathbf{M}_d . The effect of \mathbf{M}_d on the closed-loop damping matrix \mathbf{D}_d , as well as its dependence on the additional interconnection matrix \mathbf{J}_a , is also highlighted. The relation between \mathbf{M}_d , \mathbf{D}_d and \mathbf{J}_a can be deduced from equation (5.34). For this purpose, \mathbf{J}_a and \mathbf{D}_d are parameterised as follows,

$$\mathbf{J}_a = \begin{bmatrix} 0 & -j_{a1} & -j_{a2} & -j_{a3} \\ j_{a1} & 0 & -j_{a4} & -j_{a5} \\ j_{a2} & j_{a4} & 0 & -j_{a6} \\ j_{a3} & j_{a5} & j_{a6} & 0 \end{bmatrix} \quad (5.45)$$

and

$$\mathbf{D}_d = \begin{bmatrix} d_1 & d_2 & d_3 & d_4 \\ d_2 & d_5 & d_6 & d_7 \\ d_3 & d_6 & d_8 & d_9 \\ d_4 & d_7 & d_9 & d_{10} \end{bmatrix} \quad (5.46)$$

5.3.1 Controller-I: Potential Energy Shaping and Damping Injection (PESADI)

In this scenario, the desired inertia matrix is selected as $\mathbf{M}_{d1} = \mathbf{M}$, suggesting that energy shaping is accomplished solely by modifying potential energy. Desired potential energy $\nu_d(\mathbf{q})$ is a function of \mathbf{K}_d , which must be Positive definite and symmetric is constructed using equation (5.31), and is given by

$$\mathbf{K}_{d1} = \begin{bmatrix} k_{sfd1} & \alpha_1 k_{sc1} & 0 & 0 \\ \alpha_1 k_{sc1} & k_{srd1} & 0 & 0 \\ 0 & 0 & k_{tf} & 0 \\ 0 & 0 & 0 & k_{tr} \end{bmatrix} \quad (5.47)$$

where $k_{sc1} = (k_{sfd1} \cdot k_{srd1})^{\frac{1}{2}}$ and $0 \leq \alpha_1^2 < 1$. The state-feedback gain vector λ_b corresponding to displacement vector \mathbf{q} can be deduced from equation (5.47). Closed-loop potential energy $\nu_d(\mathbf{q})$ can be shaped by varying the free parameters k_{sfd1}, k_{srd1}

and α_1 in the closed-loop stiffness matrix \mathbf{K}_{d1} . In this case, there is no direct control over tire stiffnesses, and cannot be altered explicitly, and can be seen by comparing diagonal entries \mathbf{k}_{33} and \mathbf{k}_{44} of \mathbf{K} with \mathbf{k}_{d133} and \mathbf{k}_{d144} of \mathbf{K}_{d1} . The desired damping matrix \mathbf{D}_{d1} is given as

$$\mathbf{D}_{d1} = \begin{bmatrix} d_1 & d_2 & d_3 & d_4 \\ d_2 & d_5 & d_6 & d_7 \\ d_3 & d_6 & d_8 & d_9 \\ d_4 & d_7 & d_9 & d_{10} \end{bmatrix} = \begin{bmatrix} d_1 & j_{a1} & j_{a2} & j_{a3} \\ j_{a1} & d_5 & j_{a4} & j_{a5} \\ j_{a2} & j_{a4} & b_{tf} & * \\ j_{a3} & j_{a5} & * & b_{tr} \end{bmatrix} \quad (5.48)$$

where $\mathbf{D}_{d1} > 0$. From \mathbf{D} and \mathbf{D}_{d1} in equation (5.8) and equation (5.48), d_1 and d_5 correspond to the closed-loop front and rear suspension damping coefficients, respectively, with \mathbf{J}_a terms acting as coupling between various velocity states $\dot{\mathbf{q}}$. The tire damping coefficients cannot be modified and remain the same as that of open-loop structure, as seen in terms \mathbf{D}_{d1ii} and \mathbf{D}_{ii} , with $i = 3, 4$. The free parameters to tune the closed-loop damping matrix are $d_1, d_5, j_{a1}, j_{a2}, j_{a3}, j_{a4}$ and j_{a5} . The term d_9 represents the coupling between front and rear tire damping coefficients, which cannot be modified, and hence represented by * notation.

5.3.2 Controller-II: Inertial Decoupling

The inertia matrix \mathbf{M}_d is chosen such that the coefficients in the inertia matrix which couple the unsprung mass momenta p_3 and p_4 to the sprung mass momenta p_1 and p_2 in the kinetic energy $\tau_d(\mathbf{p})$ are zero. The desired inertia matrix \mathbf{M}_{d2} is given by equation (5.49).

$$\mathbf{M}_{d2} = \begin{bmatrix} m_1 & m_3 & 0 & 0 \\ m_3 & m_2 & 0 & 0 \\ 0 & 0 & (m_1 + m_{wf}) & m_3 \\ 0 & 0 & m_3 & (m_2 + m_{wr}) \end{bmatrix} \quad (5.49)$$

Corresponding stiffness matrix \mathbf{K}_{d2} is then constructed as,

$$\mathbf{K}_{d2} = \begin{bmatrix} k_{sfd2} & \alpha_2 k_{sc2} & k_{sfd2} & \alpha_2 k_{sc2} \\ \alpha_2 k_{sc2} & k_{srd2} & \alpha_2 k_{sc2} & k_{srd2} \\ k_{sfd2} & \alpha_2 k_{sc2} & k_{sfd2} + \beta_1 k_{tf} & \alpha_2 k_{sc2} - \beta_3 k_{tf} \\ \alpha_2 k_{sc2} & k_{srd2} & \alpha_2 k_{sc2} - \beta_3 k_{tf} & k_{srd2} + \beta_2 k_{tr} \end{bmatrix} \quad (5.50)$$

where $k_{sfd2} > 0$, $k_{srd2} > 0$ and $0 \leq \alpha_2 < 1$ are free variables that can be used to modify $\nu_d(\mathbf{q})$, and $k_{sc2} = (k_{sfd2} \cdot k_{srd2})^{\frac{1}{2}}$. The terms β_1 , β_2 and β_3 are system parameters given by

$$\beta_1 = \frac{m_{wf}(m_2 + m_{wr})}{(m_1 + m_{wf})(m_2 + m_{wr}) - m_3^2} \quad (5.51a)$$

$$\beta_2 = \frac{m_{wr}(m_1 + m_{wf})}{(m_1 + m_{wf})(m_2 + m_{wr}) - m_3^2} \quad (5.51b)$$

$$\beta_3 = \frac{m_3 m_{wr}}{(m_1 + m_{wf})(m_2 + m_{wr}) - m_3^2} \quad (5.51c)$$

From matrix \mathbf{K}_{d2} in equation (5.50), it is evident that the effective (virtual) stiffness of all the springs in the system can be modified using this structure. Closed-loop damping matrix \mathbf{D}_{d2} is given by

$$\mathbf{D}_{d2} = \begin{bmatrix} d_1 & j_{a1} & j_{a2} - \frac{b_{tf} m_1}{m_{wf}} & j_{a3} - \frac{b_{tr} m_3}{m_{wr}} \\ j_{a1} & d_5 & j_{a4} - \frac{b_{tf} m_3}{m_{wf}} & j_{a5} - \frac{b_{tr} m_2}{m_{wr}} \\ j_{a2} - \frac{b_{tf} m_1}{m_{wf}} & j_{a4} - \frac{b_{tf} m_3}{m_{wf}} & \frac{b_{tf}(m_1 + m_{wf})}{m_{wf}} & * \\ j_{a3} - \frac{b_{tr} m_3}{m_{wr}} & j_{a5} - \frac{b_{tr} m_2}{m_{wr}} & * & \frac{b_{tr}(m_2 + m_{wr})}{m_{wr}} \end{bmatrix} \quad (5.52)$$

where the dissipative power can be shaped using free parameters d_1 , d_5 , j_{a1} , j_{a2} , j_{a3} , j_{a4} and j_{a5} .

The proposed half car controller cases are compared with controller designed by decoupling the half-car model into two quarter-car models, and designing IDA-PBC for front and rear systems independently.

5.3.3 Quarter-Car IDA-PBC Method (QCAR IDA-PBC)

The half-car system is decoupled into two quarter-car models whose mass sprung mass is distributed as:

$$m_{bf} = m_b \frac{l_r}{l_f + l_r} \quad , \quad m_{br} = m_b \frac{l_f}{l_f + l_r} \quad (5.53)$$

The PCH models of the front and rear systems are given by

$$\dot{\mathbf{x}}_i = [\mathbf{J}_i - \mathbf{R}_i] \nabla H_i(\mathbf{x}_i) + \mathbf{g}_i u_i + \mathbf{d}_i f_i \quad (5.54)$$

where, in this section, (i=f) corresponds to front, (i=r) corresponds to rear quarter-car system, $\mathbf{x}_i = (\mathbf{p}_i, \mathbf{q}_i) \in \mathbb{R}^n$ ($n = 4$) is the state vector, and $u_i \in \mathbb{R}^m$ ($m = 1$) is the actuator input vector. Road velocity input to the system is represented by $f_i = \dot{x}_{ri}(t) \in \mathbb{R}$. Vectors $\mathbf{q}_i \in \mathbb{R}^2$ and $\mathbf{p}_i \in \mathbb{R}^2$ represent the generalised displacement and momenta coordinates, respectively, defined as

$$\mathbf{q}_i = \begin{bmatrix} q_{1i} \\ q_{2i} \end{bmatrix} \triangleq \begin{bmatrix} x_{bi} - x_{wi} \\ x_{wi} - x_{ri} \end{bmatrix} \quad (5.55a)$$

$$\mathbf{p}_i = \begin{bmatrix} p_{1i} \\ p_{2i} \end{bmatrix} = \begin{bmatrix} m_{bi} x_{bi} \\ m_{bi} x_{bi} + m_{wi} x_{wi} \end{bmatrix} \quad (5.55b)$$

The Hamiltonian $H_i(\mathbf{x}_i) = H_i(\mathbf{p}_i, \mathbf{q}_i)$, written in terms of its kinetic and potential energies, $\tau_i(\mathbf{p}_i)$ and $\nu_i(\mathbf{q}_i)$, respectively as,

$$H_i(\mathbf{x}) = \tau_i(\mathbf{p}_i) + \nu_i(\mathbf{q}_i) = \frac{1}{2} \mathbf{p}_i^T \mathbf{M}_i^{-1} \mathbf{p}_i + \frac{1}{2} \mathbf{q}_i^T \mathbf{K}_i \mathbf{q}_i \quad (5.56a)$$

$$= \frac{1}{2} \begin{bmatrix} \mathbf{p}_i^T & \mathbf{q}_i^T \end{bmatrix} \begin{bmatrix} \mathbf{M}_i^{-1} & \mathbf{0} \\ \mathbf{0} & \mathbf{K}_i \end{bmatrix} \begin{bmatrix} \mathbf{p}_i \\ \mathbf{q}_i \end{bmatrix} = \frac{1}{2} \mathbf{x}_i^T \bar{\mathbf{H}}_i \mathbf{x}_i \quad (5.56b)$$

where the inertia and stiffness matrices \mathbf{M}_i and \mathbf{K}_i are given by,

$$\mathbf{M}_i = \begin{bmatrix} m_{bi} & m_{bi} \\ m_{bi} & m_{bi} + m_{wi} \end{bmatrix} \quad , \quad \mathbf{K}_i = \begin{bmatrix} k_{si} & 0 \\ 0 & k_{ti} \end{bmatrix} \quad (5.57)$$

The interconnection and dissipative structures \mathbf{J}_i and \mathbf{R}_i are given by,

$$\mathbf{J}_i = \begin{bmatrix} \mathbf{0} & -\mathbf{I} \\ \mathbf{I} & \mathbf{0} \end{bmatrix} \quad \text{and} \quad \mathbf{R}_i = \begin{bmatrix} \mathbf{D}_i & \mathbf{0} \\ \mathbf{0} & \mathbf{0} \end{bmatrix} \quad (5.58)$$

Damping matrices \mathbf{D}_i are defined as

$$\mathbf{D}_i = \begin{bmatrix} b_{si} & 0 \\ 0 & b_{ti} \end{bmatrix} \quad (5.59)$$

The matrices \mathbf{g}_i and \mathbf{d}_i are defined as $\mathbf{g}_i = [1 \ 0 \ 0 \ 0]^T$, and $\mathbf{d}_i = [0 \ b_{ti} \ 0 \ -1]^T$. The closed-loop control system design for the Quarter car is not shown here, and can be derived using the algebraic method proposed in previous sections, or conventional method of solving PDEs, which is shown in chapter 3. The structure of the closed-loop system for quarter-car models is given by

$$\dot{\mathbf{x}}_i = [\mathbf{J}_{\mathbf{d}i} - \mathbf{R}_{\mathbf{d}i}] \nabla \mathbf{H}_{\mathbf{d}i}(\mathbf{x}_i) + \mathbf{d}_i f_i \quad (5.60)$$

where $\mathbf{J}_{\mathbf{d}i}$ and $\mathbf{R}_{\mathbf{d}i}$ is given by

$$\mathbf{J}_{\mathbf{d}i} = \begin{bmatrix} \mathbf{J}_{\mathbf{q}i} & -\mathbf{M}_{\mathbf{d}i} \mathbf{M}_i^{-1} \\ \mathbf{M}_i^{-1} \mathbf{M}_{\mathbf{d}i} & \mathbf{0} \end{bmatrix}, \quad \mathbf{R}_{\mathbf{d}i} = \begin{bmatrix} \mathbf{D}_{\mathbf{d}i} & \mathbf{0} \\ \mathbf{0} & \mathbf{0} \end{bmatrix} \quad (5.61)$$

The closed-loop energy functions of the quarter car systems are denoted as:

$$H_{\mathbf{d}i}(\mathbf{x}_i) = \frac{1}{2} \begin{bmatrix} \mathbf{p}_i^T & \mathbf{q}_i^T \end{bmatrix} \begin{bmatrix} \mathbf{M}_{\mathbf{d}i}^{-1} & \mathbf{0} \\ \mathbf{0} & \mathbf{K}_{\mathbf{d}i} \end{bmatrix} \begin{bmatrix} \mathbf{p}_i \\ \mathbf{q}_i \end{bmatrix} = \frac{1}{2} \mathbf{x}_i^T \bar{\mathbf{H}}_{\mathbf{d}i} \mathbf{x}_i \quad (5.62)$$

The closed-loop inertia and stiffness matrices for the quarter-car active suspension design are chosen from case of ESDIID in chapter 3 as follows,

$$\mathbf{M}_{\mathbf{d}i} = \begin{bmatrix} m_{bi} & 0 \\ 0 & m_{bi} + m_{wi} \end{bmatrix} \quad (5.63)$$

$$\mathbf{K}_{\mathbf{d}i} = \begin{bmatrix} k_{zi} & k_{zi} \\ k_{zi} & k_{ti} \left(\frac{m_{wi}}{m_{bi} + m_{wi}} \right) + k_{zi} \end{bmatrix} \quad (5.64)$$

$$\mathbf{D}_{di} = \begin{bmatrix} b_{1i} & j_{qi} - b_{ti} \frac{m_{bi}}{m_{wi}} \\ j_{qi} - b_{ti} \frac{m_{bi}}{m_{wi}} & b_{ti} \left(\frac{m_{bi} + m_{wi}}{m_{wi}} \right) \end{bmatrix} \quad (5.65)$$

where $k_{zf}, k_{zr}, b_{1f}, b_{1r}, j_{qf}$ and j_{qr} are the free parameters to tune the closed-loop front and rear quarter car models.

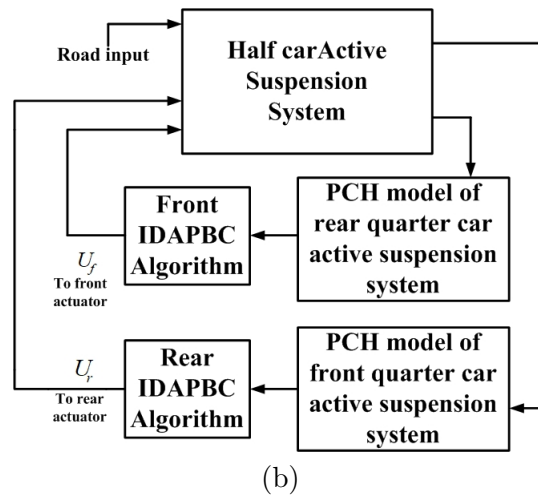
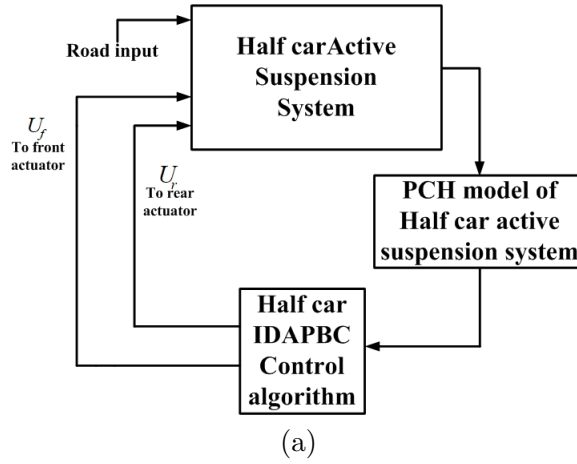


Figure 5.2: Control configurations (a) for PESADI, Inertial decoupling (b) QCAR IDAPBC

5.4 Simulation and Discussion

In this section, the effectiveness of the proposed method is discussed using an illustration example. The half car parameters are taken from Liu et al. (2016), given as $m_b = 1200$ kg, $m_{wf} = m_{wr} = 100$ kg, $I_\phi = 600$ kg.m², $k_{sf} = k_{sr} = 15000$ N/m, $b_{sf} = b_{sr} = 1500$ N.s/m, $k_{tf} = k_{tr} = 200000$ N/m, $b_{tf} = b_{tr} = 2000$ N.s/m, $l_f = 1.5$ m and $l_r = 1.2$ m. The suspension deflection limit SS_{max} is considered as 0.1 m. The maximum force deliverable by the actuators is limited to 5 kN. Road profile given in Ma and Chen (2011) is used for analysis, which is mathematically expressed as,

$$\dot{x}_{rf}(t) = \begin{cases} \frac{\pi VA}{L} \sin \frac{2\pi V}{L} t & 0 \leq t \leq \frac{L}{V} \\ 0 & t > \frac{L}{V} \end{cases} \quad (5.66)$$

where A is height of the bump, V is the forward velocity of the vehicle, and L is the length of the bump. The road input for rear tire $\dot{x}_{rr}(t)$ is considered same as that of front tire, except that it is delayed in time by $\frac{L}{V}$. The parameters of the road profile are chosen as $L = 5m$, $A = 0.1m$ and $V = 45\text{kmph}$, representing an isolated bump on a smooth road surface when vehicle is moving with a forward velocity of $V = 45\text{kmph}$. The closed-loop parameters for PESADI are chosen as follows:

- $\mathbf{M}_d = \mathbf{M}_{d1} = \mathbf{M}$, $k_{sfd1} = 15$, $k_{srd1} = 15$, $\alpha_1 = 0.9$, $d_1 = b_{sf} = 1500$, $d_5 = b_{sr} = 1500$, $j_{a1} = 0$, $j_{a2} = 0$, $j_{a3} = 0$, $j_{a4} = 0$, $j_{a5} = 0$.

In PESADI, the virtual tire stiffnesses of tires in the closed-loop cannot be altered, as seen from the stiffness matrix \mathbf{K}_d in equation (5.47). Lower values of the closed-loop suspension stiffness coefficients k_{sfd1} and k_{srd1} are used while the damping coefficients remain unchanged. This makes the suspension softer and isolates the chassis from road disturbances by reducing the force on chassis due to road excitations. This can be confirmed by comparing the uncontrolled system time responses of the forces \dot{p}_1 and \dot{p}_2 with the responses using PESADI, shown in Figure 5.3. Front and rear suspension strokes can be controlled by tuning the corresponding closed-loop damping coefficients d_1 and d_5 , respectively, along with the other coefficients in the matrix D_d in Equation (5.48). However, the tire responses cannot be altered directly as there are no control parameters directly influencing their performances. The corresponding RDTLs of front and rear tires are shown in Figure 5.8.

The closed-loop control parameters of the proposed Inertial decoupling controller are

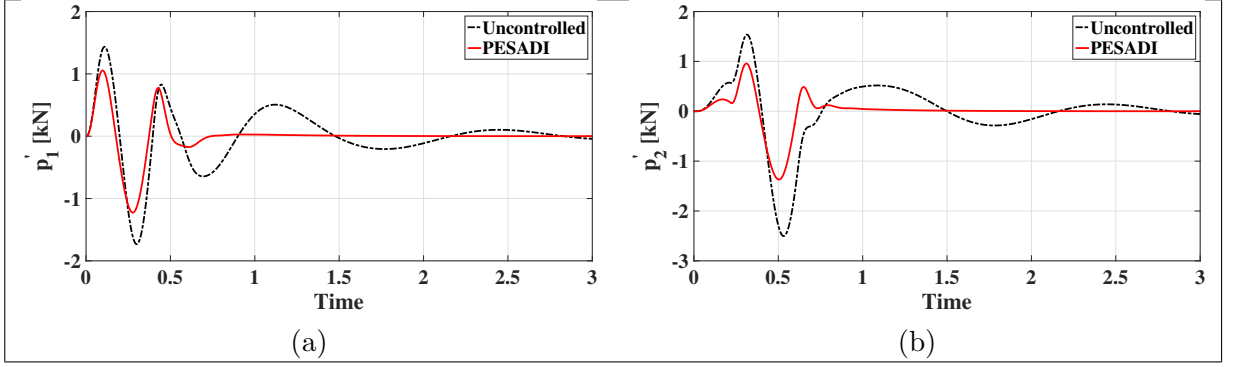


Figure 5.3: Time responses of PESADI Controller design: (a) \dot{p}_1 , (b) \dot{p}_2

given as: $k_{sfd2} = 300000$, $k_{srd2} = 480000$ and $\alpha_2 = -0.5$, $d_1 = 66000$, $d_5 = 75000$, $j_{a1} = 15000$, $j_{a2} = 12000$, $j_{a3} = 9000$, $j_{a4} = 4279$ and $j_{a5} = 6000$.

The process of energy shaping and damping injection for controller design is shown in Figure 5.4. Set1 corresponds to the case of kinetic energy shaping via selection of desired inertia matrix \mathbf{M}_{d2} , and setting the closed-loop free parameters in the desired stiffness and damping matrices \mathbf{K}_{d2} and \mathbf{D}_{d2} same as the of the uncontrolled parameters. The change in structure of \mathbf{M}_d increases the effective tire damping in this case. This can be observed by comparing the coefficients \mathbf{D}_{33} , \mathbf{D}_{44} of the damping matrix in equation (5.8) with closed-loop damping matrix coefficients \mathbf{D}_{d233} , \mathbf{D}_{d244} in equation (5.52). Increase in the effective tire stiffnesses is also observed by comparing the tire stiffness matrices \mathbf{K} and \mathbf{K}_{d2} , along with coupling between the stiffness coefficients in \mathbf{K}_{d2} . Increase in the tire stiffness and damping coefficients results in reduction in tire deflections and velocities, resulting in significant improvement in RDTLs of the system, whose responses are shown in Figures 5.5(a) and 5.5(b). Disturbance is attenuated at unsprung mass and sprung mass is isolated from the effect of disturbance, which can be seen from the time response of the forces \dot{p}_1 and \dot{p}_2 in Figure 5.5(c) and Figure 5.5(d).

Increased suspension strokes of front and rear suspensions as a result of higher tire stiffness and damping coefficients in set1 are controlled by shaping the closed-loop potential energy via free parameters k_{sfd} , k_{srd} and α in matrix \mathbf{K}_{d1} . Front suspension stroke can be modified by tuning the parameter k_{sfd} , while k_{srd} is used to control rear suspension stroke. The parameter α acts as coupling coefficient between front and rear suspension strokes, which can alter the vertical and angular displacements x_c and ϕ of the sprung mass. Time responses of the suspension strokes for set1 and

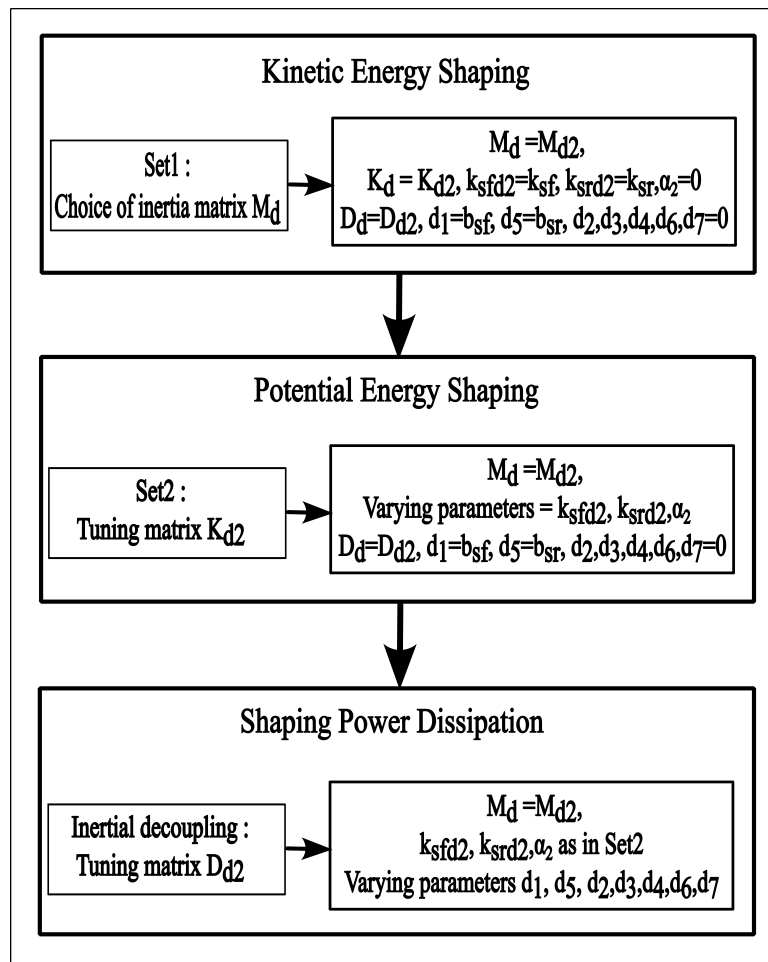


Figure 5.4: Sequence of Inertial decoupling controller tuning

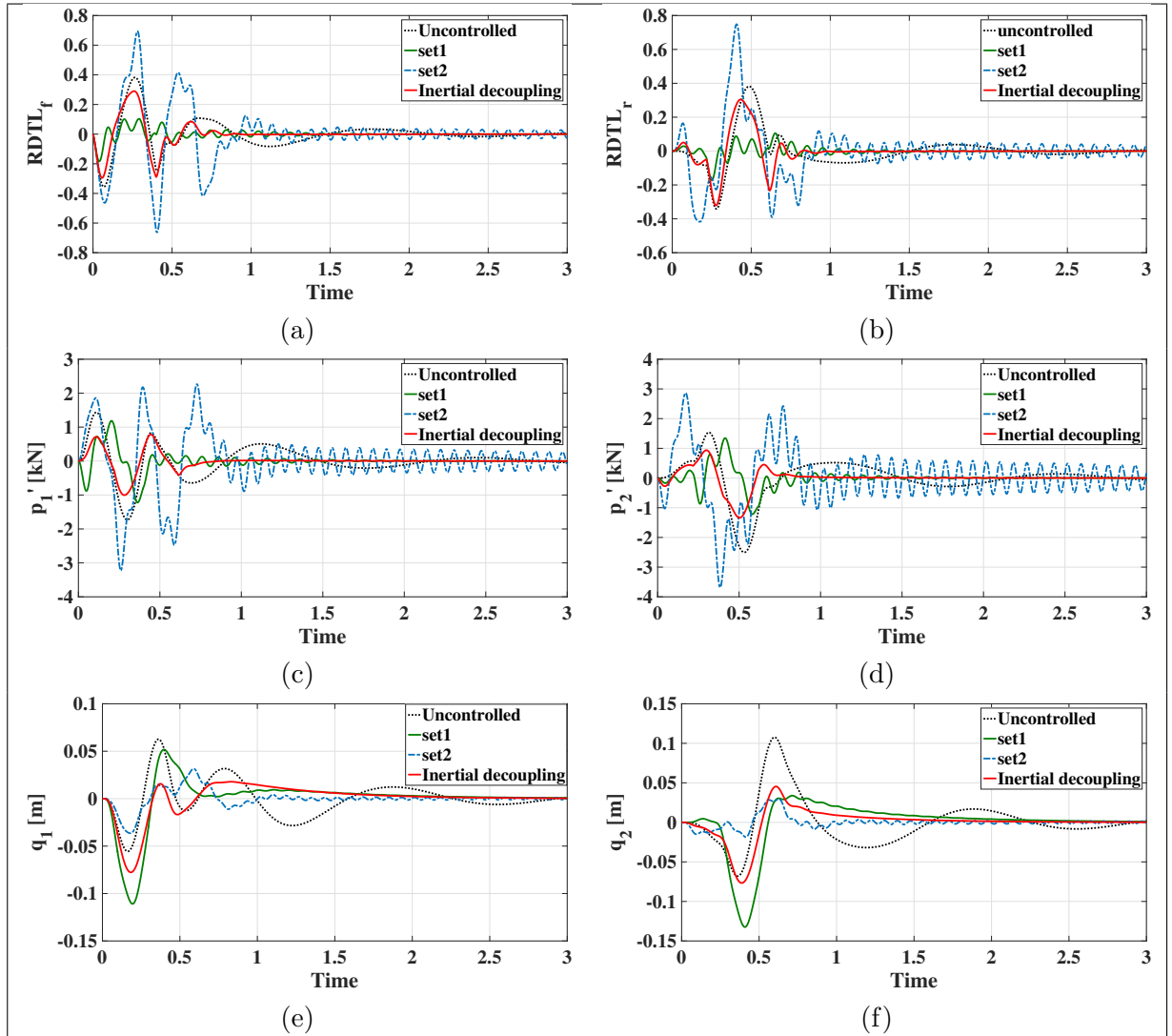


Figure 5.5: Time responses of Inertial decoupling Controller design: (a) $RDTL_f$, (b) $RDTL_r$, (c) \dot{p}_1 , (d) \dot{p}_2 , (e) q_1 and (f) q_2

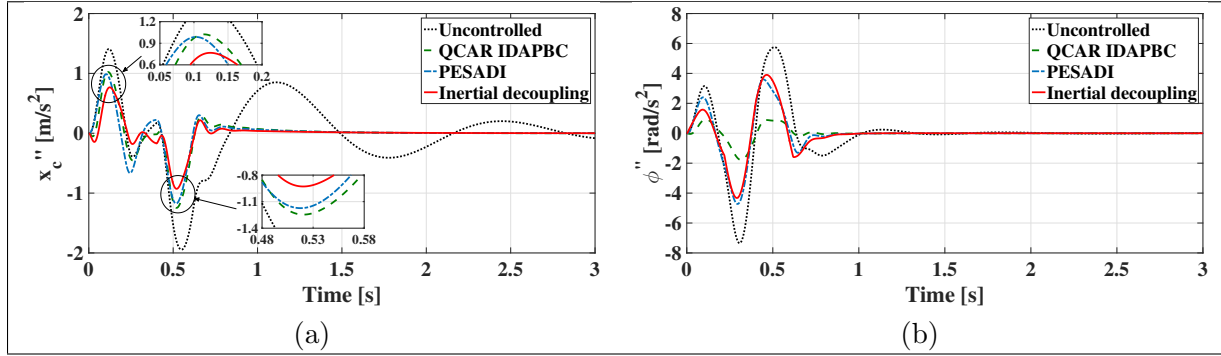


Figure 5.6: Simulation results for Acceleration: (a) Heave acceleration and (b) Pitch acceleration

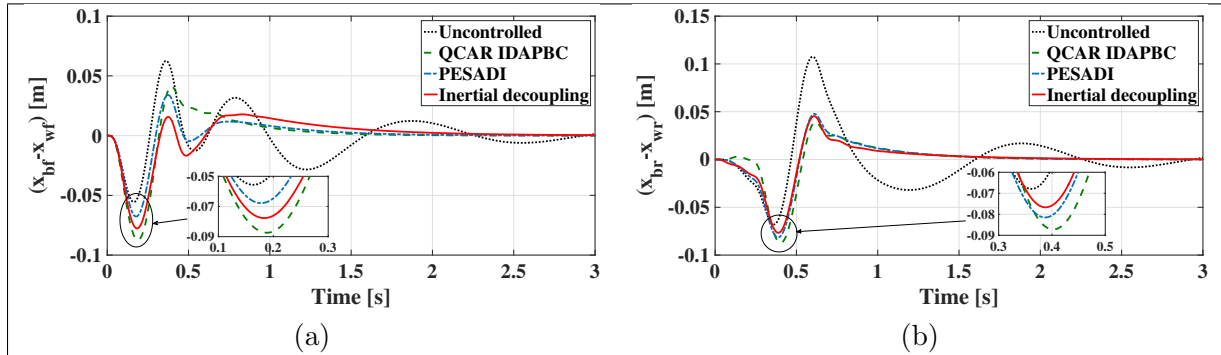


Figure 5.7: Simulation results for Suspension deflection: (a) front and (b) rear

set2 conditions are presented in Figure 5.5(e) and Figure 5.5(f). Finally, the power dissipation is shaped by tuning free variables in damping matrix \mathbf{D}_{d1} in Equation (5.52) to improve the overall response and settling time of the system.

Figure 5.6 illustrates the comparison of responses of vertical and angular accelerations of the uncontrolled system and the proposed control method. Results of the closed-loop system designed by decoupling the half car model into quarter car model and designing IDA-PBC for front and rear actuators are also shown for comparison purposes. Both PESADI and Inertial decoupling controller minimise the peak value of accelerations and settling times, thus improving the ride comfort of the closed-loop system. Significant improvement can be seen in the angular acceleration with PESADI when compared to performance of inertial decoupling controller. However, control over RDTL is limited with PESADI, as there are no direct control parameters associated with RDTL in PESADI. Whereas in inertial decoupling, the

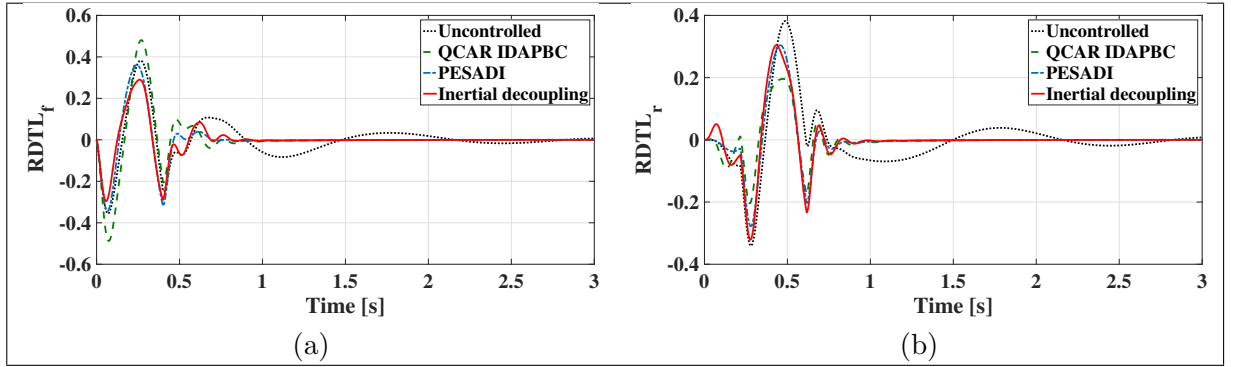


Figure 5.8: Simulation results for Relative dynamic tire load: (a) front and (b) rear

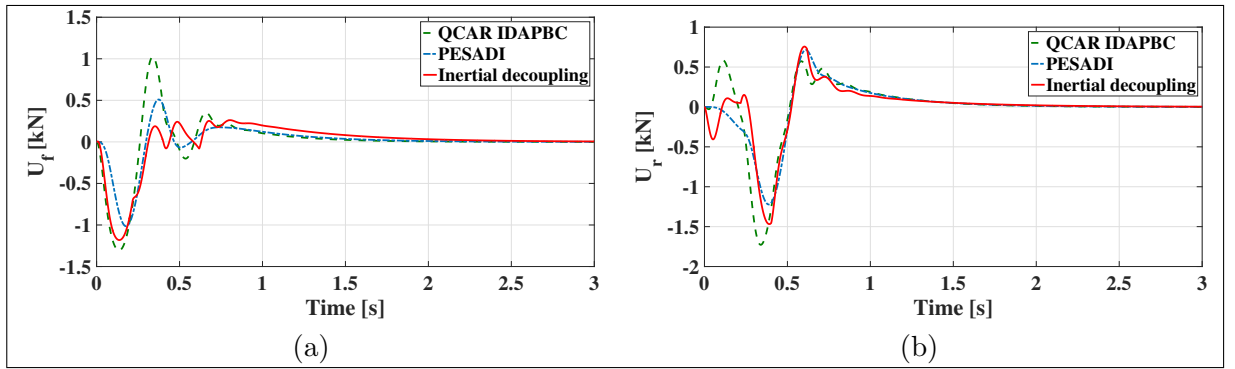


Figure 5.9: Simulation results for Actuator forces: (a) front and (b) rear

Table 5.1: RMS values of performance indices

Type of Controller	Acceleration		Suspension deflection	
	Heave	Pitch	front	rear
	\ddot{x}_c (m/s^2)	$\ddot{\phi}$ (rad/s^2)	$q_1(m)$	$q_2(m)$
Uncontrolled	0.5831	1.8848	0.02	0.0308
QCAR IDAPBC	0.2859	0.3908	0.0207	0.0207
PESADI	0.2797	1.1475	0.0151	0.0208
Inertial decoupling	0.2072	1.1159	0.0179	0.0189

Table 5.2: RMS values of performance indices

Type of Controller	RDTL		Actuator force	
	front	rear	front	rear
	ratio	ratio	$u_f(\text{N})$	$u_r(\text{N})$
Uncontrolled	0.1017	0.0990	-	-
QCAR IDAPBC	0.1173	0.0558	332.52	388.47
PESADI	0.0927	0.0752	226.74	311.96
Inertial decoupling	0.0785	0.0813	277.69	320.05

change in structure of \mathbf{M}_d directly effects the RDTL, thus giving control over the ride stability. Then the ride comfort can be improved by appropriate selection of free parameters in stiffness and damping matrices. Therefore, PESADI can be considered as a *ride comfort improvement oriented method*, whereas inertial decoupling can be considered as *ride stability improvement method*, as the controller tuning in inertial decoupling method starts with improvement in RDTL. The suspension deflections can be minimised in both inertial decoupling and PESADI methods by tuning the control parameters as explained in the previous sections, and the time responses of the same are shown in Figure 5.7. Comparison of RDTLs of the closed-loop system with proposed controller along with uncontrolled system are illustrated in Figure 5.8, which show good improvement with proposed method. The actuator responses of the system are plotted for different control structures in Figure 5.9, which are well within the allowable limits, and there RMS values can be found in Table 5.1. From the time responses of performance indices in Figures 5.6-5.9, it is seen that the performance of QCAR IDA-PBC, which is designed by decoupling half car model model into front and rear quarter car models is comparable to that of the proposed method. However, the major disadvantage QCAR IDA-PBC is that when the control gains are tuned independently for front and rear systems, and combined to control half car model, stability of the overall system cannot be guaranteed. Moreover, this approach loses the importance of designing the closed-loop system using physical parameters of the system as overall system is not considered while tuning the control gains.

The above discussions suggest that the performance of the half car active suspension system can be significantly improved using the proposed IDA-PBC technique.

Moreover, the proposed algebraic IDA-PBC method reduces the design complexity by avoiding the necessity of solving PDEs, which generally is a complex task. By proposer choice of desired inertia matrix \mathbf{M}_d , the orientation of control design can be changed to either ride comfort oriented or ride stability oriented, based on the type of vehicle. The change in structure of \mathbf{M}_d gives more flexibility and control over performance requirements. The choice of desired inertia matrix plays a crucial role in modifying the structure of the controller, and the system can be understood in terms of how the controller effects the physical parameters like inertia, damping and stiffness by comparing the open-loop and closed-loop matrices in each case, which is the main idea behind IDA-PBC in mechanical systems.

5.5 Summary

In this chapter, an interconnection and damping assignment passivity-based control system for a half car active suspension system was presented. The control law is designed using a port controlled hamiltonian model, which characterises the system in terms of its physical properties. By translating the problem into matrix equations and obtaining an algebraic solution, the general challenge of solving partial differential equations to determine the state-feedback law is avoided. The efficiency of the proposed controller is proved through case studies in which two specific situations are obtained by selecting the desired inertia matrix and constructing the associated effective stiffness and damping matrices for these cases. The simulation results for these scenarios are analysed and given in terms of time responses and RMS values. It is demonstrated that the suggested control law effectively meets the design objectives of increasing the active suspension system's ride comfort and ride stability.

Chapter 6

Conclusions and Future scope

Interconnection and Damping Assignment Passivity Based Control is designed for performance improvement of Active suspension systems. The proposed control method is designed for two systems, namely quarter-car and half-car active suspension systems. The control law is designed by shaping the closed-loop energy function and modifying the system's interconnection and damping structures. The main requirements of active suspension system, which are improvement in ride comfort and stability, while adhering to the limitations of suspension stroke are met by modifying the closed-loop system's physical properties. Using the port-Hamiltonian framework to model the system, physical parameters of the open-loop and closed-loop systems, such as inertia, stiffness, and damping coefficients, are used in the controller design. The contributions, main conclusive remarks and the future scope of this thesis are presented below.

6.1 Contributions

1. **Design and Development of closed-loop control of Quarter-car and Half-car active suspension systems in the PCH framework:** Designed and implementation of IDA-PBC was carried out for control of quarter-car and half-car active suspension systems modelled in PCH framework. Improvement in ride comfort and ride stability were achieved while constraining the suspension stroke within the prescribed limits. Analysis of the performance of controller in improving various requirements of the system with change in inertia matrix was also carried out. A step-by step procedure for tuning the controllers based on

time and frequency response characteristics is explained. The control algorithm developed for a quarter-car system was implemented on hardware and the design was verified.

2. **Design of a state-observer in PCH framework:** The design of the observer is performed in the PCH framework to incorporate it in the quarter-car closed loop control. Stability analysis was carried out on the observer and finally implemented on the hardware. The performance of the controller in presence of the state-estimation by the observer is demonstrated with hardware results.
3. **Development of an algebraic solution for solving matching equation in design of IDA-PBC for half-car suspension system:** Solution of matching equation was derived using an algebraic method, avoiding the obstacle of solving complex PDEs to obtain the state feedback law. The controller design is simplified into construction of a positive definite matrix which defines the closed-loop potential energy function after shaping the closed-loop kinetic energy by choice of desired inertia matrix. The desired inertia matrix was chosen based on the results derived from the quarter-car IDA-PBC design, which makes the controller design intuitive and straight forward.

6.2 Conclusions and Remarks

6.2.1 Control Of Quarter-Car Active Suspension System

A good improvement in ride comfort, stability and suspension deflection is achieved using the IDA-PBC. Choice of the closed-loop inertia matrix plays a very important role in the control configuration of the closed-loop system. Structure of closed-loop stiffness and damping coefficients depends on the structure of inertia matrix. As the structure of closed-loop inertia matrix is varied using α from zero to one, the disturbance is attenuated at the unsprung mass itself. For improvement in ride comfort, road holding and suspension stroke, it is required to modify the structure of inertia matrix. With change in the structure of inertia matrix, the control configuration requires all the states for implementation.

Port-Hamiltonian observer designed using only suspension deflection as the measurable output shows a good performance in terms of tracking the actual states in pres-

ence of road disturbances. The effectiveness of the observer is experimentally verified by implementing full-state IDA-PBC using the state-estimates obtained from the observer design. The performance of the closed-loop system is effective and comparable to that of the system controlled with full-state feedback.

6.2.2 Control Of Half-Car Active Suspension System

The algebraic solution proposed for solving the matching equation of IDA-PBC simplifies the controller design effectively compared to the conventional method, which requires solution of PDEs. The choice of the closed-loop inertia matrix, plays a very important role in deriving the closed-loop stiffness and damping matrices in algebraic IDA-PBC method. The choice of inertia matrix can be made for half-car system using the notion of inertia matrix structure used for quarter-car active suspension system controller design. This makes the controller design simple and effective. Based on the choice of inertia matrix, the controller can be designed either in ride comfort oriented or road holding oriented manner. The results of the proposed controller show good improvement of the closed-loop system in terms of peak and RMS values.

6.3 Future Scope

Based on the research carried out in this thesis, the recommendations for future research are presented.

- In the present study, the system is modelled as a linear time invariant system. However, the actual system may include non-linearities and uncertainties. The research can be extended to update the control law to address issues.
- Actual dynamics of the actuator are not linear. Research can be extended to include the actuator dynamics in the design.
- Observer design considering non-linearities and uncertainties can be researched. An extended observer design to estimate the disturbance effect can be attempted to minimise the error dynamics and design the observer accurately.
- The algebraic IDA-PBC controller method proposed for half-car active suspension can be used to design and analyse the controller for full-vehicle system to improve heave, pitch and roll dynamics.

- The controller design can be carried out to address lateral, and longitudinal dynamics of the vehicle.

Appendix A

Port-Hamiltonian Model Of Quarter-Car Active Suspension System

A lumped-parameter model of the quarter-car active suspension system is shown in figure 3.1. The coordinates x_w and x_b are the wheel and body displacements from their respective equilibrium positions, and $x_r(t)$ is the time-varying road position. The generalised coordinates $q_1 \triangleq x_w - x_r(t)$ and $q_2 \triangleq x_b - x_w$. Using these coordinates, the kinetic energy is given by

$$\tau(\dot{\mathbf{q}}, t) = \frac{1}{2}m_w(\dot{x}_r(t) + \dot{q}_1)^2 + \frac{1}{2}m_b(\dot{x}_r(t) + \dot{q}_1 + \dot{q}_2)^2 \quad (\text{A.1})$$

The potential energy is given by

$$\nu(\mathbf{q}) = \frac{1}{2}k_t q_1^2 + \frac{1}{2}k_s q_2^2 \quad (\text{A.2})$$

The Rayleigh dissipation function $\mathbf{D}(\dot{\mathbf{q}})$ represents the power lost to the environment by the dissipative elements. The power dissipated by the damper can be written as

$$\mathbb{D}(\dot{\mathbf{q}}) = \frac{1}{2}b_t \dot{q}_1^2 + \frac{1}{2}b_s \dot{q}_2^2 \quad (\text{A.3})$$

The Lagrangian for the system without considering the external forces (conserva-

tive system) is given by

$$L(\mathbf{q}, \dot{\mathbf{q}}, t) = \tau(\dot{\mathbf{q}}, t) - \nu(\mathbf{q}) \quad (\text{A.4})$$

$$L(\mathbf{q}, \dot{\mathbf{q}}, t) = \left(\frac{1}{2}m_w(\dot{x}_r(t) + \dot{q}_1)^2 + \frac{1}{2}m_b(\dot{x}_r(t) + \dot{q}_1 + \dot{q}_2)^2\right) - \left(\frac{1}{2}k_t q_1^2 + \frac{1}{2}k_s q_2^2\right) \quad (\text{A.5})$$

The conjugate momenta are given by

$$p_1 \triangleq \frac{\partial L}{\partial \dot{q}_1} = m_w(\dot{x}_r(t) + \dot{q}_1) + m_b(\dot{x}_r(t) + \dot{q}_1 + \dot{q}_2) = m_w \dot{x}_w + m_b \dot{x}_b \quad (\text{A.6})$$

$$p_2 \triangleq \frac{\partial L}{\partial \dot{q}_2} = m_b(\dot{x}_r(t) + \dot{q}_1 + \dot{q}_2) = m_b \dot{x}_b \quad (\text{A.7})$$

The Kinetic energy written in terms of the momenta is given by

$$\tau(\mathbf{p}) = \frac{1}{2} \mathbf{p}^T \mathbf{M}^{-1} \mathbf{p} \quad (\text{A.8})$$

where

$$\mathbf{M} = \begin{bmatrix} m_w + m_b & m_b \\ m_b & m_b \end{bmatrix} \quad (\text{A.9})$$

The Hamiltonian of the system which is the storage function is defined by

$$H(\mathbf{p}, \mathbf{q}) = \frac{1}{2} \mathbf{p}^T \mathbf{M}^{-1} \mathbf{p} + \nu(\mathbf{q}) \quad (\text{A.10})$$

Generalised velocities \dot{q}_1 and \dot{q}_2 can be written in terms of the Hamiltonian as

$$\dot{q}_1 = \frac{\partial H}{\partial p_1} - \dot{x}_r(t) \quad (\text{A.11})$$

$$\dot{q}_2 = \frac{\partial H}{\partial p_2} \quad (\text{A.12})$$

Differentiating Rayleigh dissipation function with respect to generalised velocities,

$$\frac{\partial \mathbb{D}}{\partial \dot{q}_1} = b_t \dot{q}_1 = b_t \left(\frac{\partial H}{\partial p_1} - \dot{x}_r(t) \right) \quad (\text{A.13})$$

$$\frac{\partial \mathbb{D}}{\partial \dot{q}_2} = b_s \dot{q}_2 = b_s \frac{\partial H}{\partial p_2} \quad (\text{A.14})$$

The momenta dynamics are given by

$$\dot{p}_1 = -\frac{\partial H}{\partial q_1} - \frac{\partial \mathbb{D}}{\partial \dot{q}_1} \quad (\text{A.15})$$

$$\dot{p}_1 = -\frac{\partial H}{\partial q_1} - b_t \left(\frac{\partial H}{\partial p_1} - \dot{x}_r(t) \right) \quad (\text{A.16})$$

$$\dot{p}_1 = -\frac{\partial H}{\partial q_1} - b_t \frac{\partial H}{\partial p_1} + b_t \dot{x}_r(t) \quad (\text{A.17})$$

$$\dot{p}_2 = -\frac{\partial H}{\partial q_2} - \frac{\partial \mathbb{D}}{\partial \dot{q}_2} + u_s \quad (\text{A.18})$$

$$\dot{p}_2 = -\frac{\partial H}{\partial q_2} - b_s \frac{\partial H}{\partial p_2} + u_s \quad (\text{A.19})$$

The equations A.11 to A.18 can be written in matrix forms as

$$\begin{bmatrix} \dot{p}_1 \\ \dot{p}_2 \\ \dot{q}_1 \\ \dot{q}_2 \end{bmatrix} = \begin{bmatrix} -b_t & 0 & -1 & 0 \\ 0 & -b_s & 0 & -1 \\ 1 & 0 & 0 & 0 \\ 0 & 1 & 0 & 0 \end{bmatrix} \begin{bmatrix} \frac{\partial H}{\partial p_1} \\ \frac{\partial H}{\partial p_2} \\ \frac{\partial H}{\partial q_1} \\ \frac{\partial H}{\partial q_2} \end{bmatrix} + \begin{bmatrix} 0 \\ 1 \\ 0 \\ 0 \end{bmatrix} u_s + \begin{bmatrix} b_t \\ 0 \\ -1 \\ 0 \end{bmatrix} \dot{x}_r(t) \quad (\text{A.20})$$

Matrix equation A.20 represents the system in Port-Hamiltonian form with force and velocity inputs,

$$\begin{bmatrix} \dot{\mathbf{p}} \\ \dot{\mathbf{q}} \end{bmatrix} = \begin{bmatrix} -\mathbf{D} & -\mathbf{I} \\ \mathbf{I} & \mathbf{0} \end{bmatrix} \begin{bmatrix} \nabla_{\mathbf{p}} H \\ \nabla_{\mathbf{q}} H \end{bmatrix} + \begin{bmatrix} \mathbf{G} \\ \mathbf{0} \end{bmatrix} u_s + \begin{bmatrix} \mathbf{G}_1 \\ \mathbf{G}_2 \end{bmatrix} \dot{x}_r(t) \quad (\text{A.21})$$

where, $\dot{\mathbf{p}} = [\dot{p}_1 \ \dot{p}_2]^T$, $\dot{\mathbf{q}} = [\dot{q}_1 \ \dot{q}_2]^T$, $\nabla_{\mathbf{p}} H = \left[\frac{\partial H}{\partial p_1} \ \frac{\partial H}{\partial p_2} \right]^T$, $\nabla_{\mathbf{q}} H = \left[\frac{\partial H}{\partial q_1} \ \frac{\partial H}{\partial q_2} \right]^T$, $\mathbf{G} = [0 \ 1]^T$, $\mathbf{G}_1 = [b_t \ 0]^T$ and $\mathbf{G}_2 = [-1 \ 0]^T$. The matrix \mathbf{D} is given by,

$$\mathbf{D} = \begin{bmatrix} b_t & 0 \\ 0 & b_s \end{bmatrix} \quad (\text{A.22})$$

Appendix B

Port-Hamiltonian Model Of Half-Car Active Suspension System

A lumped-parameter model of the half-car active suspension system is shown in figure 5.1. The open loop potential energy of the system is given by

$$\nu = \frac{1}{2}k_{sf}(x_{bf} - x_{wf})^2 + \frac{1}{2}k_{sr}(x_{br} - x_{wr})^2 + \frac{1}{2}k_{tf}(x_{wf} - x_{rf})^2 + \frac{1}{2}k_{tr}(x_{wr} - x_{rr})^2 \quad (\text{B.1})$$

Open loop kinetic energy is given by

$$\tau = \frac{1}{2}m_{wf}\dot{x}_{wf}^2 + \frac{1}{2}m_{wr}\dot{x}_{wr}^2 + \frac{1}{2}m_b\dot{x}_c^2 + \frac{1}{2}I_\phi\dot{\phi}^2 \quad (\text{B.2})$$

Defining the generalised displacement coordinates $q_1 \triangleq (z_{sf} - z_{uf})$, $q_2 \triangleq (z_{sr} - z_{ur})$, $q_3 \triangleq (z_{uf} - z_{rf})$ and $q_4 \triangleq (z_{ur} - z_{rr})$. If $E(\mathbf{x})$ is a continuously differential function, partial derivative of E , $\partial E/\partial \mathbf{x}$ is denoted as $\nabla_{\mathbf{x}}E$.

Some useful relations

- $x_{bf} = x_c + l_f\phi$
- $x_{br} = x_c - l_r\phi$
- $\phi = \frac{1}{l}(x_{bf} - x_{br})$
writing ϕ in terms of displacement coordinates
- $\phi = \frac{1}{l}[(q_1 + q_3 + x_{rf}) - (q_2 + q_4 + x_{rr})]$

- $x_c = \frac{l_f}{l}x_{br} + \frac{l_r}{l}x_{bf} \implies x_c = \frac{l_f}{l}[q_2 + q_4 + x_{rr}] + \frac{l_r}{l}[q_1 + q_3 + x_{rf}]$

Writing potential energy in terms of displacement coordinates:

$$\nu(\mathbf{q}) = \frac{1}{2}k_{sf}q_1^2 + \frac{1}{2}k_{sr}q_2^2 + \frac{1}{2}k_{tf}q_3^2 + \frac{1}{2}k_{tr}q_4^2 \quad (\text{B.3})$$

kinetic energy $\tau(\dot{q})$,

$$\begin{aligned} \tau(\dot{\mathbf{q}}, t) &= \frac{1}{2}m_{wf}(\dot{q}_3 + \dot{x}_{rf})^2 + \frac{1}{2}m_{wr}(\dot{q}_4 + \dot{x}_{rr})^2 \\ &\quad + \frac{1}{2}m_b \left[\frac{l_f}{l}(\dot{q}_2 + \dot{q}_4 + \dot{x}_{rr}) + \frac{l_r}{l}(\dot{q}_1 + \dot{q}_3 + x_{rf}) \right]^2 \\ &\quad + \frac{1}{2}I_\phi \left[\frac{1}{l}(\dot{q}_1 + \dot{q}_3 - \dot{q}_2 - \dot{q}_4 + \dot{x}_{rf} - \dot{x}_{rr}) \right]^2 \end{aligned} \quad (\text{B.4})$$

The Lagrangian is given by $L(\mathbf{q}, \dot{\mathbf{q}}) = \tau(\dot{\mathbf{q}}, t) - \nu(\mathbf{q})$. The conjugate momenta \mathbf{p} can be derived from Lagrangian as

$$\mathbf{p} = \begin{bmatrix} p_1 \\ p_2 \\ p_3 \\ p_4 \end{bmatrix} = \begin{bmatrix} \nabla_{\dot{q}_1} L \\ \nabla_{\dot{q}_2} L \\ \nabla_{\dot{q}_3} L \\ \nabla_{\dot{q}_4} L \end{bmatrix} \quad (\text{B.5})$$

$$\begin{aligned} p_1 &= m_b \frac{l_r}{l} \left[\frac{l_f}{l}(\dot{q}_2 + \dot{q}_4 + \dot{x}_{rr}) + \frac{l_r}{l}(\dot{q}_1 + \dot{q}_3 + \dot{x}_{rf}) \right] + \frac{I_\phi}{l} \left[\frac{1}{l}(\dot{q}_1 + \dot{q}_3 - \dot{q}_2 - \dot{q}_4 + \dot{x}_{rf} - \dot{x}_{rr}) \right] \\ &= m_b \frac{l_r}{l} \dot{x}_c + \frac{I_\phi}{l} \dot{\phi} \end{aligned} \quad (\text{B.6})$$

$$\begin{aligned} p_2 &= m_b \frac{l_f}{l} \left[\frac{l_f}{l}(\dot{q}_2 + \dot{q}_4 + \dot{x}_{rr}) + \frac{l_r}{l}(\dot{q}_1 + \dot{q}_3 + \dot{x}_{rf}) \right] - \frac{I_\phi}{l} \left[\frac{1}{l}(\dot{q}_1 + \dot{q}_3 - \dot{q}_2 - \dot{q}_4 + \dot{x}_{rf} - \dot{x}_{rr}) \right] \\ &= m_b \frac{l_f}{l} \dot{x}_c - \frac{I_\phi}{l} \dot{\phi} \end{aligned} \quad (\text{B.7})$$

$$\begin{aligned} p_3 &= m_b \frac{l_r}{l} \left[\frac{l_f}{l}(\dot{q}_2 + \dot{q}_4 + \dot{x}_{rr}) + \frac{l_r}{l}(\dot{q}_1 + \dot{q}_3 + \dot{x}_{rf}) \right] + \frac{I_\phi}{l} \left[\frac{1}{l}(\dot{q}_1 + \dot{q}_3 - \dot{q}_2 - \dot{q}_4 + \dot{x}_{rf} - \dot{x}_{rr}) \right] + m_{wf}(\dot{q}_3 + \dot{x}_{rf}) \\ &= m_b \frac{l_r}{l} \dot{x}_c + \frac{I_\phi}{l} \dot{\phi} + m_{wf} \dot{x}_{wf} \end{aligned} \quad (\text{B.8})$$

$$\begin{aligned}
p_4 &= m_b \frac{l_f}{l} \left[\frac{l_f}{l} (\dot{q}_2 + \dot{q}_4 + \dot{x}_{rr}) + \frac{l_r}{l} (\dot{q}_1 + \dot{q}_3 + \dot{x}_{rf}) \right] - \frac{I_\phi}{l} \left[\frac{1}{l} (\dot{q}_1 + \dot{q}_3 - \dot{q}_2 - \dot{q}_4 + \dot{x}_{rf} - \dot{x}_{rr}) \right] + m_{wr} (\dot{q}_4 + \dot{x}_{rr}) \\
&= m_b \frac{l_f}{l} \dot{x}_c - \frac{I_\phi}{l} \dot{\phi} + m_{wr} \dot{x}_{wr} \quad (\text{B.9})
\end{aligned}$$

Therefore,

$$\mathbf{p} = \begin{bmatrix} p_1 \\ p_2 \\ p_3 \\ p_4 \end{bmatrix} = \begin{bmatrix} m_b \frac{l_r}{l} \dot{x}_c + \frac{I_\phi}{l} \dot{\phi} \\ m_b \frac{l_f}{l} \dot{x}_c - \frac{I_\phi}{l} \dot{\phi} \\ m_b \frac{l_r}{l} \dot{x}_c + \frac{I_\phi}{l} \dot{\phi} + m_{wf} \dot{x}_{wf} \\ m_b \frac{l_f}{l} \dot{x}_c - \frac{I_\phi}{l} \dot{\phi} + m_{wr} \dot{x}_{wr} \end{bmatrix} \quad (\text{B.10})$$

Now, the Kinetic energy can be written as a function of p as

$$\tau(\mathbf{p}) = \frac{1}{2} \mathbf{p} \mathbf{M}^{-1} \mathbf{p} \quad (\text{B.11})$$

The Hamiltonian $H(\mathbf{p}, \mathbf{q})$ which is the energy stored is written as

$$H(\mathbf{p}, \mathbf{q}) = \tau(\mathbf{p}) + \nu(\mathbf{q}) \quad (\text{B.12})$$

Now, we have to find \mathbf{M} (inertia matrix), whose inverse is required to compute $\tau(\mathbf{p})$. Consider a vector of velocity coordinates \mathbf{v} , defined as $\mathbf{v} = \begin{bmatrix} \dot{x}_c & \dot{\phi} & \dot{x}_{wf} & \dot{x}_{wr} \end{bmatrix}^T$. Kinetic energy τ in B.2 can be written in terms of \mathbf{v} as,

$$\tau = \frac{1}{2} \mathbf{v}^T \mathbf{M}_T \mathbf{v} = \frac{1}{2} \begin{bmatrix} \dot{x}_c & \dot{\phi} & \dot{x}_{wf} & \dot{x}_{wr} \end{bmatrix} \begin{bmatrix} m_b & 0 & 0 & 0 \\ 0 & I_\phi & 0 & 0 \\ 0 & 0 & m_{wf} & 0 \\ 0 & 0 & 0 & m_{wr} \end{bmatrix} \begin{bmatrix} \dot{x}_c \\ \dot{\phi} \\ \dot{x}_{wf} \\ \dot{x}_{wr} \end{bmatrix} \quad (\text{B.13})$$

writing \mathbf{p} from equation B.10 in terms of \mathbf{v} ,

$$\mathbf{p} = \mathbf{\Lambda} \mathbf{v} = \begin{bmatrix} m_b \frac{l_r}{l} & \frac{I_\phi}{l} & 0 & 0 \\ m_b \frac{l_f}{l} & -\frac{I_\phi}{l} & 0 & 0 \\ m_b \frac{l_r}{l} & \frac{I_\phi}{l} & m_{wf} & 0 \\ m_b \frac{l_f}{l} & -\frac{I_\phi}{l} & 0 & m_{wr} \end{bmatrix} \begin{bmatrix} \dot{x}_c \\ \dot{\phi} \\ \dot{x}_{wf} \\ \dot{x}_{wr} \end{bmatrix} \quad (\text{B.14})$$

$\implies \mathbf{\Lambda}^{-1} \mathbf{p} = \mathbf{v}$. Let $\mathbf{\Lambda}^{-1} = \mathbf{f}_T$. Then equation B.13 can be written as

$$\tau = \frac{1}{2} \mathbf{v}^T \mathbf{M}_T \mathbf{v} = \frac{1}{2} \mathbf{p}^T \mathbf{f}_T^T \mathbf{M}_T \mathbf{f}_T \mathbf{p} \quad (\text{B.15})$$

Comparing equations B.11 and B.15,

$$\mathbf{M}^{-1} = \mathbf{f}_T^T \mathbf{M}_T \mathbf{f}_T \quad (\text{B.16})$$

$$\mathbf{f}_T = \mathbf{\Lambda}^{-1} = \begin{bmatrix} \frac{1}{m_b} & \frac{1}{m_b} & 0 & 0 \\ \frac{l_f}{I_\phi} & -\frac{l_r}{I_\phi} & 0 & 0 \\ -\frac{1}{m_{wf}} & 0 & \frac{1}{m_{wf}} & 0 \\ 0 & -\frac{1}{m_{wr}} & 0 & \frac{1}{m_{wr}} \end{bmatrix} \quad (\text{B.17})$$

$$\mathbf{M}^{-1} = \begin{bmatrix} \frac{1}{m_b} + \frac{l_f^2}{I_\phi} + \frac{1}{m_{wf}} & \frac{1}{m_b} - \frac{l_f l_r}{I_\phi} & -\frac{1}{m_{wf}} & 0 \\ \frac{1}{m_b} - \frac{l_f l_r}{I_\phi} & \frac{1}{m_b} + \frac{l_r^2}{I_\phi} + \frac{1}{m_{wr}} & 0 & -\frac{1}{m_{wr}} \\ -\frac{1}{m_{wf}} & 0 & \frac{1}{m_{wf}} & 0 \\ 0 & -\frac{1}{m_{wr}} & 0 & \frac{1}{m_{wr}} \end{bmatrix} \quad (\text{B.18})$$

Inertia matrix $\mathbf{M} = (\mathbf{M}^{-1})^{-1} = (\mathbf{f}_T^T \mathbf{M}_T \mathbf{f}_T)^{-1} = \mathbf{f}_T^{-1} \mathbf{M}_T^{-1} \mathbf{f}_T^{-T}$

$$\mathbf{M} = \begin{bmatrix} \frac{m_b l_r^2 + I_\phi}{l^2} & \frac{m_b l_f l_r - I_\phi}{l^2} & \frac{m_b l_r^2 + I_\phi}{l^2} & \frac{m_b l_f l_r - I_\phi}{l^2} \\ \frac{m_b l_f l_r - I_\phi}{l^2} & \frac{m_b l_f^2 + I_\phi}{l^2} & \frac{m_b l_f l_r - I_\phi}{l^2} & \frac{m_b l_f^2 + I_\phi}{l^2} \\ \frac{m_b l_r^2 + I_\phi}{l^2} & \frac{m_b l_f l_r - I_\phi}{l^2} & \frac{m_b l_r^2 + I_\phi}{l^2} + m_{wf} & \frac{m_b l_f l_r - I_\phi}{l^2} \\ \frac{m_b l_f l_r - I_\phi}{l^2} & \frac{m_b l_f^2 + I_\phi}{l^2} & \frac{m_b l_f l_r - I_\phi}{l^2} & \frac{m_b l_f^2 + I_\phi}{l^2} + m_{wr} \end{bmatrix} \quad (\text{B.19})$$

Hamiltonian $H(\mathbf{p}, \mathbf{q})$ in terms of Inertia matrix,

$$H(\mathbf{p}, \mathbf{q}) = \frac{1}{2} \mathbf{p}^T \mathbf{M}^{-1} \mathbf{p} + \nu(\mathbf{q}) \quad \implies \quad \nabla_{\mathbf{p}} H = \mathbf{M}^{-1} \mathbf{p} \quad (\text{B.20})$$

Defining state variables (\mathbf{p}, \mathbf{q}) : $\mathbf{p} = [p_1 \ p_2 \ p_3 \ p_4]^T$ and $\mathbf{q} = [q_1 \ q_2 \ q_3 \ q_4]^T$.
From equation B.20,

$$\nabla_{\mathbf{p}} H = \mathbf{M}^{-1} \mathbf{p} = \begin{bmatrix} \nabla_{p_1} H \\ \nabla_{p_2} H \\ \nabla_{p_3} H \\ \nabla_{p_4} H \end{bmatrix} = \begin{bmatrix} \dot{q}_1 \\ \dot{q}_2 \\ \dot{q}_3 + \dot{x}_{rf} \\ \dot{q}_4 + \dot{x}_{rr} \end{bmatrix} \quad (\text{B.21})$$

Therefore,

$$\begin{bmatrix} \dot{q}_1 \\ \dot{q}_2 \\ \dot{q}_3 \\ \dot{q}_4 \end{bmatrix} = \begin{bmatrix} \nabla_{p_1} H \\ \nabla_{p_2} H \\ \nabla_{p_3} H \\ \nabla_{p_4} H \end{bmatrix} + \begin{bmatrix} 0 & 0 \\ 0 & 0 \\ -1 & 0 \\ 0 & -1 \end{bmatrix} \begin{bmatrix} \dot{x}_{rf} \\ \dot{x}_{rr} \end{bmatrix} \quad (\text{B.22})$$

Dissipated power \mathbb{D} by dampers,

$$\mathbb{D}(\dot{\mathbf{q}}) = \frac{1}{2} b_{sf} \dot{q}_1^2 + \frac{1}{2} b_{sr} \dot{q}_2^2 + \frac{1}{2} b_{tf} \dot{q}_3^2 + \frac{1}{2} b_{tr} \dot{q}_4^2 \quad (\text{B.23})$$

Therefore,

$$\frac{\partial \mathbb{D}}{\partial \dot{q}_1} = b_{sf} \dot{q}_1, \quad \frac{\partial \mathbb{D}}{\partial \dot{q}_2} = b_{sr} \dot{q}_2, \quad \frac{\partial \mathbb{D}}{\partial \dot{q}_3} = b_{tf} \dot{q}_3, \quad \frac{\partial \mathbb{D}}{\partial \dot{q}_4} = b_{tr} \dot{q}_4 \quad (\text{B.24})$$

$$\nabla_{\dot{\mathbf{q}}} \mathbb{D} = \begin{bmatrix} b_{sf} & 0 & 0 & 0 \\ 0 & b_{sr} & 0 & 0 \\ 0 & 0 & b_{tf} & 0 \\ 0 & 0 & 0 & b_{tr} \end{bmatrix} \begin{bmatrix} \dot{q}_1 \\ \dot{q}_2 \\ \dot{q}_3 \\ \dot{q}_4 \end{bmatrix} \quad (\text{B.25})$$

From equations B.22 and B.25,

$$\nabla_{\dot{\mathbf{q}}}\mathbb{D} = \begin{bmatrix} b_{sf} & 0 & 0 & 0 \\ 0 & b_{sr} & 0 & 0 \\ 0 & 0 & b_{tf} & 0 \\ 0 & 0 & 0 & b_{tr} \end{bmatrix} \begin{bmatrix} \nabla_{p1}H \\ \nabla_{p2}H \\ \nabla_{p3}H \\ \nabla_{p4}H \end{bmatrix} - \begin{bmatrix} 0 & 0 \\ 0 & 0 \\ b_{tf} & 0 \\ 0 & b_{tr} \end{bmatrix} \begin{bmatrix} \dot{x}_{rf} \\ \dot{x}_{rr} \end{bmatrix} \quad (\text{B.26})$$

Also

$$\nabla_{\mathbf{q}}H = \begin{bmatrix} \nabla_{q1}H \\ \nabla_{q2}H \\ \nabla_{q3}H \\ \nabla_{q4}H \end{bmatrix} = \begin{bmatrix} k_{sf} & 0 & 0 & 0 \\ 0 & k_{sr} & 0 & 0 \\ 0 & 0 & k_{tf} & 0 \\ 0 & 0 & 0 & k_{tr} \end{bmatrix} \begin{bmatrix} q_1 \\ q_2 \\ q_3 \\ q_4 \end{bmatrix} = \mathbf{K}\mathbf{q} \quad (\text{B.27})$$

Hamiltonian model of a simple mechanical system with added velocity controlled dissipation and external force inputs Renton et al. (2012) is given by,

$$\begin{bmatrix} \dot{\mathbf{p}} \\ \dot{\mathbf{q}} \end{bmatrix} = \begin{bmatrix} \mathbf{0} & -\mathbf{I} \\ \mathbf{I} & \mathbf{0} \end{bmatrix} \begin{bmatrix} \nabla_{\mathbf{p}}H \\ \nabla_{\mathbf{q}}H \end{bmatrix} - \begin{bmatrix} \nabla_{\dot{\mathbf{q}}}\mathbb{D} \\ \mathbf{0} \end{bmatrix} + \begin{bmatrix} \mathbf{G} \\ \mathbf{0} \end{bmatrix} \mathbf{u} \quad (\text{B.28})$$

There are two kinds of input forces acting of the system

1. Road inputs x_{rf} and x_{rr}
2. Actuator forces u_f and u_r

$$\text{Let } \mathbf{f} = \begin{bmatrix} \dot{x}_{rf}(t) \\ \dot{x}_{rr}(t) \end{bmatrix} \text{ and } \mathbf{u}_a = \begin{bmatrix} u_f \\ u_r \end{bmatrix}. \text{ Define } \mathbf{G}_1 = \begin{bmatrix} 0 & 0 \\ 0 & 0 \\ b_{tf} & 0 \\ 0 & b_{tr} \end{bmatrix}, \mathbf{D} = \begin{bmatrix} b_{sf} & 0 & 0 & 0 \\ 0 & b_{sr} & 0 & 0 \\ 0 & 0 & b_{tf} & 0 \\ 0 & 0 & 0 & b_{tr} \end{bmatrix},$$

$$\mathbf{G}_2 = \begin{bmatrix} 0 & 0 \\ 0 & 0 \\ -1 & 0 \\ 0 & -1 \end{bmatrix} \text{ and } \mathbf{G} = \begin{bmatrix} 1 & 0 \\ 0 & 1 \\ 0 & 0 \\ 0 & 0 \end{bmatrix}$$

Now, equation B.26 can be written as,

$$\nabla_{\dot{\mathbf{q}}}\mathbb{D} = \mathbf{D}\nabla_{\mathbf{p}}H - \mathbf{G}_1\mathbf{f} \quad (\text{B.29})$$

Equation B.22 can be written as,

$$\dot{\mathbf{q}} = \nabla_{\mathbf{p}}H + \mathbf{G}_2\mathbf{f} \quad (\text{B.30})$$

$$\dot{\mathbf{p}} = -\nabla_{\mathbf{q}}H - \nabla_{\dot{\mathbf{q}}}\mathbb{D} + \mathbf{G}\mathbf{u}_a \quad (\text{B.31})$$

Substituting equation B.29 in B.31

$$\dot{\mathbf{p}} = -\nabla_{\mathbf{q}}H - [\mathbf{D}\nabla_{\mathbf{p}}H - \mathbf{G}_1\mathbf{f}] + \mathbf{G}\mathbf{u}_a \quad (\text{B.32})$$

$$= -\nabla_{\mathbf{q}}H - \mathbf{D}\nabla_{\mathbf{p}}H + \mathbf{G}_1\mathbf{f} + \mathbf{G}\mathbf{u}_a \quad (\text{B.33})$$

Therefore, writing equations B.32 and B.30 in matrix form,

$$\begin{bmatrix} \dot{\mathbf{p}} \\ \dot{\mathbf{q}} \end{bmatrix} = \begin{bmatrix} -\mathbf{D} & -\mathbf{I} \\ \mathbf{I} & \mathbf{0} \end{bmatrix} \begin{bmatrix} \nabla_{\mathbf{p}}H \\ \nabla_{\mathbf{q}}H \end{bmatrix} + \begin{bmatrix} \mathbf{G} \\ \mathbf{0} \end{bmatrix} \mathbf{u}_a + \begin{bmatrix} \mathbf{G}_1 \\ \mathbf{G}_2 \end{bmatrix} \mathbf{f} \quad (\text{B.34})$$

Equation B.34 is the PCHD form of Half car active suspension system, which can be written in extended form as

$$\begin{bmatrix} \dot{p}_1 \\ \dot{p}_2 \\ \dot{p}_3 \\ \dot{p}_4 \\ \dot{q}_1 \\ \dot{q}_2 \\ \dot{q}_3 \\ \dot{q}_4 \end{bmatrix} = \begin{bmatrix} -b_{sf} & 0 & 0 & 0 & -1 & 0 & 0 & 0 \\ 0 & -b_{sr} & 0 & 0 & 0 & -1 & 0 & 0 \\ 0 & 0 & -b_{tf} & 0 & 0 & 0 & -1 & 0 \\ 0 & 0 & 0 & -b_{tr} & 0 & 0 & 0 & -1 \\ 1 & 0 & 0 & 0 & 0 & 0 & 0 & 0 \\ 0 & 1 & 0 & 0 & 0 & 0 & 0 & 0 \\ 0 & 0 & 1 & 0 & 0 & 0 & 0 & 0 \\ 0 & 0 & 0 & 1 & 0 & 0 & 0 & 0 \end{bmatrix} \begin{bmatrix} \nabla_{p1}H \\ \nabla_{p2}H \\ \nabla_{p3}H \\ \nabla_{p4}H \\ \nabla_{q1}H \\ \nabla_{q2}H \\ \nabla_{q3}H \\ \nabla_{q4}H \end{bmatrix} + \begin{bmatrix} 1 & 0 \\ 0 & 1 \\ 0 & 0 \\ 0 & 0 \\ 0 & 0 \\ 0 & 0 \\ 0 & 0 \\ 0 & 0 \end{bmatrix} \begin{bmatrix} u_f \\ u_r \end{bmatrix} + \begin{bmatrix} 0 & 0 \\ 0 & 0 \\ b_{tf} & 0 \\ 0 & b_{tr} \\ 0 & 0 \\ 0 & 0 \\ -1 & 0 \\ 0 & -1 \end{bmatrix} \begin{bmatrix} \dot{x}_{rf} \\ \dot{x}_{rr} \end{bmatrix} \quad (\text{B.35})$$

Equation B.34 can be written in general well known port-controlled Hamiltonian form as

$$\dot{\mathbf{x}} = [\mathbf{J} - \mathbf{R}]\nabla\mathbf{H}(\mathbf{x}) + \mathbf{g}\mathbf{u}_a + \mathbf{d}\mathbf{f}(\mathbf{t}) \quad (\text{B.36})$$

where $\mathbf{x} = (\mathbf{p}, \mathbf{q}) \in \mathbb{R}^n$ ($n = 8$) is the state vector of displacement and momenta coordinates. Matrices \mathbf{J} and \mathbf{R} represent the interconnection and resistive structures,

respectively.

$$\mathbf{J} = \begin{bmatrix} \mathbf{0} & -\mathbf{I} \\ \mathbf{I} & \mathbf{0} \end{bmatrix} \quad \text{and} \quad \mathbf{R} = \begin{bmatrix} \mathbf{D} & \mathbf{0} \\ \mathbf{0} & \mathbf{0} \end{bmatrix} \quad (\text{B.37})$$

The matrices \mathbf{g} and \mathbf{d} are defined as $\mathbf{g} = [\mathbf{G}^T \quad \mathbf{0}]^T$, and $\mathbf{d} = [\mathbf{G}_1^T \quad \mathbf{G}_2^T]^T$.

Bibliography

- Afshar, K. K., Javadi, A., and Jahed-Motlagh, M. R. (2018). Robust h_∞ control of an active suspension system with actuator time delay by predictor feedback. *IET Control Theory & Applications*, 12(7):1012–1023.
- Al Aela, A. M., Kenne, J.-P., and Mintsa, H. A. (2022). Adaptive neural network and nonlinear electrohydraulic active suspension control system. *Journal of Vibration and Control*, 28(3-4):243–259.
- Alkrunz, M. and Yalçın, Y. (2019). Discrete-time i&i adaptive control for a class of uncertain port-controlled hamiltonian systems. In *2019 6th International Conference on Electrical and Electronics Engineering (ICEEE)*, pages 207–214. IEEE.
- Alves, U. N. L., Garcia, J. P. F., Teixeira, M., Garcia, S. C., and Rodrigues, F. B. (2014). Sliding mode control for active suspension system with data acquisition delay. *Mathematical Problems in Engineering*, 2014.
- Aoki, T., Yamashita, Y., and Tsubakino, D. (2016). Vibration suppression for mass-spring-damper systems with a tuned mass damper using interconnection and damping assignment passivity-based control. *International journal of robust and nonlinear control*, 26(2):235–251.
- Astolfi, A., Ortega, R., and Venkatraman, A. (2010). A globally exponentially convergent immersion and invariance speed observer for mechanical systems with non-holonomic constraints. *Automatica*, 46(1):182–189.
- Barman, S., Samanta, S., Mishra, J. P., Roy, P., and Roy, B. K. (2018). Design and implementation of an ida-pbc for a grid connected inverter used in a photovoltaic system. *IFAC-PapersOnLine*, 51(1):680–685.

- Biedermann, B., Rosenzweig, P., and Meurer, T. (2018). Passivity-based observer design for state affine systems using interconnection and damping assignment. In *2018 IEEE Conference on Decision and Control (CDC)*, pages 4662–4667. IEEE.
- Borja, P., Cisneros, R., and Ortega, R. (2016). A constructive procedure for energy shaping of port—hamiltonian systems. *Automatica*, 72:230–234.
- Chen, H. and Guo, K.-H. (2005). Constrained h_∞ control of active suspensions: an lmi approach. *IEEE Transactions on Control Systems Technology*, 13(3):412–421.
- Chen, H., Liu, Z.-Y., and Sun, P.-Y. (2005). Application of constrained h_∞ control to active suspension systems on half-car models.
- Cieza, O. B. and Reger, J. (2018). Ida-pbc for polynomial systems: An sos-based approach. *IFAC-PapersOnLine*, 51(13):366–371.
- Cornejo, C. and Alvarez-Icaza, L. (2012). Passivity based control of under-actuated mechanical systems with nonlinear dynamic friction. *Journal of Vibration and Control*, 18(7):1025–1042.
- Cupelli, M., Gurumurthy, S. K., Bhandari, S. K., Yang, Z., Joebges, P., Monti, A., and De Doncker, R. W. (2019). Port controlled hamiltonian modeling and ida-pbc control of dual active bridge converters for dc microgrids. *IEEE Transactions on Industrial Electronics*, 66(11):9065–9075.
- Deshpande, V. S., Mohan, B., Shendge, P., and Phadke, S. (2014). Disturbance observer based sliding mode control of active suspension systems. *Journal of Sound and Vibration*, 333(11):2281–2296.
- Donaire, A., Ruggiero, F., Buonocore, L. R., Lippiello, V., and Siciliano, B. (2016). Passivity-based control for a rolling-balancing system: The nonprehensile disk-on-disk. *IEEE Transactions on Control Systems Technology*, 25(6):2135–2142.
- Du, H. and Zhang, N. (2008). Constrained h_∞ control of active suspension for a half-car model with a time delay in control. *Proceedings of the Institution of Mechanical Engineers, Part D: Journal of Automobile Engineering*, 222(5):665–684.

- Erol, B. and Delibaşı, A. (2018). Proportional–integral–derivative type h_{infty} controller for quarter car active suspension system. *Journal of Vibration and Control*, 24(10):1951–1966.
- Ferguson, J., Donaire, A., Ortega, R., and Middleton, R. H. (2017). New results on disturbance rejection for energy-shaping controlled port-hamiltonian systems. *arXiv preprint arXiv:1710.06070*.
- Franco, E. (2019). Adaptive ida-pbc for underactuated mechanical systems with constant disturbances. *International Journal of Adaptive Control and Signal Processing*, 33(1):1–15.
- Fujita, M., Kawai, H., and Spong, M. W. (2006). Passivity-based dynamic visual feedback control for three-dimensional target tracking: Stability and l_2 -gain performance analysis. *IEEE Transactions on Control Systems Technology*, 15(1):40–52.
- Gandarilla, I., Santibañez, V., and Sandoval, J. (2019). Control of a self-balancing robot with two degrees of freedom via ida-pbc. *ISA transactions*, 88:102–112.
- Gillespie, T. D. (1992). Fundamentals of vehicle dynamics. Technical report, SAE Technical Paper.
- Gupta, S., Ginoya, D., Shendge, P., and Phadke, S. B. (2016). An inertial delay observer-based sliding mode control for active suspension systems. *Proceedings of the institution of mechanical engineers, Part D: Journal of Automobile Engineering*, 230(3):352–370.
- Haddad, N. K., Chemori, A., and Belghith, S. (2018). Robustness enhancement of ida-pbc controller in stabilising the inertia wheel inverted pendulum: theory and real-time experiments. *International Journal of Control*, 91(12):2657–2672.
- Hao, S., Yamashita, Y., and Kobayashi, K. (2022). Robust passivity-based control design for active nonlinear suspension system. *International Journal of Robust and Nonlinear Control*, 32(1):373–392.
- Harandi, M. R. J. and Taghirad, H. D. (2021a). On the matching equations of kinetic energy shaping in ida-pbc. *Journal of the Franklin Institute*, 358(16):8639–8655.

- Harandi, M. R. J. and Taghirad, H. D. (2021b). Solution of matching equations of ida-pbc by pfaffian differential equations. *International Journal of Control*, pages 1–11.
- Karim Afshar, K. and Javadi, A. (2019). Constrained h_∞ control for a half-car model of an active suspension system with actuator time delay by predictor feedback. *Journal of Vibration and Control*, 25(10):1673–1692.
- Khefifi, N., Houari, A., Machmoum, M., Ghanes, M., and Ait-Ahmed, M. (2019). Control of grid forming inverter based on robust ida-pbc for power quality enhancement. *Sustainable Energy, Grids and Networks*, 20:100276.
- Lapique, M., Pang, S., Martin, J.-P., Pierfederici, S., Weber, M., and Zaim, S. (2022). Enhanced ida-pbc applied to a 3-phase pwm-rectifier for stable interfacing between ac and dc microgrids embedded in more electrical aircraft. *IEEE Transactions on Industrial Electronics*.
- Li, H., Jing, X., and Karimi, H. R. (2013a). Output-feedback-based h_∞ control for vehicle suspension systems with control delay. *IEEE Transactions on industrial electronics*, 61(1):436–446.
- Li, H., Liu, H., Hand, S., and Hilton, C. (2012). Multi-objective h_∞ control for vehicle active suspension systems with random actuator delay. *International Journal of systems science*, 43(12):2214–2227.
- Li, H., Liu, H., Hilton, C., and Hand, S. (2013b). Non-fragile h_∞ control for half-vehicle active suspension systems with actuator uncertainties. *Journal of Vibration and Control*, 19(4):560–575.
- Li, W., Xie, Z., Wong, P. K., Cao, Y., Hua, X., and Zhao, J. (2019). Robust nonfragile h_∞ optimum control for active suspension systems with time-varying actuator delay. *Journal of Vibration and Control*, 25(18):2435–2452.
- Lian, R.-J. (2012). Enhanced adaptive self-organizing fuzzy sliding-mode controller for active suspension systems. *IEEE Transactions on Industrial Electronics*, 60(3):958–968.

- Liu, B., Saif, M., and Fan, H. (2016). Adaptive fault tolerant control of a half-car active suspension systems subject to random actuator failures. *IEEE/ASME Transactions on Mechatronics*, 21(6):2847–2857.
- Liu, H., Gao, H., and Li, P. (2013). *Handbook of vehicle suspension control systems*. Institution of Engineering and Technology.
- Liu, Z., Geng, Z., and Hu, X. (2018). An approach to suppress low frequency oscillation in the traction network of high-speed railway using passivity-based control. *IEEE Transactions on Power Systems*, 33(4):3909–3918.
- Lu, T.-T. and Shiou, S.-H. (2002). Inverses of 2×2 block matrices. *Computers & Mathematics with Applications*, 43(1-2):119–129.
- Ma, M.-M. and Chen, H. (2011). Disturbance attenuation control of active suspension with non-linear actuator dynamics. *IET control theory & applications*, 5(1):112–122.
- Mattioni, M., Monaco, S., and Normand-Cyrot, D. (2020). Ida-pbc for lti dynamics under input delays: a reduction approach. *IEEE Control Systems Letters*, 5(4):1465–1470.
- Montoya, O. D., Serra, F. M., Gil-González, W., Asensio, E. M., and Bosso, J. E. (2021). An ida-pbc design with integral action for output voltage regulation in an interleaved boost converter for dc microgrid applications. In *Actuators*, volume 11, page 5. MDPI.
- Nagesh Rao, S. P., Lopes, G. A., Jeltsema, D., and Babuška, R. (2015). Port-hamiltonian systems in adaptive and learning control: A survey. *IEEE Transactions on Automatic Control*, 61(5):1223–1238.
- Nunna, K., Sassano, M., and Astolfi, A. (2015). Constructive interconnection and damping assignment for port-controlled hamiltonian systems. *IEEE Transactions on Automatic Control*, 60(9):2350–2361.
- Ortega, R., Perez, J. A. L., Nicklasson, P. J., and Sira-Ramirez, H. J. (2013). *Passivity-based control of Euler-Lagrange systems: mechanical, electrical and electromechanical applications*. Springer Science & Business Media.

- Ortega, R., Van Der Schaft, A., Castanos, F., and Astolfi, A. (2008). Control by interconnection and standard passivity-based control of port-hamiltonian systems. *IEEE Transactions on Automatic control*, 53(11):2527–2542.
- Ortega, R., Van Der Schaft, A., Maschke, B., and Escobar, G. (2002). Interconnection and damping assignment passivity-based control of port-controlled hamiltonian systems. *Automatica*, 38(4):585–596.
- Ortega, R., Van Der Schaft, A. J., Mareels, I., and Maschke, B. (2001). Putting energy back in control. *IEEE Control Systems Magazine*, 21(2):18–33.
- Ozer, H. O., Hacıoglu, Y., and Yagiz, N. (2018). High order sliding mode control with estimation for vehicle active suspensions. *Transactions of the Institute of Measurement and Control*, 40(5):1457–1470.
- Pan, H., Sun, W., Gao, H., and Yu, J. (2015). Finite-time stabilization for vehicle active suspension systems with hard constraints. *IEEE transactions on intelligent transportation systems*, 16(5):2663–2672.
- Pang, H., Shang, Y., and Yang, J. (2020). An adaptive sliding mode-based fault-tolerant control design for half-vehicle active suspensions using t-s fuzzy approach. *Journal of Vibration and Control*, 26(17-18):1411–1424.
- Pang, H., Zhang, X., Yang, J., and Shang, Y. (2019a). Adaptive backstepping-based control design for uncertain nonlinear active suspension system with input delay. *International Journal of Robust and Nonlinear Control*, 29(16):5781–5800.
- Pang, S., Nahid-Mobarakeh, B., Pierfederici, S., Huangfu, Y., Luo, G., and Gao, F. (2019b). Toward stabilization of constant power loads using ida-pbc for cascaded lc filter dc/dc converters. *IEEE Journal of Emerging and Selected Topics in Power Electronics*, 9(2):1302–1314.
- Pare Jr, T. E. (2001). *Passivity-based analysis and control of nonlinear systems*. stanford university.
- Qin, W., Shangguan, W.-B., and Yin, Z. (2020a). Sliding mode control of double-wishbone active suspension systems based on equivalent 2-degree-of-freedom model. *Proceedings of the Institution of Mechanical Engineers, Part D: Journal of Automobile Engineering*, 234(13):3164–3179.

- Qin, W., Shangguan, W.-B., and Zhao, K. (2020b). A research of sliding mode control method with disturbance observer combining skyhook model for active suspension systems. *Journal of Vibration and Control*, 26(11-12):952–964.
- Rajamani, R. (2011). *Vehicle dynamics and control*. Springer Science & Business Media.
- Rath, J. J., Defoort, M., Karimi, H. R., and Veluvolu, K. C. (2016). Output feedback active suspension control with higher order terminal sliding mode. *IEEE Transactions on Industrial Electronics*, 64(2):1392–1403.
- Renton, C., Teo, Y. R., Donaire, A., and Perez, T. (2012). Active control of car suspension systems using ida-pbc. In *2012 2nd Australian Control Conference*, pages 361–366. IEEE.
- Ryalat, M. (2015). *Design and implementation of nonlinear and robust control for Hamiltonian systems: the passivity-based control approach*. PhD thesis, University of Southampton.
- SCHAFT, A. v. d. (2000). Robust nonlinear control. port-controlled hamiltonian systems: Towards a theory for control and design of nonlinear physical systems. *Journal of the Society of Instrument and Control Engineers of Japan (SICE)*, 39(2):91–98.
- Sun, W., Gao, H., and Kaynak, O. (2012). Adaptive backstepping control for active suspension systems with hard constraints. *IEEE/ASME transactions on mechatronics*, 18(3):1072–1079.
- Sun, W., Pan, H., and Gao, H. (2015). Filter-based adaptive vibration control for active vehicle suspensions with electrohydraulic actuators. *IEEE Transactions on Vehicular Technology*, 65(6):4619–4626.
- Sun, W., Pan, H., Zhang, Y., and Gao, H. (2014). Multi-objective control for uncertain nonlinear active suspension systems. *Mechatronics*, 24(4):318–327.
- Sun, W., Zhao, Y., Li, J., Zhang, L., and Gao, H. (2011). Active suspension control with frequency band constraints and actuator input delay. *IEEE Transactions on Industrial Electronics*, 59(1):530–537.

- Taghirad, H. D. and Esmailzadeh, E. (1998). Automobile passenger comfort assured through lqg/lqr active suspension. *Journal of vibration and control*, 4(5):603–618.
- Van Der Schaft, A. and Jeltsema, D. (2014). Port-hamiltonian systems theory: An introductory overview. *Foundations and Trends in Systems and Control*, 1(2-3):173–378.
- Venkatraman, A. (2010). *Control of port-Hamiltonian systems: observer design and alternate passive input-output pairs*. PhD thesis. Relation: <http://www.rug.nl/> Rights: University of Groningen.
- Venkatraman, A., Ortega, R., Sarras, I., and van der Schaft, A. (2008). Control of underactuated mechanical systems: Observer design and position feedback stabilization. In *2008 47th IEEE Conference on Decision and Control*, pages 4969–4975. IEEE.
- Venkatraman, A. and Van der Schaft, A. (2010). Full-order observer design for a class of port-hamiltonian systems. *Automatica*, 46(3):555–561.
- Viola, G., Ortega, R., Banavar, R., Acosta, J. Á., and Astolfi, A. (2007). Total energy shaping control of mechanical systems: simplifying the matching equations via coordinate changes. *IEEE Transactions on Automatic Control*, 52(6):1093–1099.
- Vu, N. T. and Lefèvre, L. (2018). A connection between optimal control and ida-pbc design. *IFAC-PapersOnLine*, 51(3):205–210.
- Wang, Y., Ge, S. S., and Cheng, D. (2005). Observer and observer-based h_∞ control of generalized hamiltonian systems. *Science in China Series F: Information Sciences*, 48(2):211–224.
- Xiao, L. and Zhu, Y. (2014). Passivity-based integral sliding mode active suspension control. *IFAC Proceedings Volumes*, 47(3):5205–5210.
- Yaghmaei, A. and Yazdanpanah, M. J. (2018). Structure preserving observer design for port-hamiltonian systems. *IEEE Transactions on Automatic Control*, 64(3):1214–1220.
- Yilmaz, C. T. and Basturk, H. I. (2019). Adaptive backstepping control design for active suspension systems with output feedback. In *2019 American Control Conference (ACC)*, pages 1712–1717. IEEE.

- Yu, S., Jin, L., Zheng, K., and Du, J. (2013). Continuous finite-time terminal sliding mode ida-pbc design for pmsm with the port-controlled hamiltonian model. *Mathematical Problems in Engineering*, 2013.
- Yüksel, B., Secchi, C., Bühlhoff, H. H., and Franchi, A. (2019). Aerial physical interaction via ida-pbc. *The International Journal of Robotics Research*, 38(4):403–421.
- Zhang, M., Borja, P., Ortega, R., Liu, Z., and Su, H. (2017). Pid passivity-based control of port-hamiltonian systems. *IEEE Transactions on Automatic Control*, 63(4):1032–1044.

PUBLICATIONS BASED ON THE THESIS

Papers in refereed journals

1. **Sistla, P.**, Figarado, S., Chemmangat, K., Manjarekar, N. S., & Kallu Valappil, G. (2021). Design and performance comparison of interconnection and damping assignment passivity-based control for vibration suppression in active suspension systems. *Journal of Vibration and Control*, 27(7–8), 893–911. <https://doi.org/10.1177/1077546320933749>
2. **Sistla, P.**, Chemmangat, K., Figarado, S., Design and Implementation of Passivity-Based controller for Active Suspension System using port-Hamiltonian observer. *Proceedings of the Institution of Mechanical Engineers, Part D: Journal of Automobile Engineering*. 2023;0(0). doi:10.1177/09544070221147364
3. **Sistla, P.**, Chemmangat, K., Figarado, S., Control of Half Car Active Suspension system using Algebraic Interconnection and Damping Assignment Passivity based control. *IEEE Transactions on Control Systems Technology* (Manuscript in Preparation)

Bio-data

Name : S V Pramod

Date of birth: 19-04-1990

E-mail: pramod.sistla@gmail.com

Mobile: +91-9052783935

Education

- **M.Tech**, Power Electronic Systems and Control, Manipal Institute of Technology, Manipal, Karnataka, 2015.
- **B.Tech.**, Electrical & Electronics Engineering, ACE Engineering College, Hyderabad, Telangana, 2011.

Address

H.No:27-16-22/10A (WSK11), West Srikrishna Nagar Colony

Near community hall, RK Puram (PO)

Malkajgiri, Secunderabad Telangana -500056, India.